IMMUNOMETABOLISM AND THE ROLE OF COMPLEMENT FACTOR 5 IN INSULIN ACTION

By
Kristin Rose Peterson

Dissertation

Submitted to the Faculty of the

Graduate School of Vanderbilt University

in partial fulfillment of the requirements

for the degree of

DOCTOR OF PHILOSOPHY

in

Pharmacology

May 10, 2019

Nashville, Tennessee

Approved:

Brian Wadzinski, Ph.D.
Raymond Blind, Ph.D.
Sean Davies, Ph.D.
Owen McGuinness, Ph.D.
Alyssa Hasty, Ph.D.

This Dissertation is dedicated to
my mom and dad
who have always prioritized my education
&
my husband for the endless support

ACKNOWLEDGEMENTS

I would like to first acknowledge my mentor, Dr. Alyssa Hasty. Thank you for guiding and supporting me throughout my time at Vanderbilt, and for establishing a laboratory environment of collaboration and learning among colleagues and friends. I am thankful that I found your lab in which to develop my skills as a scientist. I think what makes our lab unique is that you get to know each person you work with, and mentor based on his or her individual skills and goals. Aside from scientific and critical thinking skills, I have also learned from you about perseverance, hard work, and the definition of success. I will most certainly use all of these things as I continue my career. I appreciate the support you have given me and will always look back fondly on the time I spent learning under your guidance.

Next, I would like to thank the members of my dissertation committee, Drs. Brian Wadzinski, Ray Blind, Sean Davies, and Owen McGuinness. I know that my project was not typical of a student in Pharmacology, and I appreciate you learning with me and contributing each of your expertise. I have enjoyed getting to know you and am confident that I am a better scientist because of your guidance.

I would also like to thank the department of Pharmacology, of which I feel fortunate to have been a part. Especially, thank you to Dr. Joey Barnett for welcoming Alyssa and I in to the department, and to Karen Gieg and Cindi Kellam for helping me navigate Vanderbilt and becoming my friends in the process.

Thank you to the friends I've made through IGP, Pharmacology, and MPB, and to the members of the Hasty Lab. I appreciate your support and friendship, and look forward to seeing where each of us ends up.

I would like to thank my parents, Mike and Rita Peterson, who have worked extremely hard to prioritize my education, and in doing so have motivated me to pursue learning and discovery. I appreciate your sacrifices and support.

Finally, thank you to my husband, Danny Driscoll. You've been by my side the last (almost) ten years and have supported my interests and goals from Virginia to Tennessee. I can't wait to see what our future holds.

This research was supported by the NIH: Training in Pharmacological Sciences, GM007628 & Immunobiology of Blood & Vascular Systems, HL069765.

TABLE OF CONTENTS

Page

LIST OF FIGURES

Page

LIST OF ABBREVIATIONS

2DG: 2[^{14}C]deoxyglucose

AdC5: Adenovirus containing C5

AdGFP: Adenovirus containing GFP

ANOVA: Analysis of variance

AT: Adipose tissue

AUC: Area under the curve

BAT: Brown adipose tissue

BMI: Body mass index

BWA: Burrows-Wheeler aligner

C3: Complement factor 3

C3a$_{desArg}$: "Inactive" form of C3 with terminal arginine removed

C5: Complement factor 5

C5a$_{desArg}$: "Inactive" form of C5 with terminal arginine removed

C5$_{cont}$: Congenic control for C5$_{def}$ Jackson Laboratory mouse

C5$_{def}$: Jackson Laboratory C5 deficient mouse (B10.D2-*Hc^{0} H2^{d} H2-T18^{c}*/oSnJ)

C5$_{het}$: Heterozygous mice bred from C5$_{cont}$ female and C5$_{def}$ male mice

C6: Complement factor 6

C7: Complement factor 7

C8: Complement factor 8

C9: Complement factor 9

C5b-9: Complement proteins that combine to form the membrane attack complex

CDC: Centers for Disease Control and Prevention

Cfb: Complement factor B

Cfd: Complement factor D

CLS: Crown-like structures

CVD: Cardiovascular disease

DHSR: Digital histology shared resource

EGFR: Epidermal growth factor receptor

ELISA: Enzyme-linked immunosorbent assay

EndoRa: Glucose production from the liver

ER: Endoplasmic riticulum

FOV: Field-of-view

FSC: Forward scatter for flow cytometric analyses

GC-MS: Gas chromatography-mass spectrometry

GTT: Glucose tolerance test

H & E: Hematoxylin & eosin stain

Hc: Gene name for C_5

HFD: High fat diet (60%, Research Labs)

IGV: Integrated Genomics Viewer

Igf1: Insulin-like growth factor

Igf1r: Insulin-like growth factor 1 receptor

Igfbp3: Insulin-like growth factor-binding protein 3

INSR: Insulin receptor

INSR-β: Active β subunit of the insulin receptor

IR: Insulin resistance

Irs1: Insulin signaling adaptor molecule 1

Irs2: Insulin signaling adaptor molecule 2

LDLR: Low density lipoprotein receptor

LFD: Low fat diet (10%, Research Labs)

M1-like macrophage: Polarized macrophage with pro-inflammatory properties

M2-like macrophage: Polarized macrophage with anti-inflammatory properties

MMPC: Mouse Metabolic Phenotyping Center

NAFLD: Non-alcoholic fatty liver disease

NMR: Nuclear magnetic resonance

OCT: Optimal cutting temperature solution

Pro-INSR: Proreceptor for insulin receptor

Rg: Glucose metabolic index, which is a measure of tissue-specific glucose uptake

SSC: Side scatter for flow cytometric analyses

SVF: Stromal vascular fraction

SAT: Subcutaneous adipose tissue

SEM: Standard error of the mean

T2D: Type 2 diabetes

Tfr1: transferrin receptor

TG: Triglycerides

UCP1: Uncoupling protein 1

US: United States

VANTAGE: Vanderbilt Technologies for Advanced Genomics

VAT: Visceral adipose tissue

VU: Vanderbilt University

WAT: White adipose tissue

CHAPTER 1

INTRODUCTION

Obesity and metabolic disease

The prevalence of adult and childhood obesity and associated co-morbidities has increased significantly in the United States (US) and other industrialized nations in the past several decades [1-3]. The Centers for Disease Control and Prevention (CDC) defines overweight and obesity relative to a person's height by using the Body Mass Index (BMI) as an indicator of body fat. The range for an overweight individual is a BMI of 25 to 30, and for obese is a BMI of 30 and higher. While physicians and scientists alike acknowledge that defining obesity is more complicated than BMI alone, this has proven to be a useful scale for predicting health outcomes. With these criteria the CDC reported that 39.8% of adults and 18.5% of children in the US were obese in 2015-2016 [6]. These data have been further analyzed in relation to geography, ethnicity, education, and socioeconomic status. As of 2017, the southeastern portion of the US shows the highest prevalence of obesity with seven states reporting over 35% of the adult population as obese (**Figure 1**). Hispanics and blacks reported the highest levels of obesity, and people with college degrees had less prominent obesity prevalence.

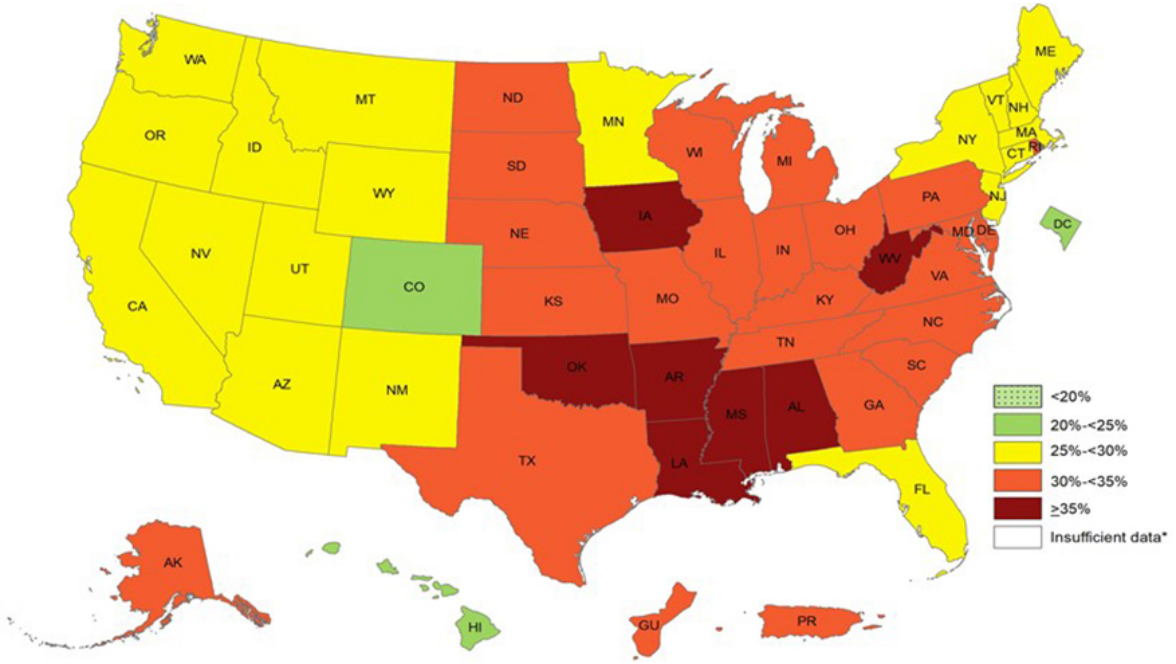

Figure 1. Obesity prevalence in the United States
The Center for Disease Control and Prevention reported obesity prevalence as of 2017. This map shows that all states had over 20% of their adult population considered to be obese, and seven states reporting over 35%. (www.cdc.gov)

Adipose tissue depots

Obesity can be caused by many things, but its physiological impacts partially stem from excessive lipid accumulation in fat cells, called adipocytes. Adipose tissue (AT) has long been known to cushion and protect internal organs and to store excess energy as triglycerides (TG). More recently, it has become appreciated that AT is in fact a dynamic endocrine organ involved in crosstalk with other metabolic tissues [9]. With TG overload, AT expands primarily via adipocyte hypertrophy, although hyperplasia can also contribute. There are many AT depots, and the site of expansion influences whether the increased adiposity contributes to increased risk for development of obesity-accelerated disease (**Figure 2**). Distinct AT depots have also been identified in mice (**Figure 3**).

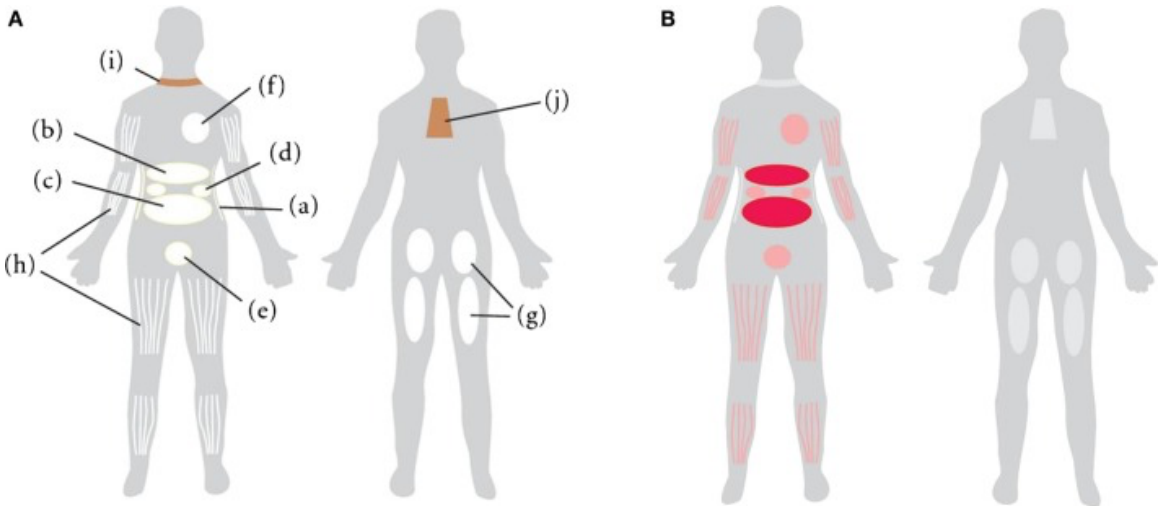

Figure 2. Human adipose tissue depots
From Chusyd *et al.*, Frontiers in Nutrition (2016) [12].
A) Adipose tissue (AT) depots including visceral (b: omental, c: mesenteric, d: retroperitoneal, e: gonadal, and f: pericardial), subcutaneous (a: abdominal, g: gluteofemoral, and h: intramuscular), and brown (i: supraclavicular and j: subscapular). B) Red color shows AT depots associated with increased obesity-associated disease risk.

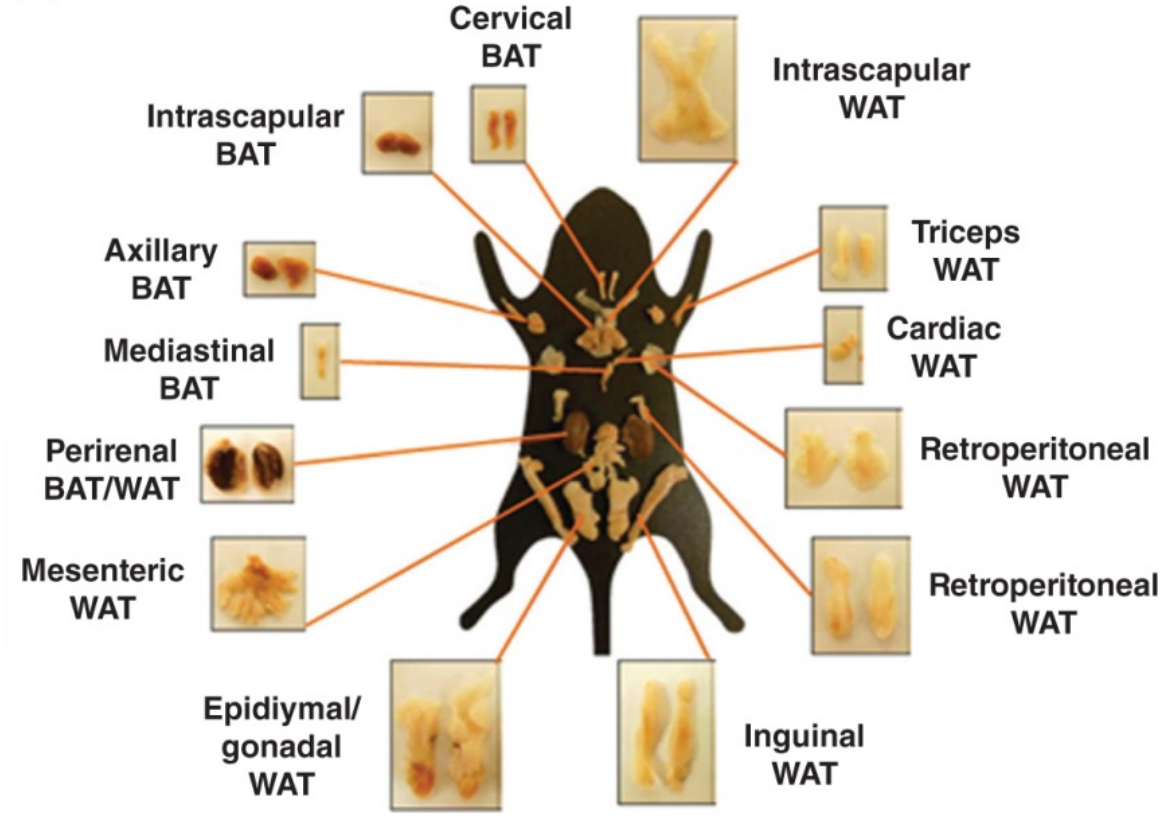

Figure 3. Murine adipose tissue depots
Adapted from Cozzo *et al.*, Comprehensive Physiology (2018) [14].
Distinct adipose tissue depots and their location in mice are indicated as labeled.

AT depots are also described based upon the tissue "color," on a spectrum from white to brown. White AT (WAT) is the most well-studied and is called such because of its role in TG storage, and consequent white appearance. WAT is characterized by adipocytes that contain a single unilocular lipid droplet (**Figure 4**). Visceral AT (VAT) is WAT that surrounds organs within the peritoneal cavity and can be further classified as gonadal, omental, mesenteric, pericardial, and retroperitoneal. Of all the WAT depots, unhealthy VAT is most strongly associated with obesity-associated metabolic disease, such as type 2 diabetes (T2D). Subcutaneous AT (SAT) is found under the skin outside the peritoneal cavity, is less metabolically active, and is thought to be more inert with regards to disease risk [16, 17].

Brown AT (BAT) contains adipocytes with several smaller lipid droplets and iron-rich mitochondria that give it its characteristic brown color (**Figure 4**). It is located near the clavicle and between the shoulder blades, and is most active early in life. Studies of BAT function in metabolism have come to the forefront because BAT is capable of producing energy through non-shivering thermogenesis [18], in contrast to WAT's role in storing energy. In fact, in humans it is estimated that 40-50 grams of maximally stimulated BAT could aid in maintaining body weight by accounting for 20% of daily energy expenditure [19]. BAT activity occurs through upregulation of uncoupling protein 1 (UCP1). While the most well-studied way to activate this pathway is through cold exposure and resultant sympathetic nerve signaling and norepinephrine [20, 21], similar effects have also been seen by adenosine [22] and BMP8B [23] in mice, and glucocorticoids in humans [24].

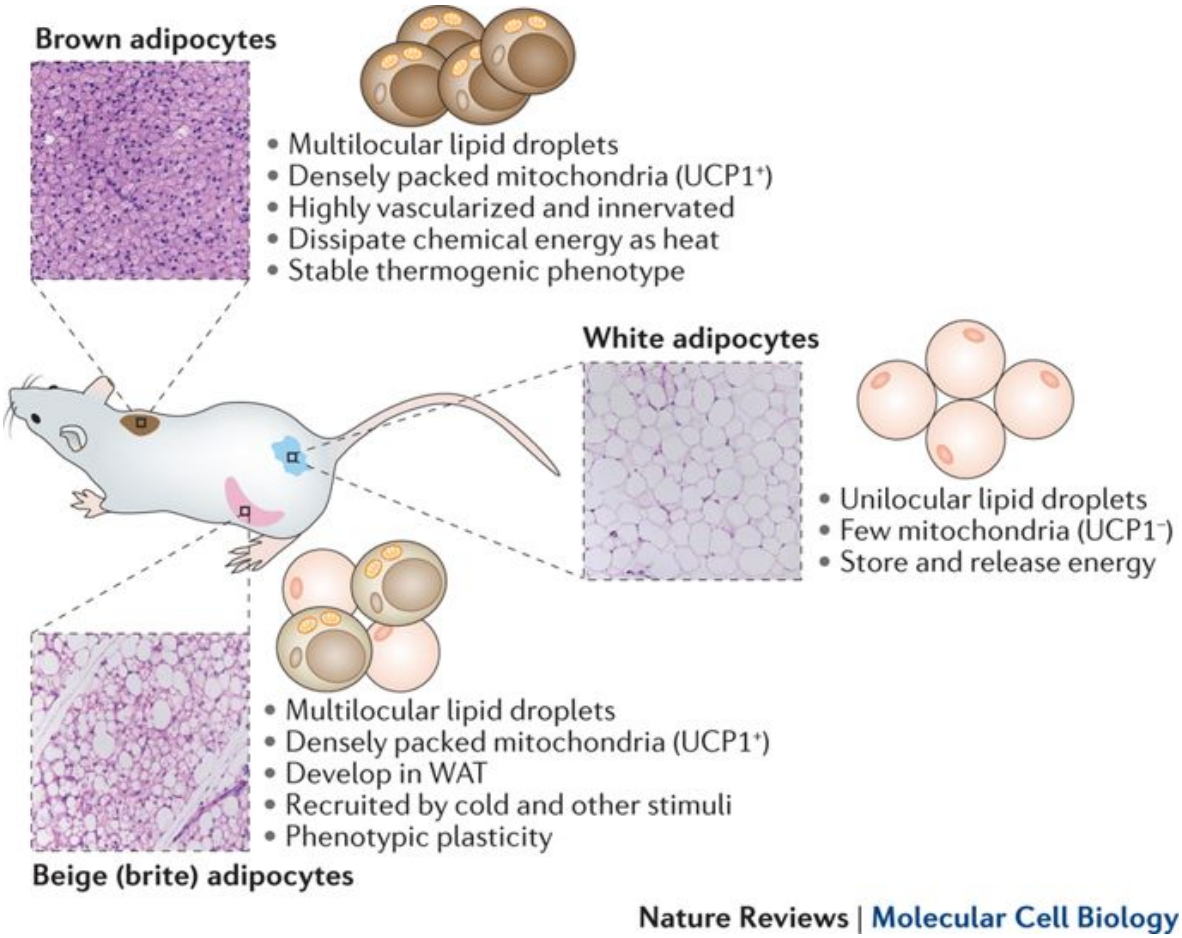

Figure 4. Schematic of white, beige, and brown adipocytes in mice
From Wang & Seale, Nature Reviews Molecular Cell Biology (2016) [25].
Characteristic summary of different types of murine adipocytes, their function, and their thermogenic potential. Differential lipid droplet size is also shown via histology.

A goal of investigators is to manipulate white adipocytes to resemble brown adipocytes in order to burn energy more efficiently, a process termed "beiging" [18, 26] (**Figure 4**). UCP1 activation in white adipocytes has been shown to be activated through expression of BMP4 [27], COX [28], FGF21 [29], and treatment with β3-adrenergic receptor [30] or PPARγ [31, 32] agonists. In mice, the inguinal/subcutaneous AT depot shows the most promising capability of beiging to increase energy expenditure [33], although it has also been reported that gene

expression patterns may differ between mice and humans [34]. Many other proteins have been implicated for their role in BAT activation and/or beiging potential [26], and this is area of continued research in the metabolism field [35].

Obesity-associated disease

Obesity has been shown to contribute to pathologies associated with many diseases including asthma [36], arthritis [37, 38], cardiovascular disease (CVD) [39], chronic obstructive lung disease [40], inflammatory bowel disease [41], kidney disease [42], neurodegeneration [43-45], non-alcoholic fatty liver disease (NAFLD) [46], T2D [47, 48], and some types of cancer [49-52]. It is associated with a state of chronic low-grade inflammation accompanied by elevated circulating levels of pro-inflammatory cytokines that lead to insulin resistance (IR) in AT, muscle, and liver [53-56]. Whether the inflammatory nature of AT in obesity contributes to systemic inflammation and the development of the chronic diseases listed above is an area of ongoing investigation by laboratories around the world.

Insulin action and resistance

Upon exposure to glucose, the body seeks to normalize blood sugar levels by stimulating glucose uptake via insulin signaling. In healthy individuals, when glucose enters the bloodstream, the pancreas responds by secreting insulin. Insulin binds to its receptor, INSR, on cells in metabolic tissues including AT, brain, liver, muscle, and pancreas. INSR is a transmembrane tyrosine kinase receptor that is activated upon ligand binding, leading to autophosphorylation of the receptor. Activation leads to recruitment of adaptor proteins, and these facilitate signaling (**Figure 5**) [57, 58]. Consequent downstream actions result in phosphorylation and activation of Akt, which can lead to diverse endpoints. Akt can activate Foxo family proteins to induce gluconeogenesis, lipid synthesis, and transcription involved in hepatic glucose control. It also induces activation of the mTORC1 complex to activate other targets involved in genetic regulation of protein synthesis, and inactivates GSK3 to regulate hepatic glycogen stores. It can mediate cell growth and survival by controlling members of the p53 and NFκB pathways. Insulin-stimulated signaling is also regulated in a tissue-dependent manner. The main downstream effect of insulin signaling in AT is inhibition of lipolysis, in skeletal muscle is glucose uptake via GLUT4, and in liver is regulation of hepatic glucose output. During IR, tissues do not effectively sense insulin, leading to impaired insulin signaling and reduction of insulin's positive metabolic effects.

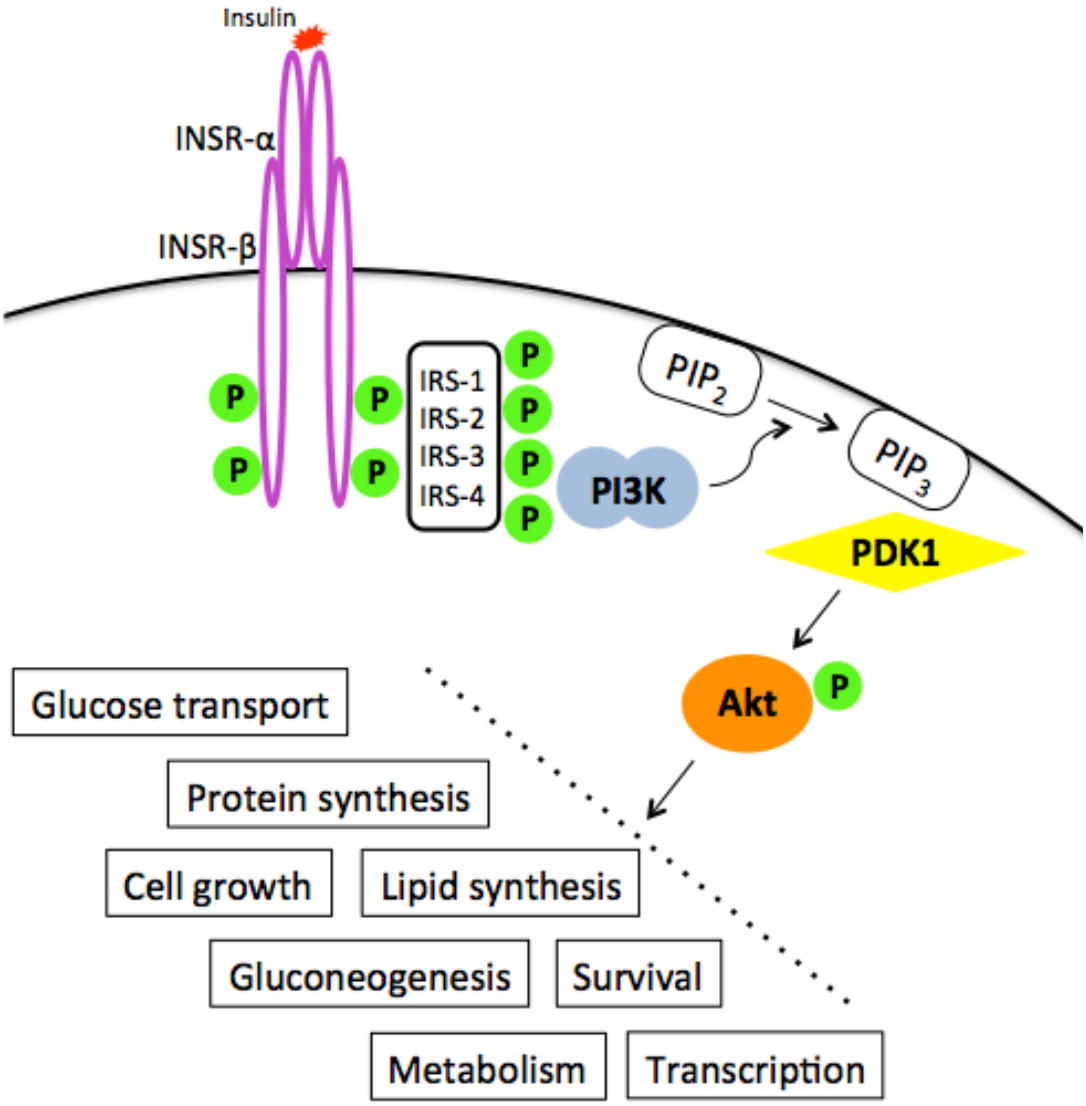

Figure 5. Insulin signaling through insulin receptor

Adipose tissue immunometabolism

There are several mechanisms by which impaired insulin action can occur, but the focus of the Hasty Lab is to determine the role of obesity-associated inflammation. Thus far, this introduction has focused on AT depots and different types of adipocytes. AT also contains many other cell types, and these populations change with the onset and progression of obesity. AT was one of the first organs in which macrophage contribution to metabolic disease was discovered, and is arguably the best studied. Less than 20 years ago it was found that the number of macrophages increases in obese compared to lean AT and that this imparts an overall inflammatory milieu [59, 60]. Macrophage recruitment requires the assistance of inflammatory cytokines, which are secreted by adipocytes, macrophages themselves, and various other immune cells. These cytokines can also interfere with insulin signaling, resulting in IR of AT. For example, IFN-γ treatment of human adipocytes leads to down-regulation of INSR and decreased activation of the downstream effector, AKT [61]. Similarly, 3T3-L1 adipocytes treated with IL-6 exhibited decreased expression in insulin signaling pathway proteins [14, 62], and with TNF-α even showed blunted autophosphorylation of the INSR [63]. These effects ultimately result in the down-regulation of GLUT4 and decreased glucose uptake. Ultimately, cytokine-induced IR can lead to unchecked basal lipolysis and ectopic lipid storage in other metabolic tissues such as muscle and liver.

Immunophenotype of white adipose tissue

Aside from macrophages, many other immune cells secrete cytokines and are involved in inflammatory responses. Since the seminal AT macrophage publications by Weisberg and Xu in 2003 [59, 60], these cell types have been evaluated for their involvement in AT homeostasis [64, 65]. A simplified schematic of the immunometabolic landscape of WAT is described in **Figure 6**. Specifically, eosinophils [66], M2-like anti-inflammatory and iron-containing MFe^{hi} macrophages [67], regulatory B cells [68, 69], and natural killer [70] and regulatory T cells [71, 72] are resident in lean WAT. In contrast, B cells [73, 74], dendritic cells [75], pro-inflammatory M1-like macrophages [76], mast cells [77], neutrophils [78], and CD4+ and CD8+ T cells [79, 80] infiltrate WAT with obese conditions.

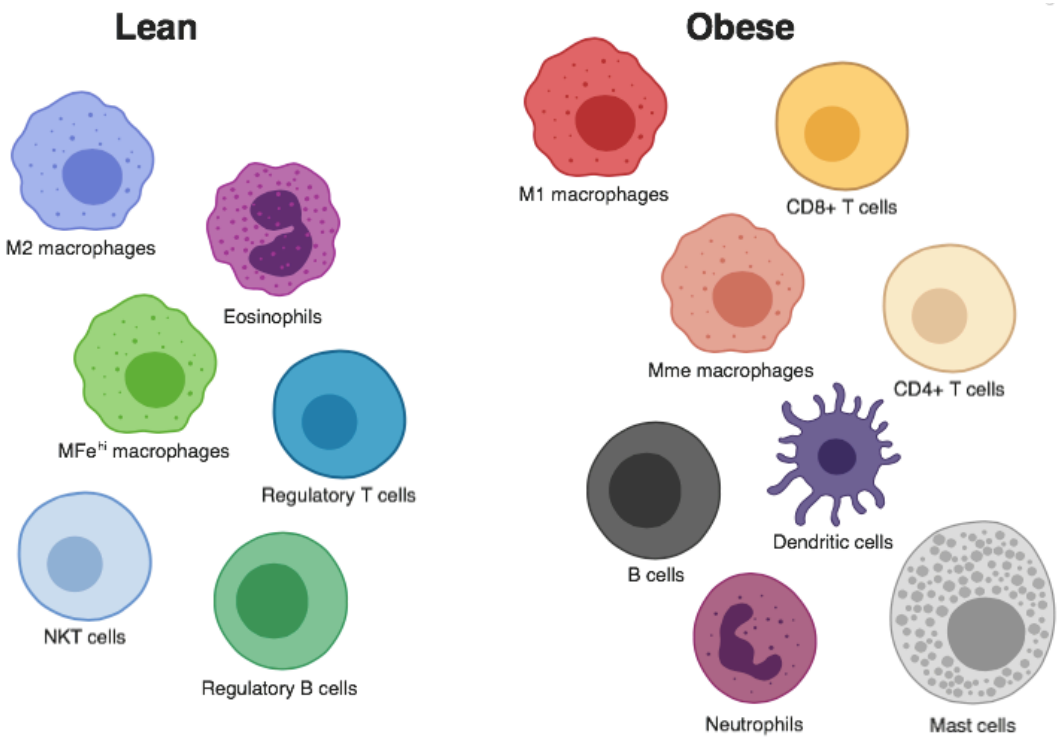

Figure 6. Immune cells of white adipose tissue
The microenvironment of adipose tissue changes with the onset and progression of obesity.

Immunophenotype of brown adipose tissue

The immune cell repertoire of BAT is much less studied than WAT. There is evidence of the presence of various immune cell types in BAT, such as eosinophils [66], macrophages and monocytes [81], and regulatory T cells [82], but many of these studies were carried out as supporting data to studies on WAT. This gap in the field led to the studies presented in Chapter 2 of this Dissertation, and the most recent discoveries regarding the immunophenotype of BAT are highlighted in the final discussion in Chapter 4 of this Dissertation.

Complement in adipose tissue inflammation

Cytokines play a central role in obesity-induced inflammation, but another major contributor is the complement system. The complement system is a vital component of both innate and adaptive immune responses and is conserved across a wide range of species [83]. Three different complement activation pathways have been described: classical, alternative, and lectin-binding [84]. In addition to AT, other sites of complement factor secretion include the liver and gastrointestinal tract. Complement proteins remain inert in the circulation until activated, at which time an amplified cascade of proteolytic steps results in cleavage of complement factor 3 (C3) into C3a and C3b, as well as complement factor 5 (C5) into C5a and C5b (**Figure 7**). C3a and C5a are further modified into their desarginated forms, $C3a_{desArg}$ and $C5a_{desArg}$, respectively. C5a is the most potent anaphylatoxin of the complement cascade, and has many functions in the immune system: it is a strong chemoattractant for all cells of the myeloid lineage and some cells of the lymphoid lineage [85], it has been shown to modulate cytokine expression in various cell

types [86], and it up-regulates adhesion molecules in neutrophils, monocytes and epithelial cells [87]. C5b binds to the membrane of target cells, serving as an anchor for the sequential binding of C6, C7, C8, and C9. This leads to the formation of the membrane attack complex (C5b-9) and subsequent cell lysis. Each of these functions can further exacerbate obesity-associated inflammation in AT, and Chapter 3 will delve into further detail about these topics.

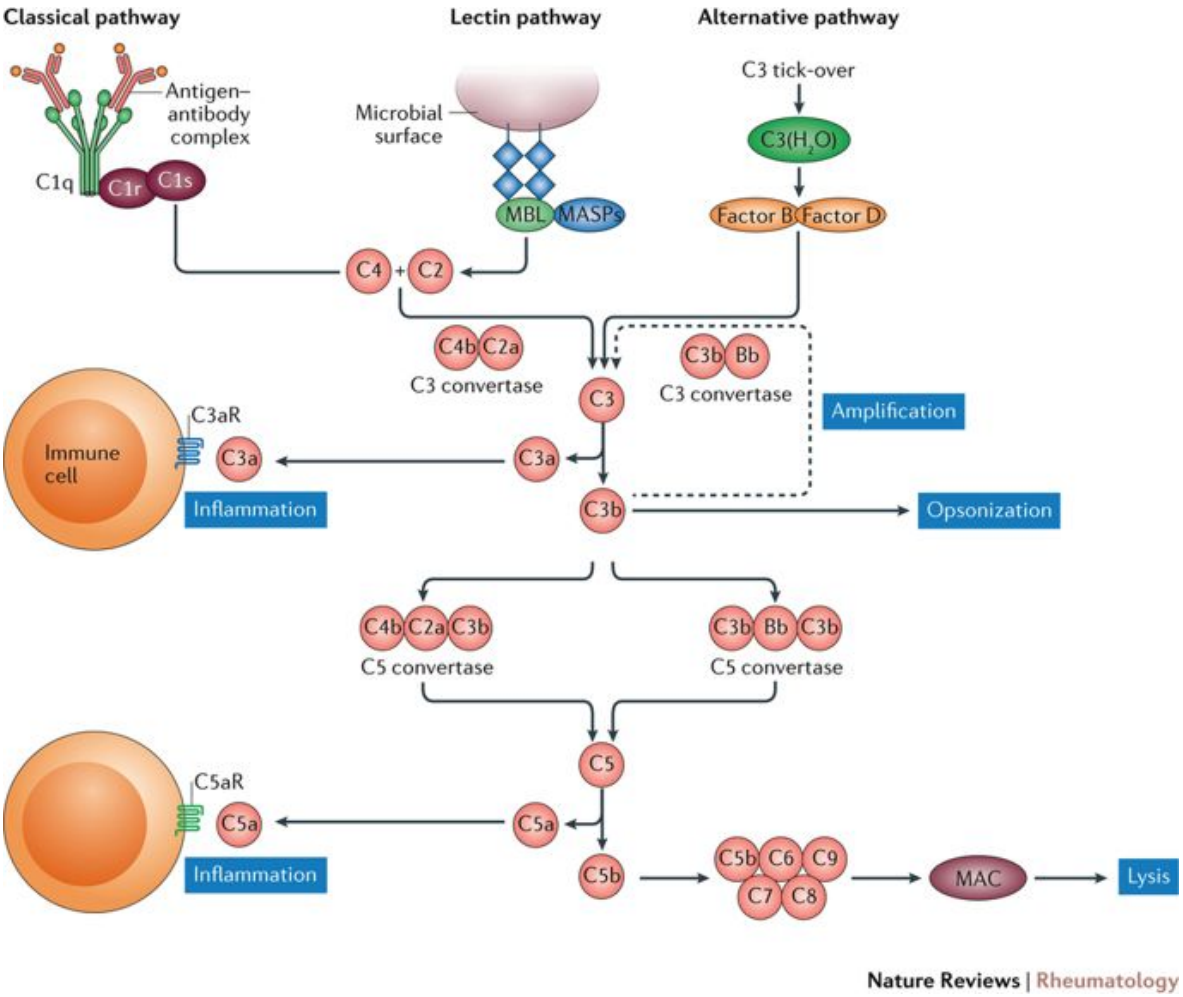

Figure 7. Complement signaling pathway
From Trouw *et al.*, Nature Reviews Rheumatology (2017) [88].

Conclusion

Obesity and associated diseases have become public health problems of epidemic proportions. The associated AT inflammation has become a major focus of the Immunometabolism field, but there are still many questions to be answered and discoveries to be made. The remainder of this Dissertation details my contributions to the field by evaluating the immunophenotype of BAT (Chapter 2) and how complement factor 5 is involved in systemic metabolism (Chapter 3). It will conclude with a discussion (Chapter 4) of how these findings contribute to the field and where the future questions may lead. An additional appendix is included, which is a review article describing the potential of macrophage-targeted therapeutics in the treatment of metabolic disease (**Appendix**).

CHAPTER 2

THE IMMUNOPHENOTYPE OF BROWN ADIPOSE TISSUE

This chapter was adapted from a published article titled,
Obesity alters B cell and macrophage populations in brown adipose tissue
written by Peterson, Flaherty, and Hasty [89].

Introduction

Properly functioning WAT is vital for systemic metabolic homeostasis. While WAT is appreciated for its role in organ protection and energy storage, BAT's evolutionary purpose is to aid in temperature regulation of animals through UCP1-driven thermogenesis. As BAT has become better understood, there has been more of a focus on the potential for beiging of WAT to burn energy and combat obesity. While this strategy shows obvious health benefits, there is not enough known about the physiology of BAT and how the tissue environment is involved in thermogenesis.

It is well-established that inflammation and associated immune cells have an important role in WAT homeostasis and progression to obesity-induced disease (**Figure 6**) [64, 65]. Accordingly, it is important to understand the role of immune cells in BAT in both obesity and aging to determine how they will be affected with a therapeutic goal of WAT beiging. Immune signaling in BAT has not been systematically studied, and the knowledge about the immune cell repertoire of BAT is limited. Because of this lack of systematic understanding, we used an "immunophenotyping" approach to determine which cell types are present. This information will be vital for further comparing the function of BAT in normal and diseased states.

Methods

Mouse studies

Animal procedures were performed following IACUC approval. Male and female C57BL/6J mice were purchased from The Jackson Laboratory (Bar Harbor, ME) and aged or fed special diets in the Vanderbilt facility. Mice were maintained on chow diet for the aging studies (1, 6-7, or 10-15 months) and on 10% low fat diet (LFD) or 60% high fat diet (HFD) (Research Diets, Inc. New Brunswick, NJ) for 3, 8, or 16 weeks for the obesity studies. Mice were fed *ad libitum*. Upon termination of the study, BAT was harvested by cutting away connecting tissue that looked more like WAT.

Flow cytometry

Stromal vascular fraction (SVF) of the total BAT from one animal per sample was collected following collagenase digestion and centrifugal separation as previously described [90]. Briefly, BAT was digested for 4 h with 2 mg/mL collagenase type 4 (Worthington, Lot #45H15909). The tissue was pressed through a 100 μm filter. The isolated SVF was incubated with Fc block for 5 min on ice, washed, and incubated with fluorophore-conjugated antibodies for 20 min at 4 ℃. The following antibodies were used: B220-FITC, CD3-APC/Cy7, CD45-PE/Cy7, F4/80-APC, and SiglecF-PE (BD Biosciences, Franklin Lakes. NJ). DAPI was used for viability staining. Flow cytometry was carried out on the entire volume from each sample at the Vanderbilt Flow Cytometry Shared Resource using a BD Special Order Research Product (SORP) LSR Fortessa. Please see **Figure 8** for the gating scheme.

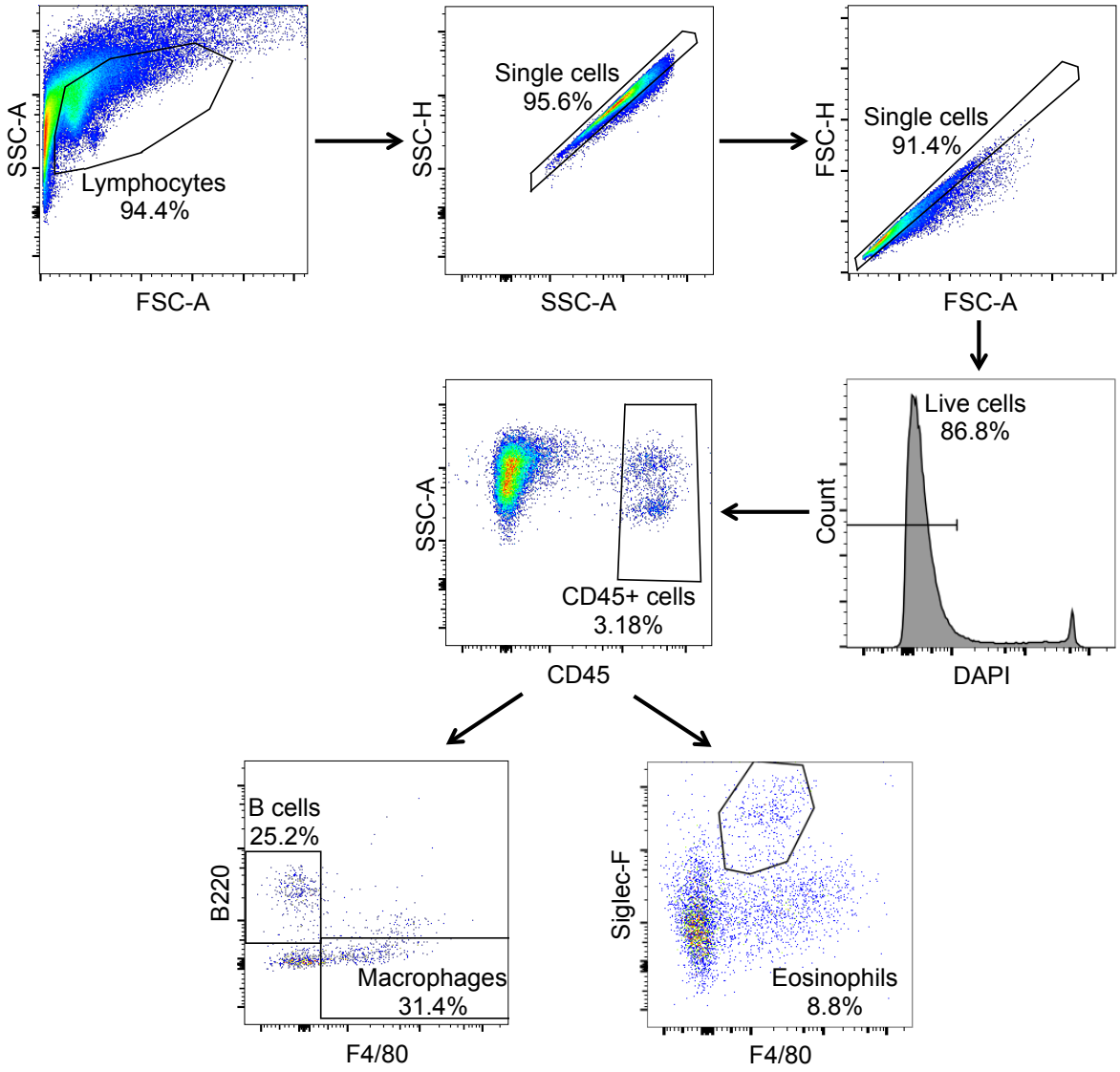

Figure 8. Flow cytometry gating scheme.
Leukocytes were identified initially by their forward scatter (FSC) and side scatter (SSC) properties. Subsequent FSC and SSC pulse geometry gates were used to eliminate aggregating cells. Viable leukocytes were identified as DAPI-, CD45+ cells. From CD45+ cells, the analysis of B cells (B220+, F4/80-) and macrophages (B220-, F4/80+) was achieved by using a dot plot. Eosinophils were gated from CD45+ leukocytes as F4/80+ and SiglecF+.

Histology & imaging

BAT tissue was fixed in 10% formalin overnight, paraffin embedded, sectioned, and stained by the Vanderbilt Translational Pathology Shared Resource for hematoxylin and eosin, CD11b (macrophages), and B220 (B cells). Images were captured and analyzed through the Vanderbilt Digital Shared Resource and Leica Digital Image Hub software.

Statistical analysis

All statistics were performed using GraphPad Prism software. BAT mass changes and all LFD:HFD cell population comparisons were analyzed by unpaired Student's *t*-test. Aging-associated differences and body weight curves were analyzed by one-way and two-way ANOVA, respectively.

Results

Metabolic parameters of mice on diet

Male and female wild type C57BL/6J mice gained weight on HFD (**Figure 9A-B**). In addition to WAT expansion, BAT mass was also increased and was significantly greater in mice fed HFD for 8 and 16 weeks (**Figure 9C-D**).

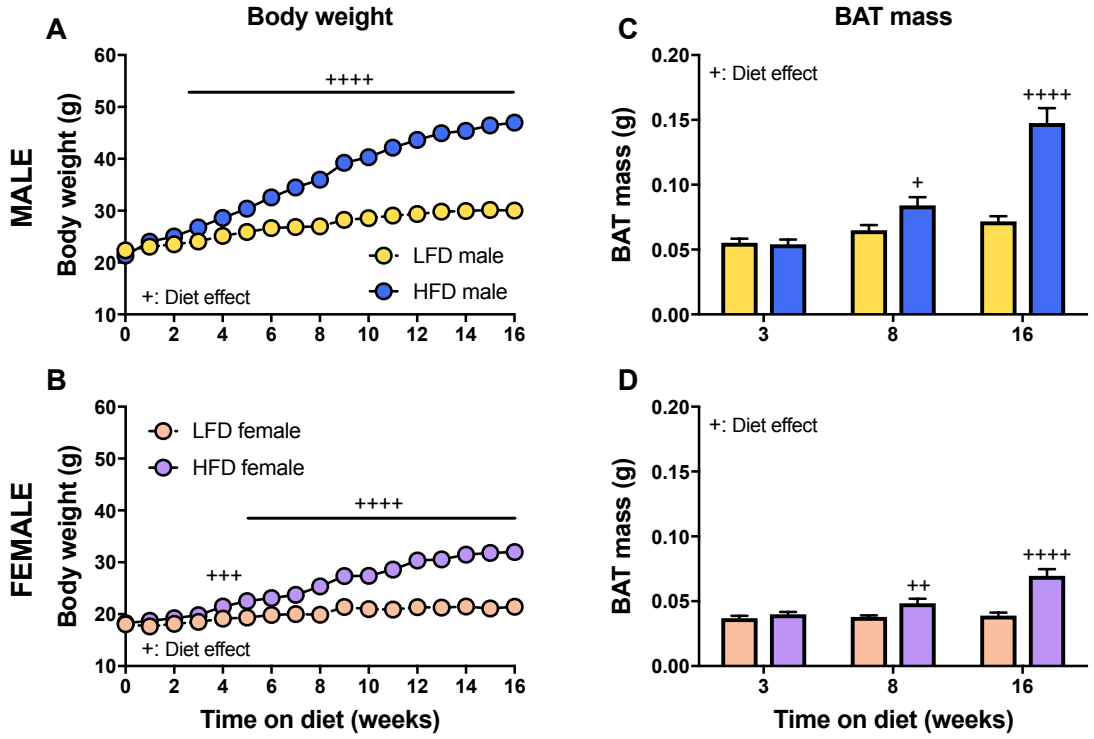

Figure 9. Metabolic parameters of mice on diet.
Wild type C57BL/6J mice were placed on 10% low fat diet (LFD) or 60% high fat (HFD) for 3, 8, or 16 weeks. Body weight was measured weekly (A: male, B: female), and brown adipose tissue was collected and weighed (C: male, D: female). Data are presented as mean ± SEM of 4-5 samples per group.
+ $p<0.05$; ++ $p<0.01$; +++ $p< 0.001$; ++++ $p< 0.0001$

Flow cytometry of brown adipose tissue stromal vascular fraction

BAT SVF was analyzed for the presence of B cells, macrophages, and eosinophils using flow cytometry (see **Figure 8** for gating scheme). CD45+ leukocytes represent less than 5% of all live cells. In general, there is a higher frequency of B220+ B cells (**Figure 10A-B**) and a lower frequency of F4/80+ macrophages (**Figure 10C-D**) in HFD- compared to LFD-fed mice.

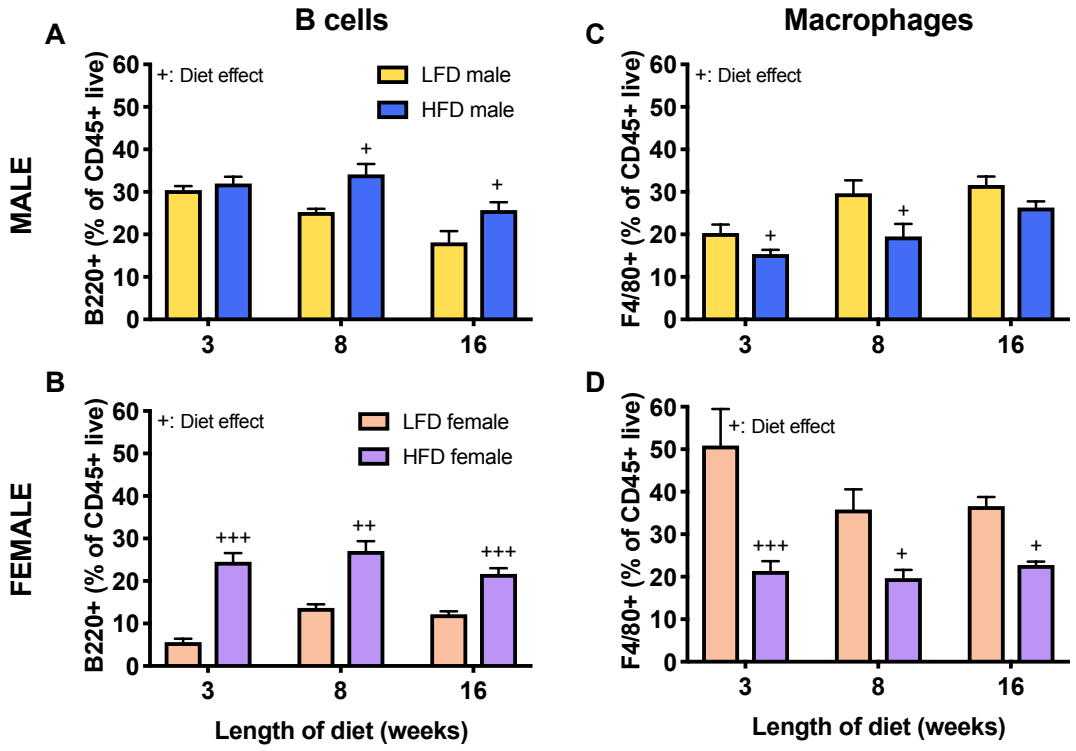

Figure 10. Flow cytometry of brown adipose tissue (BAT) stromal vascular fraction (SVF).
BAT was collected from wild type C57BL/6J mice after 3, 8, or 16 weeks of 10% low fat diet (LFD, white bars) or 60% high fat (HFD, black bars). SVF was processed and analyzed by flow cytometry for B220+ B cells (A: male, B: female) and F4/80+ macrophages (C: male, D: female) as a percent of CD45+ live cells. Data are presented as mean ± SEM of 4-5 samples per group.
+ $p<0.05$; ++ $p<0.01$; +++ $p< 0.001$

Concomitantly, there is a lower frequency of SiglecF+ eosinophils in animals with diet-induced obesity (**Figure 11**). The data show that 13.5% ± 2.1 of live leukocytes are SiglecF+ in male mice fed HFD, while 6.9% ± 1.5 ($p<0.05$) are SiglecF+ in mice fed LFD for 8 weeks.

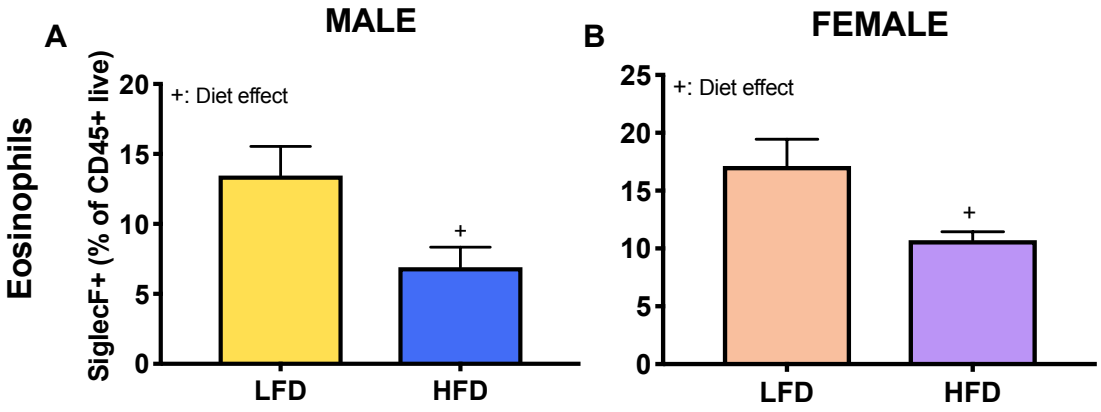

Figure 11. Flow cytometry of brown adipose tissue (BAT) stromal vascular fraction (SVF).
BAT was collected from wild type C57BL/6J mice after 8 weeks of 10% low fat diet (LFD, white bars) or 60% high fat (HFD, black bars). SVF was processed and analyzed by flow cytometry for SiglecF+ eosinophils (A: male, B: female) as a percent of CD45+ live cells. Data are presented as mean ± SEM of 5 samples per group.
+ $p<0.05$

The very low prevalence of B220+ B cells and CD11b+ macrophages was confirmed by immunohistochemical staining of BAT from male wild type animals fed LFD or HFD for 8 weeks (**Figure 12**).

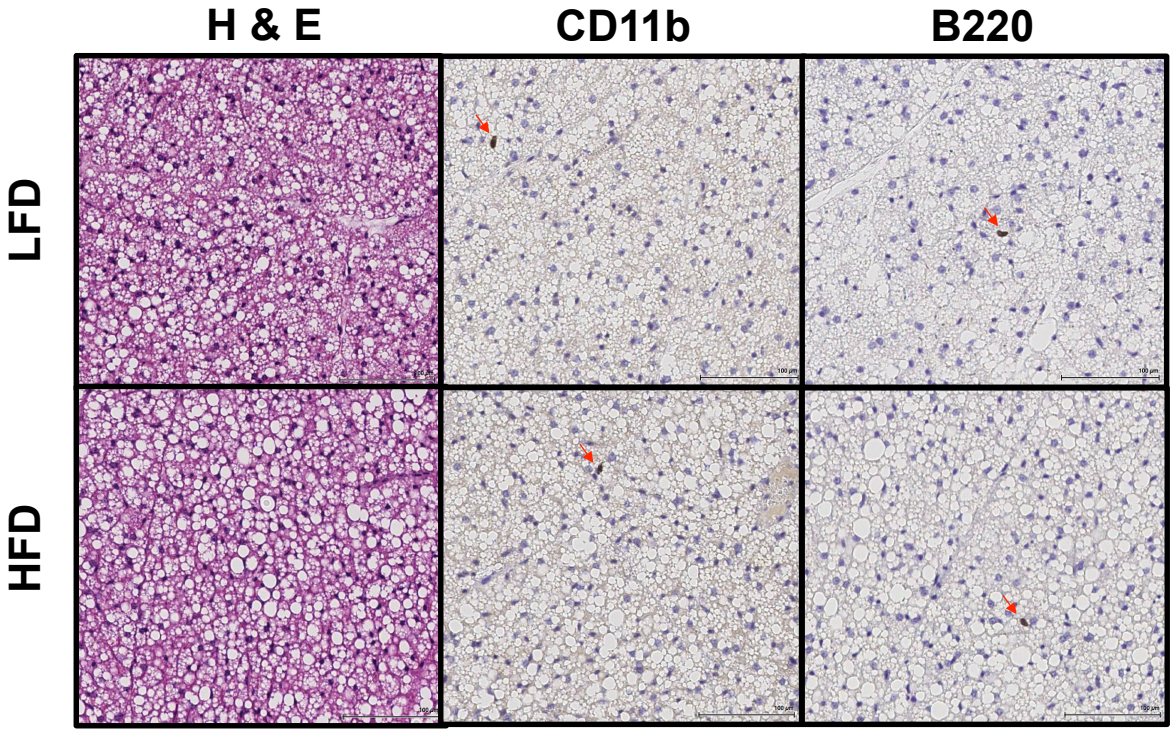

Figure 12. Brown adipose tissue (BAT) immunohistochemistry.
BAT was collected from wild type C57BL/6J mice fed 10% low-fat (LFD) or 60% high-fat (HFD) diet for 8 weeks, and fixed in 10% formalin before further processing and staining for hematoxylin & eosin (H & E), CD11b+ (macrophages), or B220+ (B cells). Red arrows indicate positively stained cells. Data presented are representative images from 3 samples per group.

Analysis of brown adipose tissue immune cells with aging

Additionally, the effect of aging on BAT immune cell repertoire was investigated. Body weights increased with age, and mice that were 6-7 month and 10-15 months old were significantly heavier than mice that were only 1 month old ($p<0.0001$; **Figure 13A-B**). BAT mass increased with age in the male, but not the female, mice in a similar pattern as the body weight ($p<0.01$; **Figure 13C-D**).

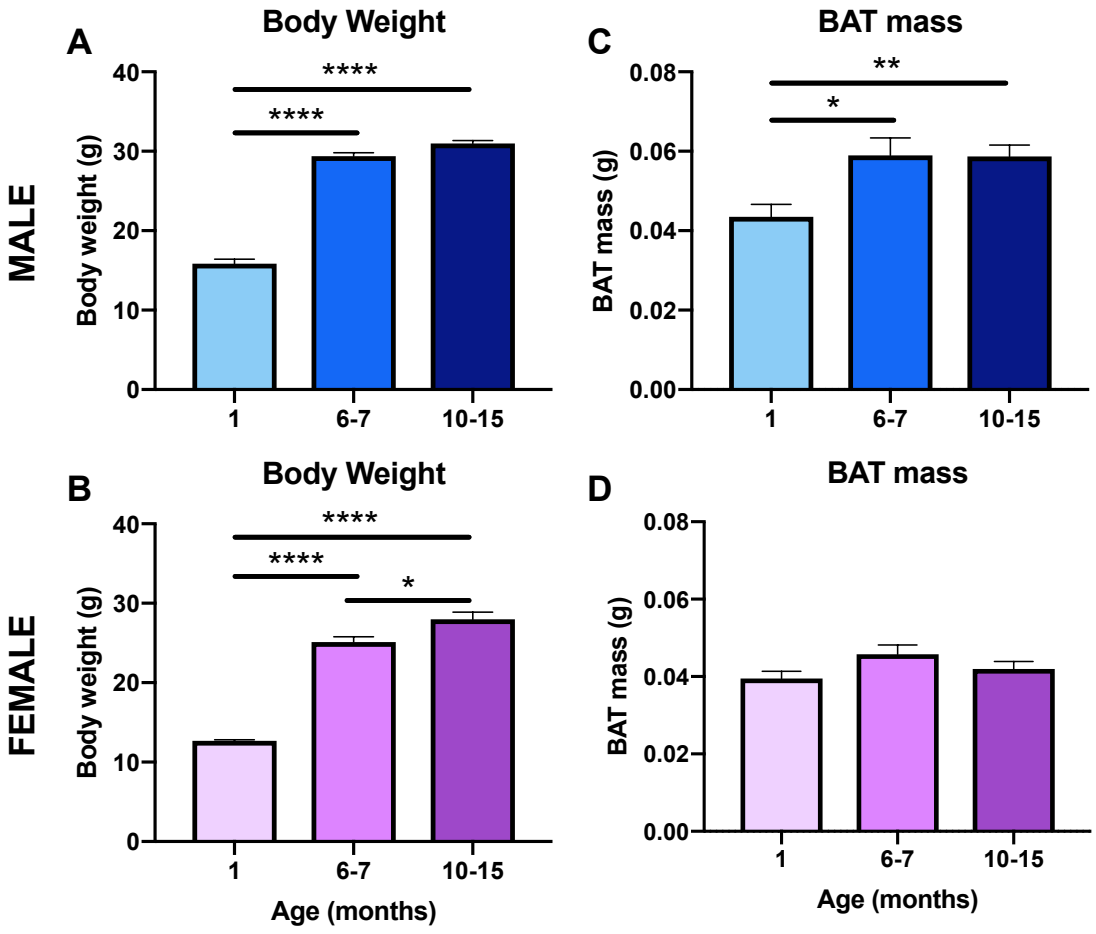

Figure 13. Analysis of brown adipose tissue (BAT) with aging.
Male and female wild type C57BL/6J mice were aged to 1, 6-7, or 10-15 months. Their final body weight was measured (A: male, B: female), and BAT was collected and weighed (C: male, D: female). Data are presented as mean ± SEM of 4-18 samples per group.
* $p<0.05$; ** $p<0.01$; **** $p<0.0001$

The SVF was analyzed by flow cytometry and there were no observed changes in B cell or macrophage repertoires in response to aging (**Figure 14A-B**).

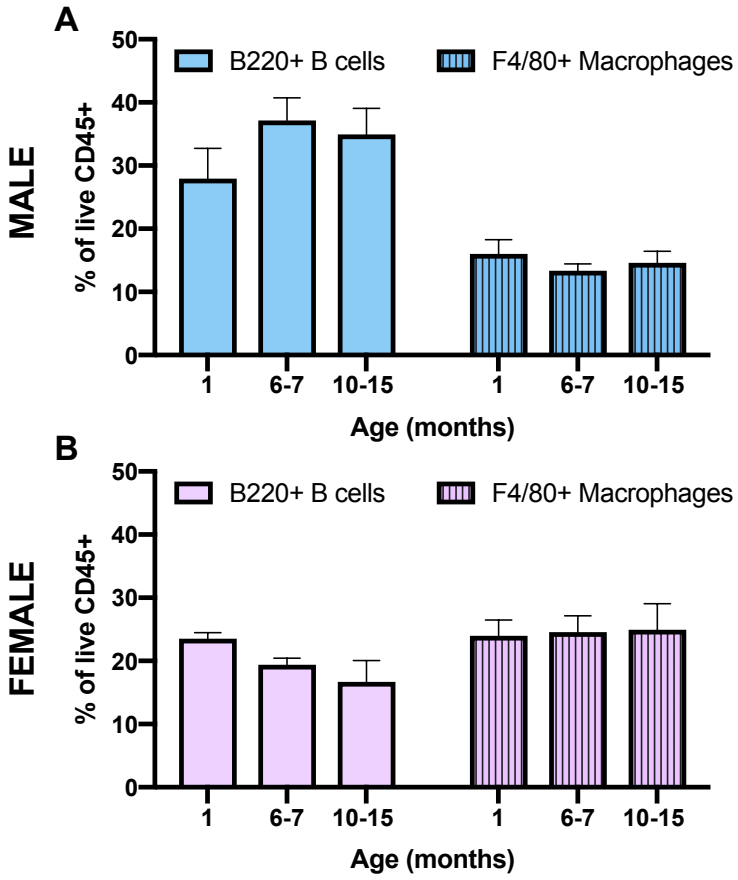

Figure 14. Analysis of brown adipose tissue (BAT) immune cells with aging.
Male and female wild type C57BL/6J mice were aged to 1, 6-7, or 10-15 months. BAT stromal vascular fraction was processed and analyzed by flow cytometry for B220+ B cells (non-patterned bars) and F4/80+ macrophages (striped bars) as a % of CD45+ live cells (A: male, B: female). Data are presented as mean ± SEM of 4-18 samples per group.

Discussion

Our data show that macrophages, eosinophils, and B cells are present in BAT, cumulatively making up about 75% of the CD45+ immune cell population. While previous reports have shown that eosinophils [66] and macrophages [81] are present in BAT, to our knowledge, this is the first report of the presence of B cells. We show a higher frequency of B cells in obese compared to lean mice, while macrophages and eosinophils show the opposite trend. These trends are present in both sexes, but the males do not appear to have as strong of a diet-driven effect.

Previous studies have assessed macrophages in BAT by flow cytometry with markers such as Cx3Cr1, F4/80, CD14, CD64, MerTK, and MHCII [91]. During the preparation of our manuscript, Wolf *et al.* beautifully showed that during development, most BAT macrophages are CX_3CR1^+MCHII-, but that they progressively form 4 distinct populations based upon CX_3CR1 and MCHII expression [91]. While our data showed a reduction in the percent of macrophages in BAT in obese mice, we did not see changes during aging. The understanding of aging WAT is that it becomes more inflammatory, with a similar phenotype to obese AT [92]. With these studies however, we cannot rule out phenotypic changes associated with aging, as we did not assess gene expression patterns of CX_3CR1, MHCII levels, or polarization markers.

The underlying tone of some work on BAT macrophages has been that they exist in relatively high numbers in the BAT and that they play an important role in BAT physiology. However, in our studies, we show that macrophages make up only 30% of the BAT immune cell population, which is already less than 5% of all live cells. Published studies showing histology for macrophages in BAT also show low

numbers. Buettner and colleagues reported that Mac-2-positive macrophages exist in only small numbers in BAT [93] and Czeck and colleagues did not observe any F4/80+ macrophages in BAT [94]. It has also been reported that the inflammatory nature of macrophages in diet-induced obesity is lower in BAT compared to WAT, and we in fact detected a reduction in BAT macrophage percentage in obese mice. Furthermore, Dowal *et al.* have shown that co-culture of macrophages with brown adipocytes has little impact on their inflammatory nature [95]. The function of BAT macrophages in homeostasis or in pathogenesis is not yet clear. A role for BAT macrophages in catecholamine synthesis and adaptive thermogenesis was suggested by one group [96] but was recently disputed [93]. Certainly, macrophages are important cells for tissue homeostasis; however, given their very low numbers, the lack of changes in gene expression of macrophages co-cultured with brown adipocytes, the absence of change with obesity or aging, and the recent publication showing no effect of M2 macrophages on catecholamine synthesis or adaptive thermogenesis [93], the physiological function of BAT macrophages is unclear.

Interestingly, we found that 20-30% of leukocytes in BAT are B cells. While B cells have traditionally been studied for their role in antigen processing and antibody secretion, their immunoregulatory role has surfaced in the context of inflammatory disease. B cell phenotypic plasticity is influenced by both norepinephrine [97] and adenosine [98], which are also known to activate thermogenesis in BAT. Additionally, norepinephrine is released in response to antigen presentation, and is necessary for normal expression of IgG [99]. Further studies are needed to characterize BAT B cells and their role in this tissue.

Due to the paucity of immune cells in BAT, we limited our analyses to macrophages, eosinophils and B cells. However, future studies could provide a more detailed analysis of their phenotype, as well as reveal other immune populations. Despite these limitations, our work adds to the field's quantification of immune populations in BAT, especially with the addition of B cells.

CHAPTER 3

THE ROLE OF COMPLEMENT FACTOR 5 IN METABOLISM

This chapter was adapted from an article under review titled,
Impaired insulin signaling in the B10.D2-HC^{o} H2D^{d} H2-T18^{c}/oSnJ
mouse model of complement factor 5 (C5) deficiency
written by Peterson, Gutierrez, Kikuchi, Anderson-Baucum,
Winn, Shuey, Bolus, McGuinness, and Hasty.

Introduction

While much work has focused on the role of specific cytokines and chemokines in obesity-associated inflammation, very little is known regarding the contribution of primitive components of immunity, such as the complement system, to systemic metabolic regulation. The complement system is an evolutionarily conserved arm of the innate immune system that when activated can promote inflammation and cell lysis. Various cells, including hepatocytes, epithelial cells of the gastrointestinal tract, adipocytes, and immune cells secrete complement proteins, which remain inert in circulation until activated (**Figure 7**). Studies suggest that, in addition to their key function in immunity (described in Chapter 1), products of the complement system also play a vital role in metabolism. Complement proteins are associated with the onset and progression of obesity-associated inflammation in AT, attributed in part to their chemoattractive properties [100]. Alternatively, studies have also demonstrated complement proteins to be important in metabolism, partially due to their ability to promote glucose uptake by various cell types, including adipocytes [101-108]. These contrasting properties, as well as our data showing increased *Hc* (i.e. C5 gene

name) expression in diet-induced obese mice (**Figure 15**), led to the experiments shown here investigating how C5 deficiency influences systemic metabolism.

The mouse strain most commonly used to study the effects of isolated C5 deficiency is the Jackson B10.D2-*Hc^{o} H2^{d} H2-T18^{c}*/oSnJ, henceforth referred to as $C5_{def}$. There are several other mouse strains known to be C5 deficient. They are historically used in other areas of physiology and disease, such as alcohol tolerance (DBA/2J) [109], arthritis (DBA/1J) [110], atherosclerosis susceptibility (AKR/J, A/J, CBA/J, DBA/2J) [111-113], cancer susceptibility (AKR/J, A/J) [114, 115], diabetes and obesity (AKR/J, NOD/ShiLtJ) [116, 117], eye defects (CBA/J, DBA/2J, FVB/NJ) [118-120], and hearing defects (AKR/J, A/J, CBA/J, DBA/1J, DBA/2J, NOD/ShiLtJ) [121-123]. Many of these models are known to have genetic variability at other loci in addition to C5, but the B10.D2-*Hc^{o} H2^{d} H2-T18^{c}*/oSnJ $C5_{def}$ strain used in the current study is reported as the model with the least confounding variables. The metabolic phenotype of C5 deficient AKR/J and NOD/ShiLtJ mice has been previously evaluated; however, that of B10.D2-*Hc^{o} H2^{d} H2-T18^{c}*/oSnJ $C5_{def}$ mice has not. The NOD/ShiLtJ mouse is well known as a model for type 1 diabetes. While it is C5 deficient, it also has other well-characterized defects in other immune pathways such as general cytokine production and adaptive immune responses (www.jax.org/strain/001976). The AKR/J mouse is commonly used in cancer biology because of its susceptibility to leukemia. In addition to being C5 deficient, it is also reported to have genetic variation in at least ten other genes (www.jax.org/strain/000648). For these reasons, we chose to focus our studies on the $C5_{def}$ B10.D2-*Hc^{o} H2^{d} H2-T18^{c}*/oSnJ strain.

In the current study, we evaluated the effects of primary deficiency of circulating C5 on insulin sensitivity in mice. We showed that $C5_{def}$ mice exhibited severe glucose intolerance and systemic IR in both lean and obese states that was inflammation-independent. IR in the $C5_{def}$ mouse strain was associated with a genetic mutation in the *Insr* gene and improper processing of the pro-insulin receptor in multiple metabolically-active tissues, as has been reported in other models of INSR haplodeficiency [124]. Interestingly, adenoviral overexpression of C5 improved insulin sensitivity in both $C5_{cont}$ and $C5_{def}$ mice, lending support for a beneficial role of C5 in metabolism.

Methods

Mice and diets

All animal procedures were performed after approval from the Institutional Animal Care and Use Committee of Vanderbilt University (VU). All mice were purchased from The Jackson Laboratory (Jx, Bar Harbor, Maine). The congenic C5 deficient ($C5_{def}$) mice were originally generated at Jx by crossing the naturally $C5_{def}$ DBA/2J mice onto the C57BL/10SnJ background for more than 10 generations and selecting for the $Hc^{o}H2^{d}$ and $H2\text{-}T18^{c}$ loci; thus generating the B10.D2-Hc^{o} $H2^{d}$ $H2\text{-}T18^{c}$/oSnJ congenic strain utilized in this study. $C5_{def}$ mice have a 2-base pair deletion in Exon 6 of the *C5* gene that leads to an early stop codon, thus rendering the mice C5 deficient [125-127]. Mice wild type for C5, B10.D2-$Hc^{1}H2^{d}H2\text{-}T18^{c}$/oSnJ, referred to as $C5_{cont}$, were used as controls. Eight-week old C57BL/6J mice were placed on 10%, 45% or 60% fat diets (Research Diets, Inc. New Brunswick, NJ, Catalog #D12492, D12451, and D12450J, respectively) for 16 weeks. Eight-week old $C5_{def}$ and $C5_{cont}$ mice were placed on either a 10% low fat diet (LFD) or 60% high fat diet (HFD) for up to 12 weeks. AKR/J, DBA/2J, A/J, CBA/J, DBA/1J, FVB/NJ, and NOD/ShiLtJ mice were purchased from Jackson Laboratory and maintained on chow diet in VU facilities prior to experiments at 8-12 weeks of age. Male mice were used in all experiments unless indicated otherwise. Mice were kept in the VU non-barrier facility, fed *ad libitum* and given free access to water.

Body weight, body composition, and food intake

Body weight was measured weekly for the duration of the study. Total lean mass, AT mass and free fluid composition were measured by nuclear magnetic resonance using a Bruker Minispec (Woodland, TX) in the Vanderbilt Mouse Metabolic Phenotyping Center (MMPC) at baseline and 6 and 12 weeks after placement on the respective diet.

Blood collection and analyses

Mice were fasted for 5 h and bled from the retro-orbital venous plexus using heparinized collection tubes. Glucose levels from whole blood were measured using a LifeScan One Touch Ultra glucometer (Johnson & Johnson, Northridge, CA). Plasma was separated by centrifugation and stored at -80 ℃ until further analysis. Plasma insulin levels were measured using an ELISA or by radioimmunoassay from Millipore (Billerica, MA).

Glucose tolerance test

Mice were morning-fasted for 5 h before the initiation of the test. Mice were bled via tail snip and baseline glucose was measured using a glucometer. Mice were then injected with 1 g of dextrose per kg of lean body mass. Glucose levels were assessed at 15, 30, 45, 60, 90, 120, and 150 min after glucose injection.

Hyperinsulinemic-euglycemic clamps

One week before hyperinsulinemic-euglycemic clamps were performed, mice had carotid artery and jugular vein catheters surgically implanted for

sampling and infusions, respectively. On the day of a study, mice were fasted for 5 h and insulin clamps were performed in conscious unrestrained mice as previously described [128, 129]. Two hours prior to the clamp a primed (1 μCi) continuous (0.05 μCi/min) tracer ([3-^{3}H]-glucose) infusion was initiated and continued for the duration of the study. After baseline blood samples for insulin and tracer measurements insulin was infused (t=0 min) at 2.0 mU·kg^{-1}·min^{-1}. Glucose was infused at a variable rate to maintain euglycemia. After 120 min a bolus of 2[^{14}C]deoxyglucose (2DG) was administered, and after 25 min had elapsed, tissues were collected. 2DG was used to determine the glucose metabolic index (R_g), a measure of tissue-specific glucose uptake [130, 131]. Washed blood cells from a donor animal were continuously infused to maintain blood volume during the clamp.

Tissue collection and weights

At the end of each study, brain, epididymal AT, liver, gastrocnemius muscle, and pancreas were collected, weighed, and snap-frozen in liquid nitrogen. For clamp studies additional tissues were collected to determine glucose uptake including BAT, inguinal WAT, heart, soleus muscle, and vastus lateralis muscle,

Real-time RT-PCR

Tissue RNA isolation and cDNA synthesis were performed as previously described [132]. FAM-conjugated primer/probe sets were purchased from Applied Biosystems (Foster City, CA). Catalog numbers will be provided upon request. All genes were normalized to glyceraldehyde-3-phosphate dehydrogenase expression,

and presented as expression relative to the $C5_{cont}$ group fed a 10% fat diet (LFD). Data were analyzed using the Pfaffl method [133].

Western blot analysis

Protein samples were collected by sonicating 50 mg of AT, liver, or gastrocnemius muscle in 2% SDS. Protein concentration was measured using a BCA assay, and equal concentrations of total protein were run on 4-20% SDS gels (BioRad) or 4-12% Bis Tris gels (Invitrogen), transferred to nitrocellulose (Invitrogen) or PVDF (BioRad) membranes, and immunoblotted for the indicated probes of interest (antibodies from Cell Signaling: 3020, 3700, 4060, 9272). The blots shown in figures 28, 31, 32, 33, 34, and 36 were visualized by enhanced chemiluminescence (Amersham Pharmacia BioTech). The blots shown in figures 35, 37, and 43 were visualized by fluorescently-tagged secondary antibodies (Li-Cor) and imaged on the Li-Cor Odyssey in the Vanderbilt Molecular Cell Biology Resource Core. Quantification of the intensity of individual bands was done using ImageJ.

Tissue histology

Liver: Liver samples were collected, frozen in Optimal Cutting Temperature (OCT) solution, and stored at -20 ℃. Seven micrometer sections of liver were cut using a cryostat and stained for Oil Red O. Images were captured using an Olympus BX51 microscope (Tokyo, Japan) at a 10X magnification. *Adipose:* Epididymal AT samples were collected and fixed in 10% formalin overnight. They were further processed, paraffin embedded, and sections were cut and stained with

anti-F4/80 antibody by the Vanderbilt Translational Pathology Shared Resource. Entire slides were imaged on a Leica SCN400 Slide Scanner by the Vanderbilt Digital Histology Shared Resource (DHSR) at a 20X magnification. F4/80 positive-stained crown-like structures (CLS) were counted per field of view using ImageJ public software.

DNA isolation, whole genome sequencing, and read alignment

Total DNA was isolated from liver of $C5_{cont}$ and $C5_{def}$ male mice according to the DNeasy Blood & Tissue Kit (Qiagen). Samples were submitted to the Vanderbilt Technologies for Advanced Genomics (VANTAGE) resource core for quality control and sequencing. Before processing, genomic DNA samples undergo quality control testing in the form of Qubit and Tapestation runs following manufacturer's protocols. Samples are normalized, sheared (Covaris LE220) and Illumina ready libraries are prepared (NEB DNA Ultra II). Final libraries are assessed for quantity and quality using Qubit and Qiagen QIAxcel runs. Successful libraries are normalized and subjected to Kapa qPCR. Libraries are pooled and loaded on the NovaSeq6000 following Illumina protocols and fastq files are generated from raw sequence data using Illumina's bcl2fastq software. Fastq reads are analyzed via FastQC for sequence quality, GC content, the presence of adaptors, overrepresented *k*-mers and duplicated reads in order to detect sequencing errors, PCR artifacts or contaminations. Reads are also mapped to the reference genome (when available) for additional contamination assessment.

Sequencing reads after quality control were mapped to the C57BL/6J reference genome (NCBI build M37/mm9) using the Burrows-Wheeler aligner

(BWA-MEM v0.7.17 [134]) on a per-mouse basis using default parameters. Using SAMtools [135], aligned SAM files were converted to BAM files that were re-sorted and then indexed. Visualization of the *Insr* gene using the Integrated Genomics Viewer (IGV.2.4.14 [136]) was used for the initial identification of variation between the control and case genes. The variants and indels in *Insr* gene identified during the visualization process were confirmed in the consensus sequences, which were created using the SAMtools mpileup function and BCFtools for each genome [135].

Adenoviral studies

Preparation of adenovirus: Adenovirus (Ad5 with E1/E3 deletion) containing human C5 (clone BC113738) was purchased from Vector BioLabs. Adenovirus containing GFP was used as the control. Mice were fed 10% LFD for 14-16 weeks prior to AdC5 or AdGFP injection. Adenovirus was provided at $1.1x10^9$ PFU/mouse in 200 μL PBS via the retro-orbital venous plexus. Four weeks following adenovirus injection, hyperinsulinemic-euglycemic clamps were performed as described above.

Statistical analyses

All statistics were performed using GraphPad Prism software. Given the multiple models used herein, details pertaining to statistical analyses are provided in each figure legend.

Results

Regulation of complement expression by HFD feeding

To determine the effects of obesity on expression of components of the complement system, male C57BL/6J mice were fed diets containing 10%, 45%, or 60% of kcals from fat for 16 weeks. AT gene expression of complement factor 5 (*Hc*) was elevated with increasing dietary fat composition: mice fed a 60% fat diet had a >10-fold increase in AT *Hc* expression when compared to mice fed a 10% fat diet ($p<0.0001$; **Figure 15A**). In contrast, AT expression of *C3*, *C9*, and Factor B (*Cfb*) were unchanged (**Figure 15B-D**), while *C6* and Factor D (*Cfd*) expressions were decreased with increasing fat in the diet ($p<0.01$; **Figure 15E-F**).

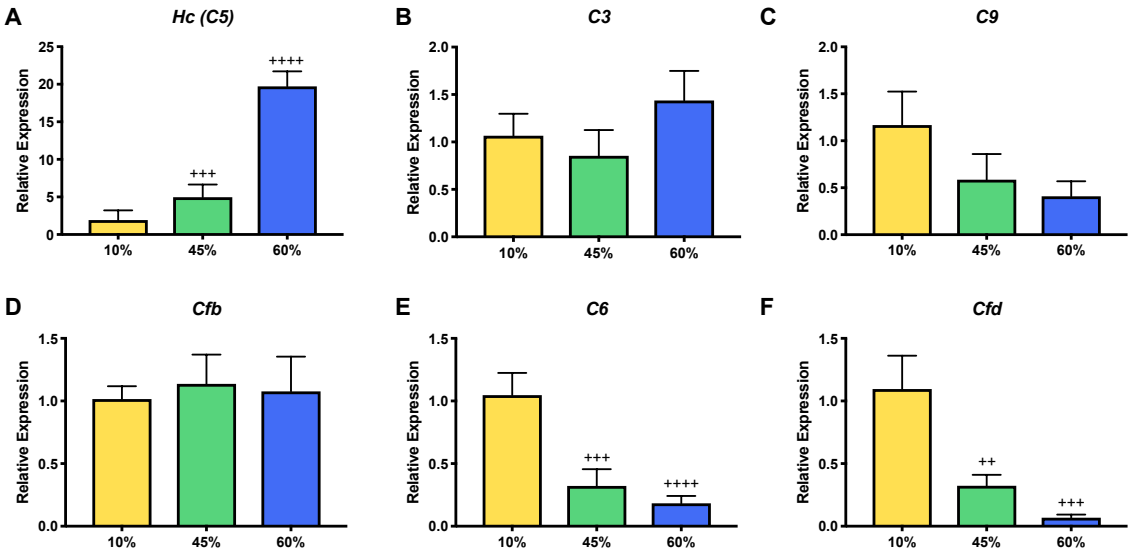

Figure 15. Regulation of adipose tissue complement expression by HFD feeding

C57BL/6J mice were placed on 10%, 45% or 60% fat diets for 16 weeks. Adipose tissue was collected and total mRNA expression was assessed by real-time RT-PCR. A) *Hc*, B) *C3*, C) *C9*, D) *Cfb*, E) *C6*, F) *Cfd*. Data are presented as mean ± SEM of 4-7 mice per group, and were analyzed by one-way ANOVA with multiple comparisons.

++ $p<0.01$; +++ $p<0.001$; ++++ $p<0.0001$

In the liver, HFD feeding did not change the expression of *Hc*, *C3*, or *C9*, but reduced the expression of *C6* ($p<0.05$ compared to 10% fat diet; **Figure 16A-D**). These data indicate that components of the complement system are dynamically regulated by obesity and dietary fat content.

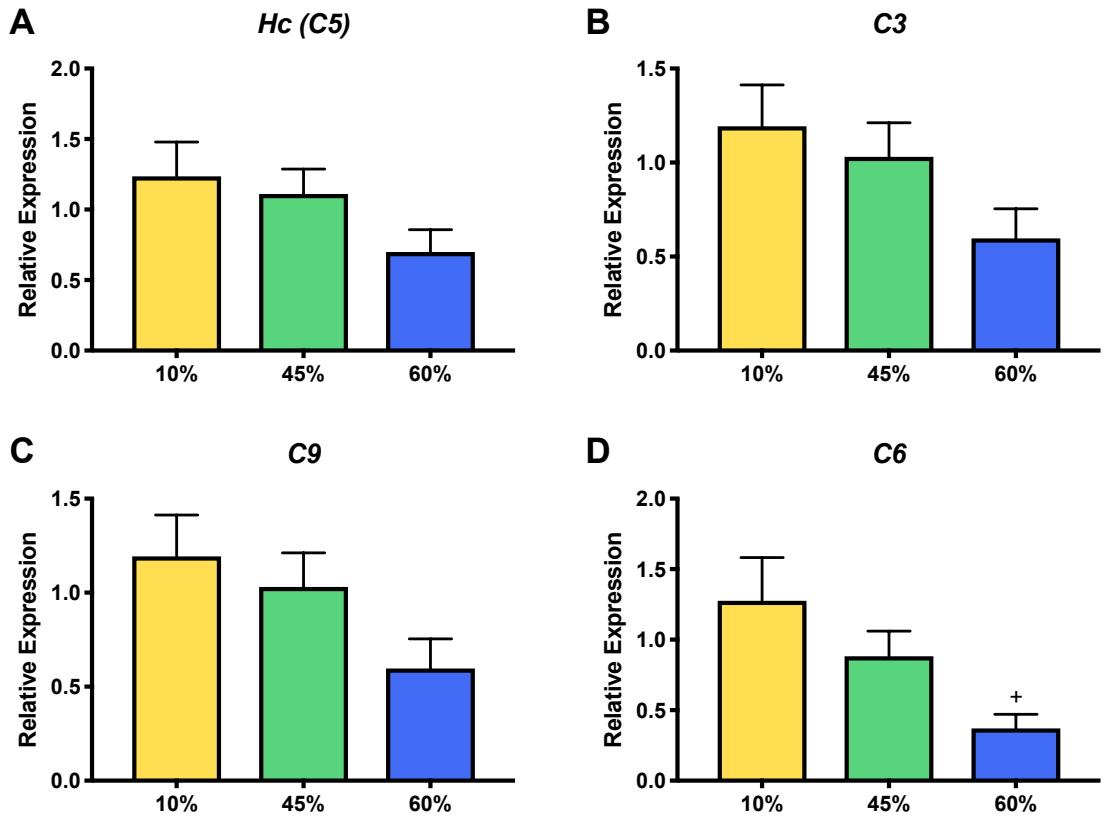

Figure 16. Regulation of liver complement expression by HFD feeding
C57BL/6J mice were placed on 10%, 45% or 60% fat diets for 16 weeks. Liver was collected and total mRNA expression was assessed by real-time RT-PCR. A) *Hc,* B) *C3*, C) *C9*, D) *C6*. Data are presented as mean ± SEM of 4-7 mice per group, and were analyzed by one-way ANOVA with multiple comparisons.
+ $p<0.05$

Metabolic characterization of $C5_{def}$ mice

Because *Hc* gene expression was the only complement factor whose expression was elevated in obese AT, we next determined whether deficiency in its encoded protein, C5, abrogates obesity-associated inflammation and metabolic dysfunction in mice. Accordingly, C5 control ($C5_{cont}$) and C5 deficient ($C5_{def}$) mice were placed on a 10% fat LFD or 60% fat HFD for 12 weeks to evaluate their metabolic phenotypes. C5 deficiency did not alter weight gain or final body weights in mice fed LFD (**Figure 17A**). In contrast, as soon as 2 weeks after beginning HFD feeding, $C5_{def}$ mice weighed less than $C5_{cont}$ mice ($p<0.05$). Food consumption was not statistically different between genotypes (data not shown). After 12-weeks of HFD feeding, both groups had increased AT mass ($p<0.0001$); however, $C5_{def}$ mice had less total AT mass than the $C5_{cont}$ animals ($p<0.0001$; **Figure 17B**). Total lean mass and liver mass were elevated by HFD feeding in the $C5_{cont}$ mice ($p<0.001$ and $p<0.01$, respectively) but not in the $C5_{def}$ mice (**Figure 17C-D**).

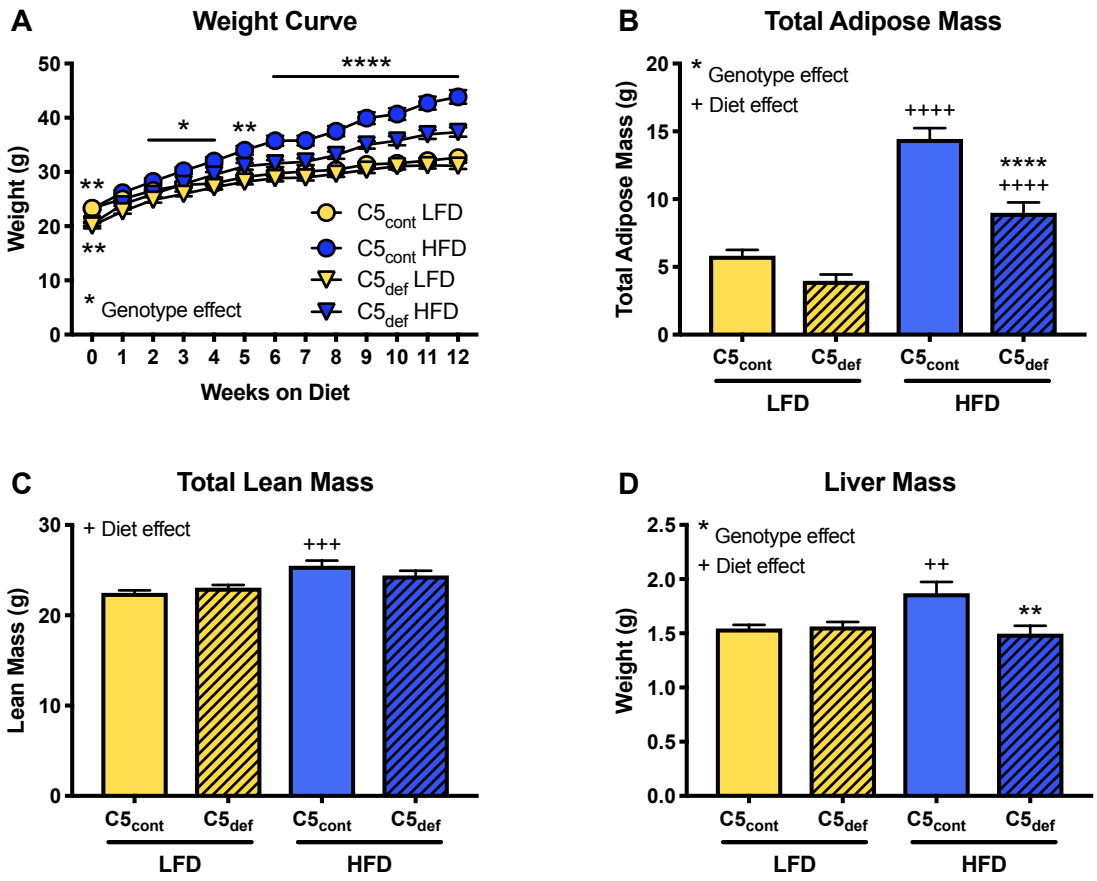

Figure 17. Metabolic characterization of $C5_{cont}$ and $C5_{def}$ mice

C5 control ($C5_{cont}$) and C5 deficient ($C5_{def}$) mice were placed on LFD or HFD for 12 weeks. A) Body weight curves. B) Total adipose tissue mass as measured by NMR. C) Total lean mass as measured by NMR. D) Liver weight. Data are presented as mean ± SEM of 11-14 mice per group, and were analyzed by two-way ANOVA with multiple comparisons, and body weight curve with repeated measures.

* $p<0.05$; ** $p<0.01$; **** $p<0.0001$ (genotype effect)

++ $p<0.01$; +++ $p<0.001$; ++++ $p<0.0001$ (diet effect)

Tissue inflammation and physiology

To determine if $C5_{def}$ mice display differences in tissue inflammation, RNA was isolated from epididymal AT and liver after 12-weeks of LFD or HFD feeding, and gene expression of macrophage and inflammatory markers was analyzed by quantitative real-time RT-PCR. Based upon expression of *Emr1* (gene for F4/80), AT macrophage content was significantly increased by HFD-feeding in both groups ($p<0.01$ for $C5_{cont}$, $p<0.05$ for $C5_{def}$; **Figure 18A**). Expression of the cytokines *Tnf*, *Il10,* and *Ccl2* also showed the expected increase with HFD feeding in both $C5_{def}$ and $C5_{cont}$ AT ($p<0.001$ for *Tnf*; $p<0.01$ $C5_{cont}$ and $p<0.05$ $C5_{def}$ for *Il10*; $p<0.001$ $C5_{cont}$ and $p<0.01$ $C5_{def}$ for *Ccl2*; **Figure 18B-D**). There was a trend toward reduced AT expression of *Emr1*, *Il10*, and *Ccl2* in $C5_{def}$ compared to $C5_{cont}$ mice, this did not reach statistical significance.

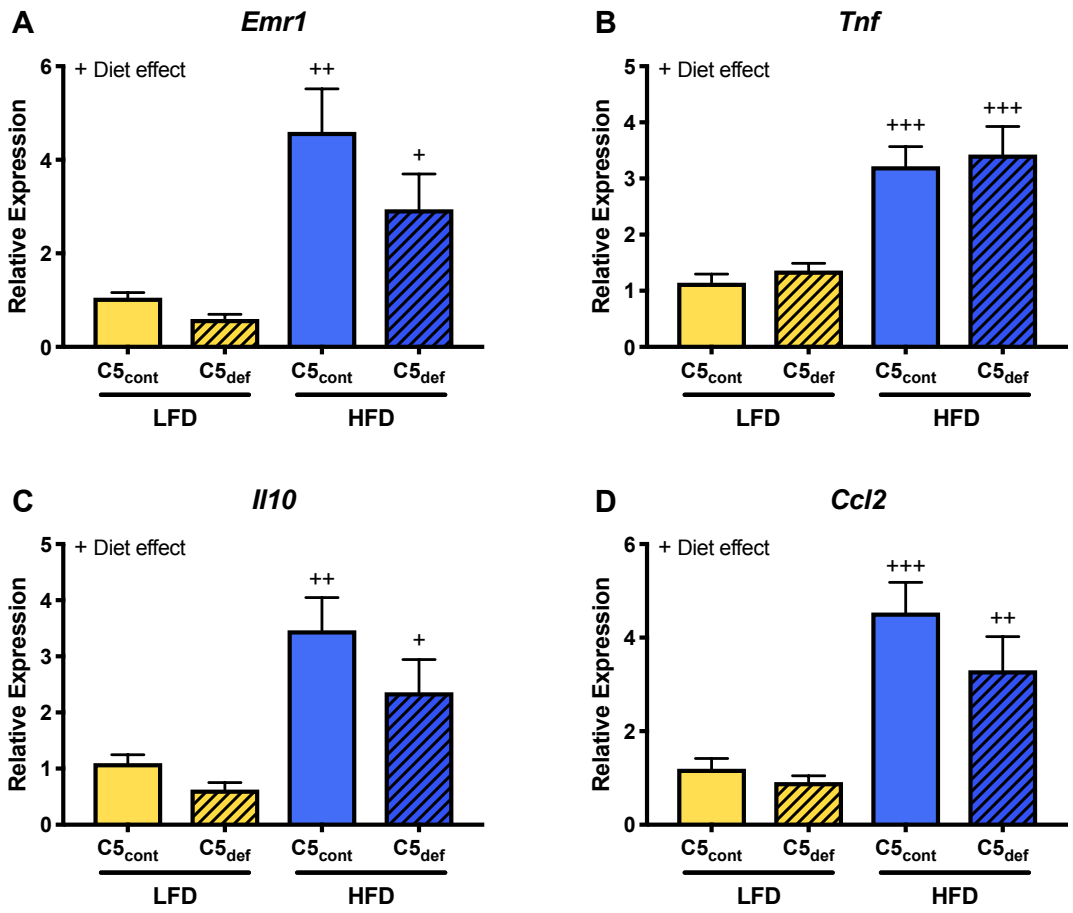

Figure 18. Adipose tissue inflammation

Adipose tissue was collected from C5 control ($C5_{cont}$) and C5 deficient ($C5_{def}$) mice after 12 weeks of LFD and HFD feeding and used for mRNA expression of: A) *Emr1*, B) *Tnf*, C) *Il10*, and D) *Ccl2*. Data are presented as mean ± SEM of 11-13 mice per group, and were analyzed by two-way ANOVA with multiple comparisons. + $p<0.05$; ++ $p<0.01$; +++ $p<0.001$ (diet effect)

Hepatic expression of *Emr1, Tnf*, and *Il10* were not changed by diet or genotype (**Figure 19A-C**), while *Ccl2* expression was increased in LFD-fed $C5_{def}$ mice ($p<0.05$, **Figure 19D**).

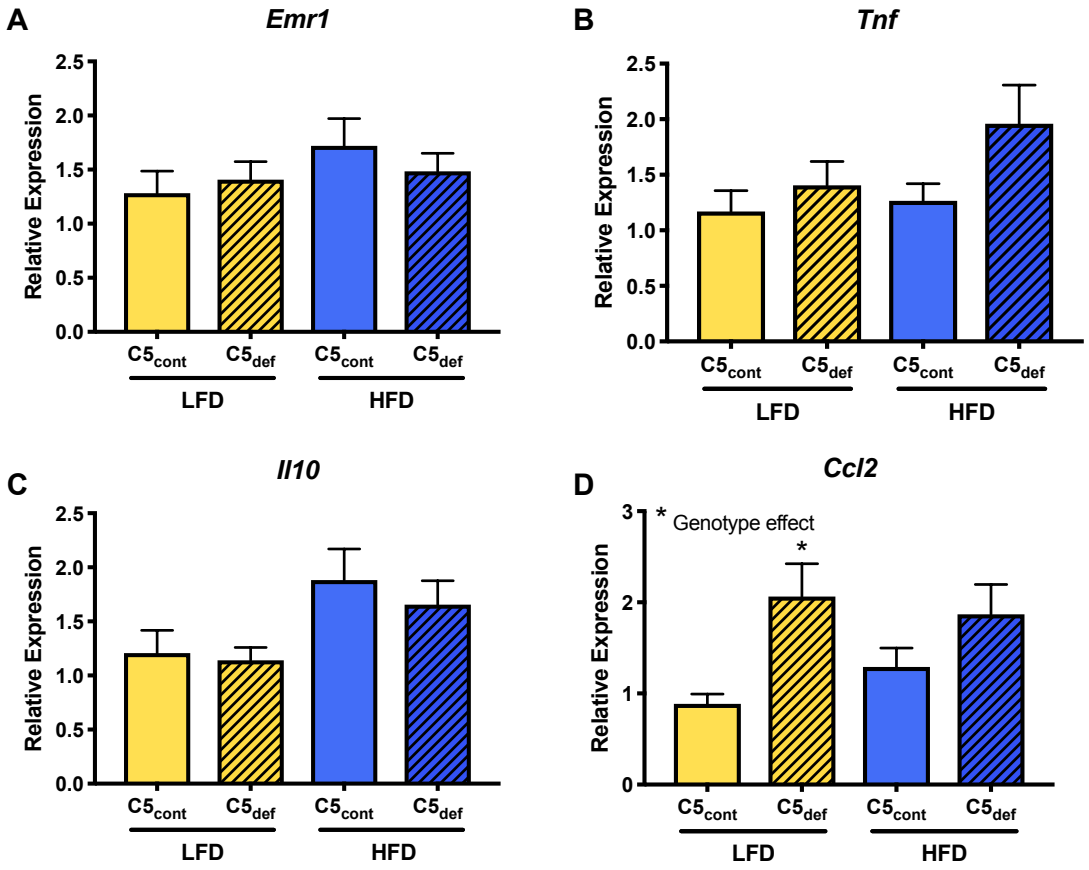

Figure 19. Liver inflammation
Liver was collected from C5 control ($C5_{cont}$) and C5 deficient ($C5_{def}$) mice after 12 weeks of LFD and HFD feeding and used for mRNA expression of: A) *Emr1*, B) *Tnf*, C) *Il10*, and D) *Ccl2*. Data are presented as mean ± SEM of 11-13 mice per group, and were analyzed by two-way ANOVA with multiple comparisons.
* $p<0.05$ (genotype effect)

AT sections were stained for F4/80 and analyzed by light microscopy. As expected, there was HFD-induced macrophage infiltration of AT; though, $C5_{def}$ mice had less HFD-induced crown-like structure formation than $C5_{cont}$ animals (**Figure 20A**, quantified in **Figure 20B**).

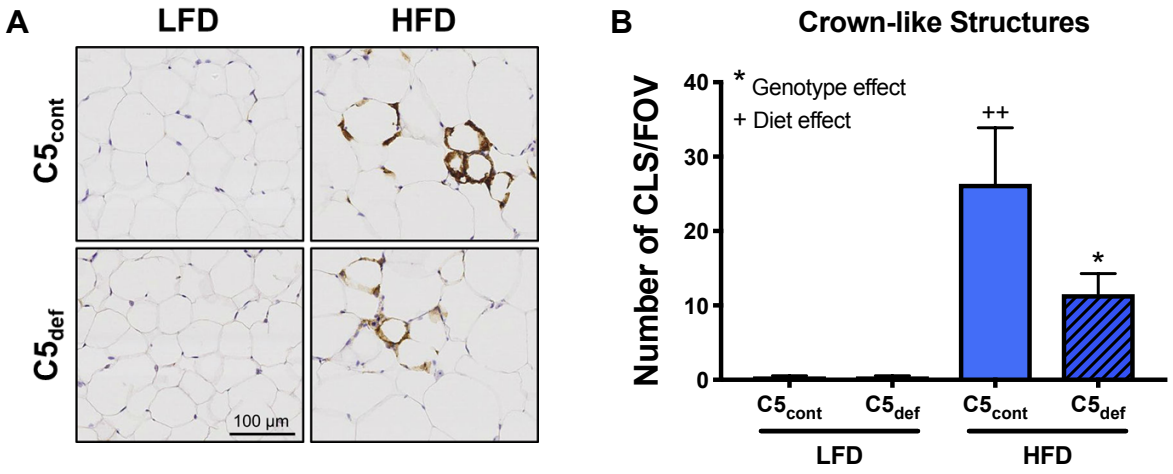

Figure 20. Adipose tissue inflammation and physiology
Adipose tissue (AT) was collected from C5 control ($C5_{cont}$) and C5 deficient ($C5_{def}$) mice after 12 weeks of LFD and HFD feeding and used for histological analyses. A) Fixed AT sections were stained with the macrophage marker F4/80. Representative images are shown are at 20X magnification. B) Quantification of crown-like structures per field-of-view (CLS/FOV). Data are presented as mean ± SEM from 3-4 mice per group, and were analyzed by two-way ANOVA with multiple comparisons.
* $p<0.05$ (genotype effect)
++ $p<0.01$ (diet effect)

Oil Red O staining of liver sections showed increased neutral lipid staining in HFD-fed compared to LFD-fed $C5_{cont}$ mice (**Figure 21A**). In contrast, HFD-induced lipid accumulation was attenuated in the livers of $C5_{def}$ mice (**Figure 21A**). Quantification of liver triglycerides confirmed these histological findings (**Figure 21B**). In fact, total triglyceride content was 70% lower in the $C5_{def}$ HFD group compared to the $C5_{cont}$ HFD group ($p<0.001$).

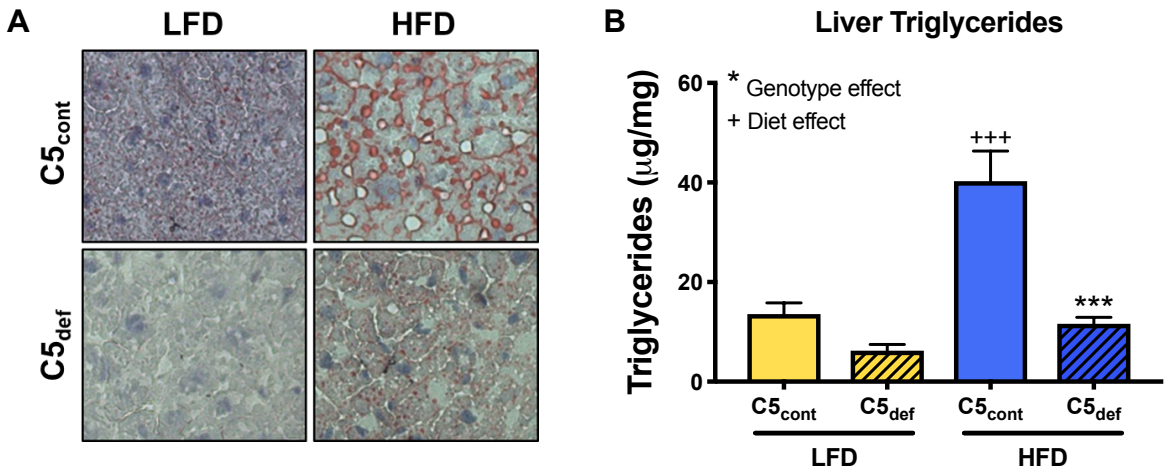

Figure 21. Liver physiology
Liver was collected from C5 control ($C5_{cont}$) and C5 deficient ($C5_{def}$) mice after 12 weeks of LFD and HFD feeding and used for triglyceride quantification and histological analyses. A) Frozen liver sections were stained for neutral lipids using Oil Red O. Representative images are shown are at 10X magnification. B) Triglyceride content was quantified by GC-MS.
Data are presented as mean ± SEM of 4-6 mice per group, and were analyzed by two-way ANOVA with multiple comparisons.
*** $p<0.001$ (genotype effect)
+++ $p<0.001$ (diet effect)

In support of decreased lipid content, liver expression of the enzyme acyl-coenzyme A carboxylase was decreased in HFD-fed $C5_{def}$ mice when compared to the HFD-fed $C5_{cont}$ group ($p<0.001$; **Figure 22A**). Expression of other enzymes involved in hepatic glucose metabolism were not different between $C5_{cont}$ and $C5_{def}$ mice (**Figure 22B-D**).

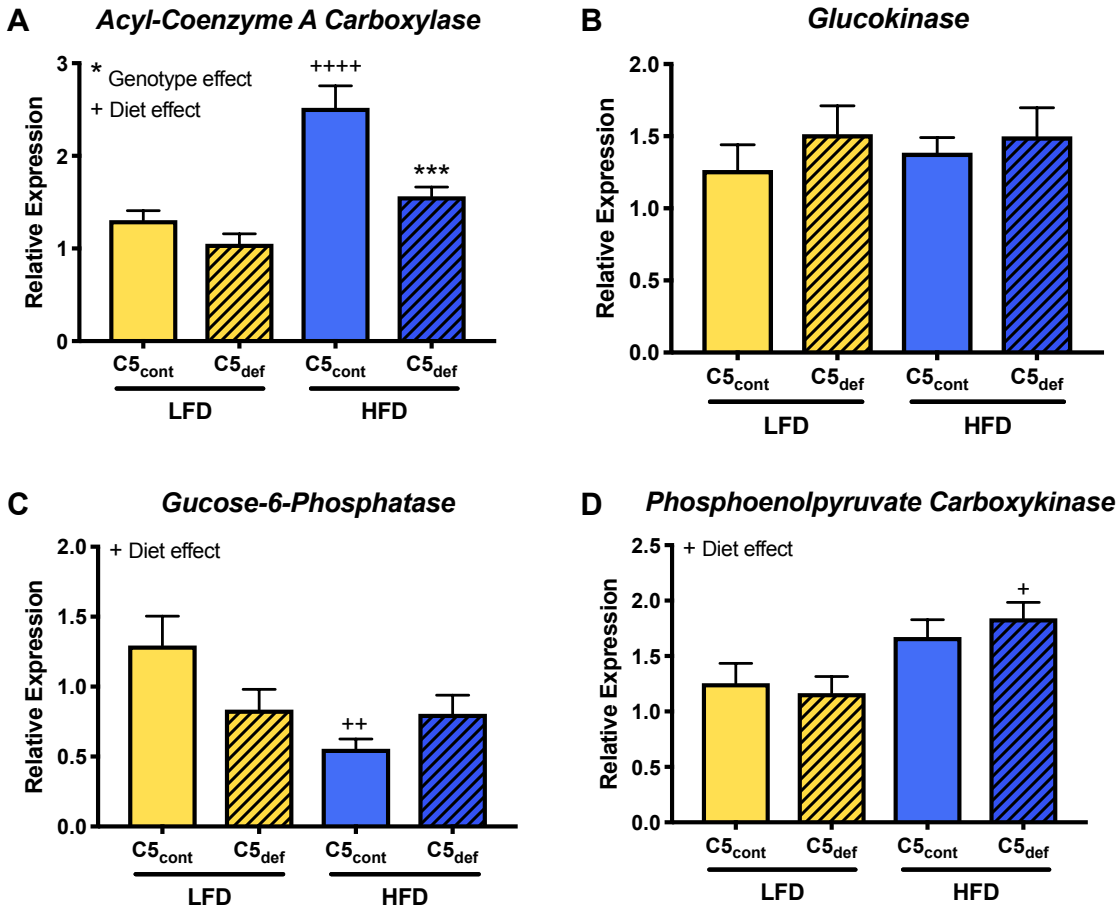

Figure 22. Hepatic glucose metabolism
Liver was collected from C5 control ($C5_{cont}$) and C5 deficient ($C5_{def}$) mice after 12 weeks of LFD and HFD feeding and used for mRNA expression of: A) *Acyl-coenzyme A carboxylase*, B) *Glucokinase*, C) *Glucose-6-phosphatase*, and D) *Phosphoenolpyruvate carboxykinase*. Data are presented as mean ± SEM of 11-13 mice per group, and were analyzed by two-way ANOVA with multiple comparisons.
*** $p<0.001$ (genotype effect)
+ $p<0.05$;++ $p<0.01$; ++++ $p<0.0001$ (diet effect)

$C5_{def}$ mice exhibit severe systemic glucose intolerance and IR

Data presented thus far shows that C5 deficiency has a relatively minimal effect on immune cell composition and inflammation in AT or liver, suggesting the altered metabolic phenotype in $C5_{def}$ mice is not immune cell mediated in those tissues. To determine if C5 deficiency impacts systemic glucose handling, intraperitoneal glucose tolerance tests (GTTs) were performed after 6 and 12 weeks of LFD or HFD feeding (**Figure 23A-B**). As expected, HFD feeding caused glucose intolerance in $C5_{cont}$ mice, and also in $C5_{def}$ mice, despite their lower body, liver, and AT weights, which are typically associated with better glucose control. $C5_{def}$ mice on both LFD and HFD were significantly more glucose intolerant than their $C5_{cont}$ counterparts ($p<0.05$ on LFD, $p<0.01$ on HFD at 12 weeks, AUC). In fact, at the 12-week time-point, $C5_{def}$ mice on LFD had the same glucose clearance rate as $C5_{cont}$ mice on HFD (**Figure 23B**). Further indication of IR in $C5_{def}$ mice, plasma insulin levels were elevated compared to control mice after 6 weeks of HFD feeding ($p<0.0001$; **Figure 23C**), although they were no longer significantly different after 12 weeks (**Figure 23D**).

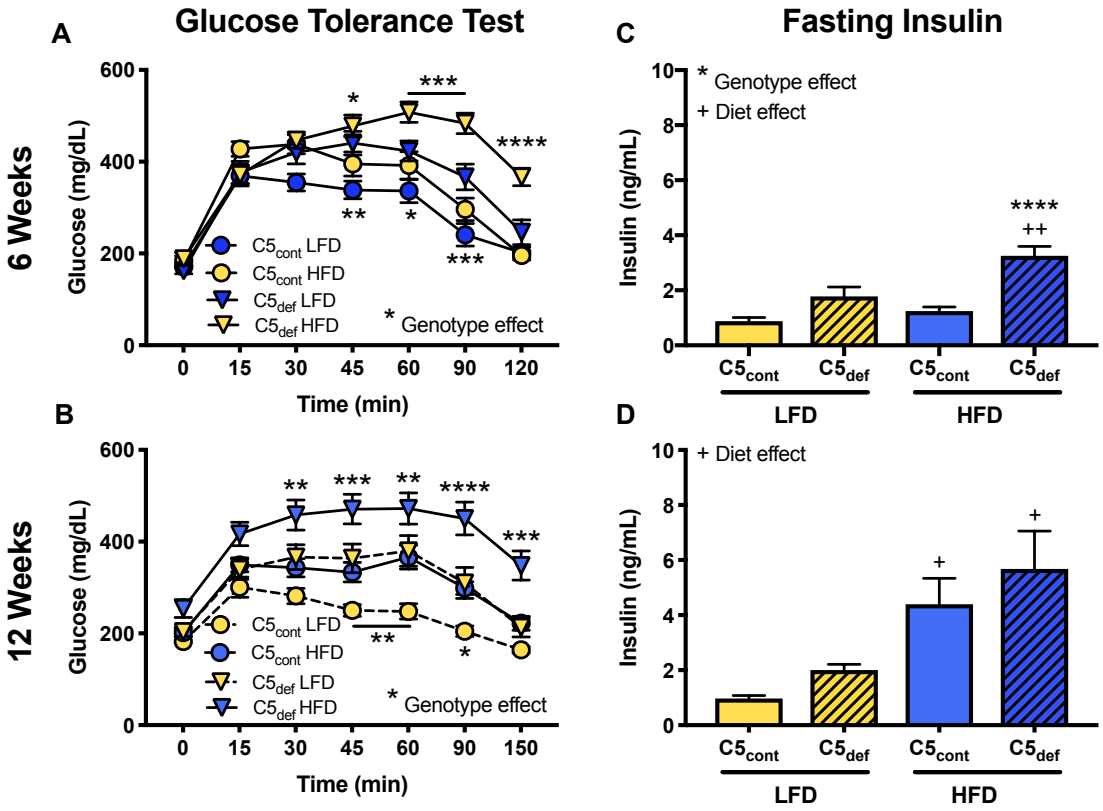

Figure 23. Glucose tolerance and fasting insulin

C5 control ($C5_{cont}$) and C5 deficient ($C5_{def}$) mice were maintained on LFD or HFD for 6 (A, C) or 12 (B, D) weeks and assessed for glucose tolerance (A-B) and fasting plasma insulin concentrations (C-D). Data are presented as mean ± SEM from 9-14 mice per group. Bar graphs were analyzed by two-way ANOVA with multiple comparisons. Curves were analyzed by two-way ANOVA with multiple comparisons and repeated measures.

* $p<0.05$; ** $p<0.01$; *** $p<0.001$; **** $p<0.0001$ (genotype effect)

+ $p<0.05$; ++ $p<0.01$ (diet effect)

To more thoroughly assess the metabolic phenotype of $C5_{def}$ mice, hyperinsulinemic-clamps were performed using $C5_{cont}$ and $C5_{def}$ mice that had been maintained on a LFD for 6 weeks. In both groups, blood glucose levels were successfully clamped at ~130 mg/dL (**Figure 24A**). However, the glucose infusion rate necessary to maintain euglycemia was strikingly lower in the $C5_{def}$ compared to $C5_{cont}$ mice (10 mg/kg/min versus 50 mg/kg/min, respectively; $p<0.0001$; **Figure 24B**), confirming that the $C5_{def}$ mice present with severe systemic IR, even on LFD.

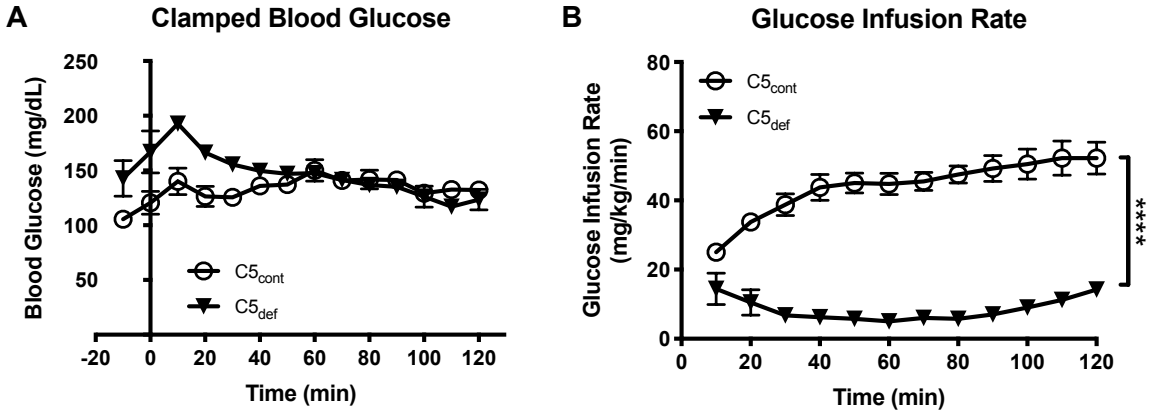

Figure 24. Hyperinsulinemic-euglycemic clamps and glucose infusion rate

C5 control ($C5_{cont}$) and C5 deficient ($C5_{def}$) mice were maintained on LFD for 6 weeks. During the last week, mice underwent surgical implantation of jugular and carotid catheters. Hyperinsulinemic-euglycemic clamps were performed as described in the Methods section. A) Blood glucose was clamped at ~130 mg/dL in each group. B) Glucose infusion rate required to clamp glucose. Data are presented as mean ± SEM from 5 mice per group. Curves were analyzed by two-way ANOVA with multiple comparisons and repeated measures.

**** $p<0.0001$ (genotype effect)

Circulating insulin but not c-peptide levels were elevated in $C5_{def}$ mice, both at baseline and during the clamp ($p<0.01$; **Figure 25A-B**), suggestive of impaired first pass insulin extraction, as opposed to a difference in endogenous insulin secretion during clamp.

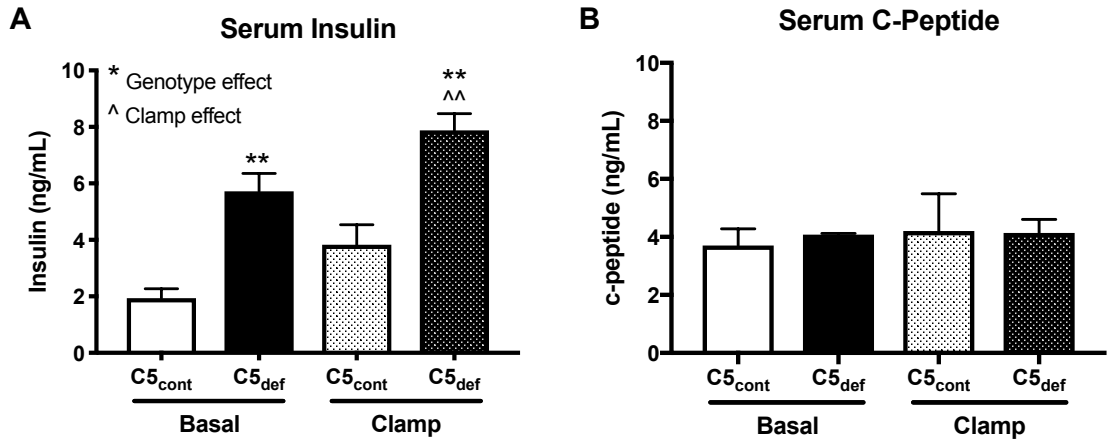

Figure 25. Hyperinsulinemic-euglycemic clamps, serum insulin and c-peptide

C5 control ($C5_{cont}$) and C5 deficient ($C5_{def}$) mice were maintained on LFD for 6 weeks. During the last week, mice underwent surgical implantation of jugular and carotid catheters. Hyperinsulinemic-euglycemic clamps were performed as described in the Methods section. A) Plasma insulin and B) c-peptide in basal and clamp periods. Data are presented as mean ± SEM from 5 mice per group, and were analyzed by two-way ANOVA with multiple comparisons.

** $p<0.01$ (genotype effect)

^^ $p<0.01$ (clamp effect)

Despite the elevated circulating insulin concentrations, glucose production from the liver (endoRa) was equally suppressed during the clamp in both groups ($p<0.001$ for $C5_{cont}$, $p<0.0001$ for $C5_{def}$; **Figure 26A**). As expected, there was a significant negative correlation between serum insulin levels and endoRa in the $C5_{cont}$ group ($r^2=0.5023$, $p<0.05$, **Figure 26B**). However, this correlation was not present in the $C5_{def}$ group ($r^2=0.1270$, $p=0.31$), and more importantly, this relationship was shifted to the right, indicating IR in the livers of $C5_{def}$ mice.

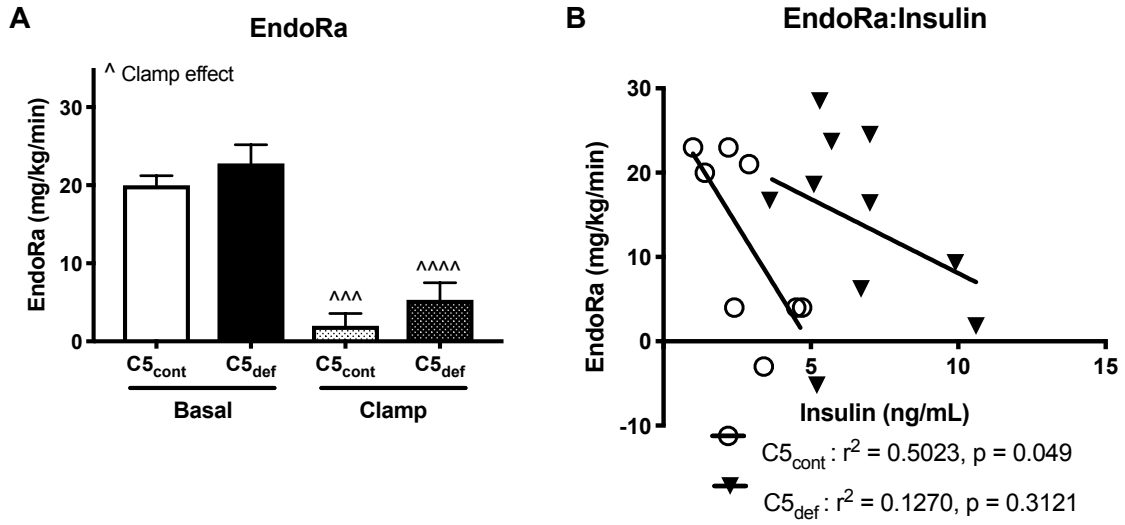

Figure 26. Hyperinsulinemic-euglycemic clamps, EndoRa and EndoRa:Insulin ratio

C5 control ($C5_{cont}$) and C5 deficient ($C5_{def}$) mice were maintained on LFD for 6 weeks. During the last week, mice underwent surgical implantation of jugular and carotid catheters. Hyperinsulinemic-euglycemic clamps were performed as described in the Methods section. A) Hepatic glucose production (EndoRa) and B) relationship between plasma insulin and EndoRa during basal and clamp periods. Data are presented as mean ± SEM from 5 mice per group. Bar graphs was analyzed by two-way ANOVA with multiple comparisons, and EndoRa:Insulin was analyzed by linear regression.

^^^ $p<0.001$; ^^^^ $p<0.0001$ (clamp effect)

In addition, tissue-specific glucose uptake in the AT, muscle (gastrocnemius, soleus, and vastus lateralis) and heart was lower in $C5_{def}$ compared to $C5_{cont}$ mice ($p<0.001$, $p<0.01$, $p<0.01$, $p<0.05$, $p<0.0001$, respectively), while glucose uptake in brain was not different between the genotypes (**Figure 27**).

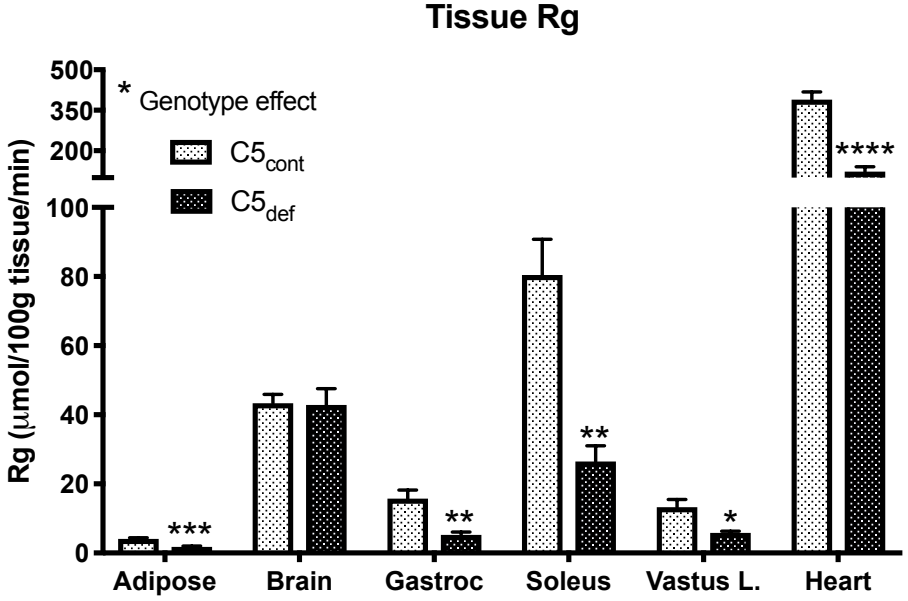

Figure 27. Hyperinsulinemic-euglycemic clamps and tissue glucose uptake

C5 control ($C5_{cont}$) and C5 deficient ($C5_{def}$) mice were maintained on LFD for 6 weeks. During the last week, mice underwent surgical implantation of jugular and carotid catheters. Hyperinsulinemic-euglycemic clamps were performed as described in the Methods section. Glucose uptake (Rg) in adipose tissue, brain, gastrocnemius, soleus, vastus lateralis, and heart. Data are presented as mean ± SEM from 5 mice per group, and were analyzed by student's t test with multiple comparisons.

* $p<0.05$; ** $p<0.01$; *** $p<0.001$; **** $p<0.0001$ (genotype effect)

IR in $C5_{def}$ mice was not associated with increased cellular stress

Based upon the surprising finding that $C5_{def}$ mice exhibit severe IR, we sought to determine the mechanism(s) underlying this metabolic defect. It has been reported in these mice that C5 is synthesized in hepatocytes, but is not secreted [126]. Therefore, it is possible that accumulation of C5 protein in hepatocytes could result in endoplasmic reticulum (ER) stress and/or oxidative stress, leading to the observed IR in the liver of $C5_{def}$ mice. Thus, several markers of ER and oxidative stress were evaluated in livers of $C5_{cont}$ and $C5_{def}$ mice by western blot analysis. The protein levels of BiP, p-JNK1/2, and SOD-2 did not differ between $C5_{cont}$ and $C5_{def}$ mice either on LFD or HFD (**Figure 28**). IRE-1α protein levels were actually slightly lower in the liver of $C5_{def}$ mice on HFD ($p<0.05$). Thus, increased liver ER or oxidative stress does not explain the IR observed in these mice.

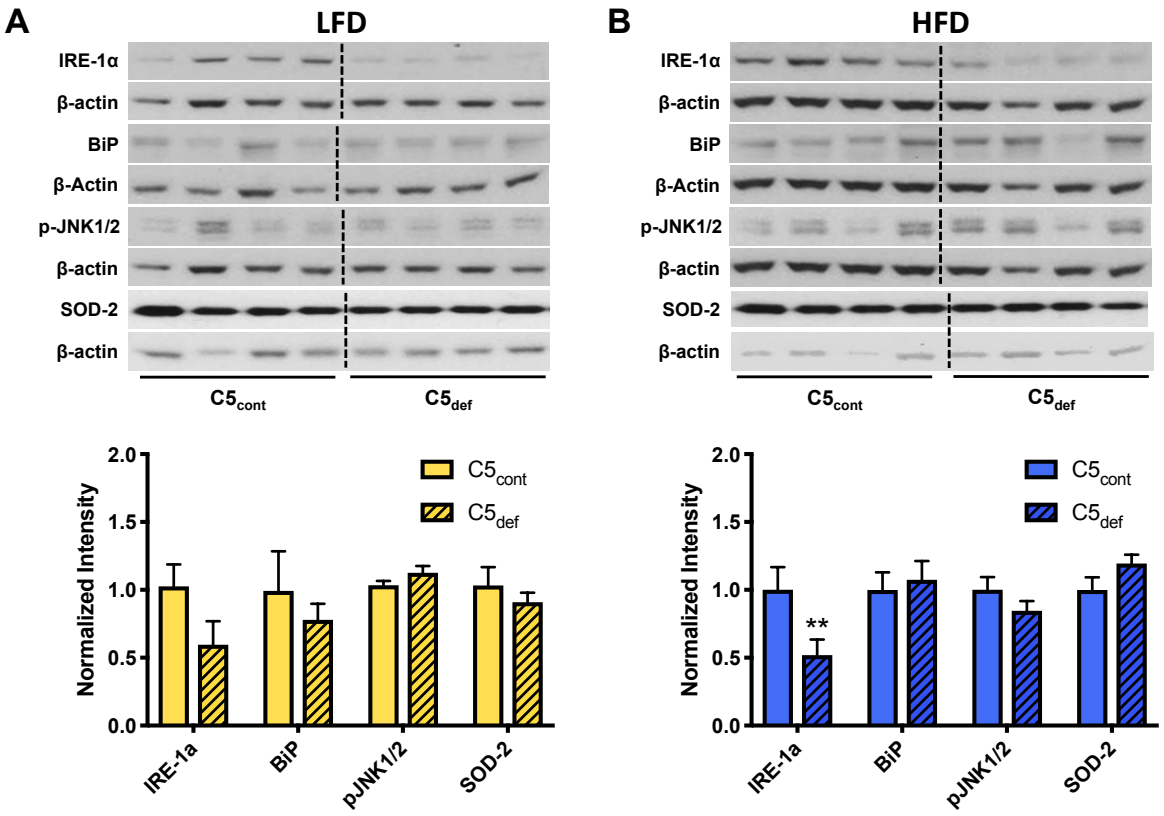

Figure 28. Hepatic ER- and oxidative-stress markers

Protein lysates were collected from liver of C5 control ($C5_{cont}$) and C5 deficient ($C5_{def}$) mice fed LFD or HFD for 12 weeks. Western blot analysis was conducted to measure the protein expression of IRE-1α, BiP, phospho-JNK, and SOD2 in A) LFD and B) HFD mice. β-actin was used as a protein loading control. Quantification data in bar graphs are presented as mean ± SEM of 8 mice per group, and were analyzed by student's t test with multiple comparisons.

** $p<0.01$

$C5_{def}$ mice have decreased levels of insulin receptor mRNA and protein

To further investigate a mechanism for the severe inflammation-independent IR in $C5_{def}$ mice, insulin receptor (INSR) gene expression (*Insr)* was measured in both liver and AT. $C5_{def}$ *Insr* expression was reduced by more than 50% in both liver and AT ($p<0.001$; **Figure 29A-B**), independent of diet.

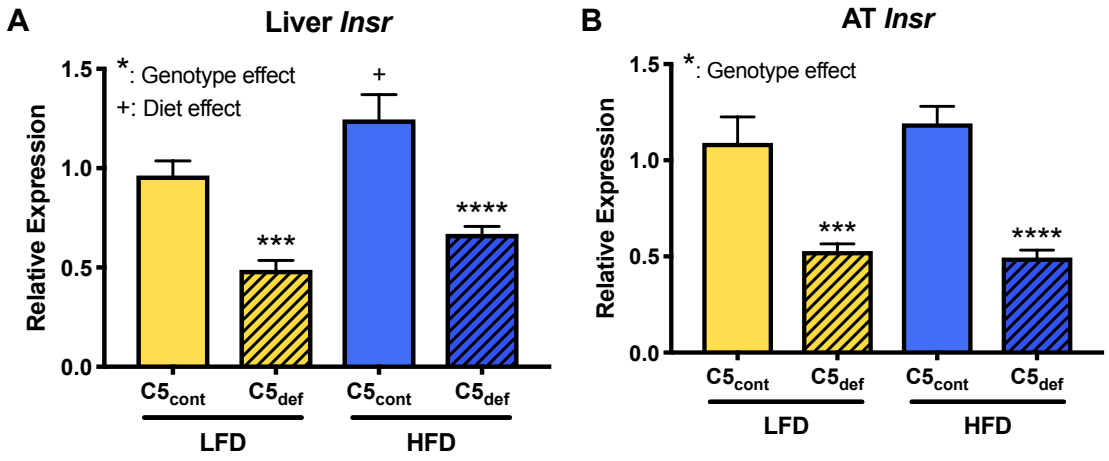

Figure 29. Insulin receptor gene expression liver and adipose tissue of $C5_{cont}$ and $C5_{def}$ mice

C5 control ($C5_{cont}$) and C5 deficient ($C5_{def}$) mice were maintained on LFD or HFD for 12 weeks. Liver (A) and AT (B) were collected and RNA was isolated for gene *Insr* expression analysis. Data are expressed as mean ± SEM of 12-13 mice per group, and were analyzed by two-way ANOVA with multiple comparisons.

*** $p<0.001$; **** $p<0.0001$ (genotype effect)

+ $p<0.05$ (diet effect)

Liver gene expression of other insulin related proteins was also evaluated. Gene expression of the insulin signaling adaptor molecular, *Irs1*, was slightly increased in $C5_{def}$ mice fed HFD compared to LFD ($p<0.05$; **Figure 30A**). However, there were no genotype-driven differences in insulin-like growth factor (*Igf1*), insulin-like growth factor 1 receptor (*Igf1r*), insulin-like growth factor-binding protein 3 (*Igfbp3*), or insulin signaling adaptor molecules (*Irs1* and *Irs2*) (**Figure 30A-E**).

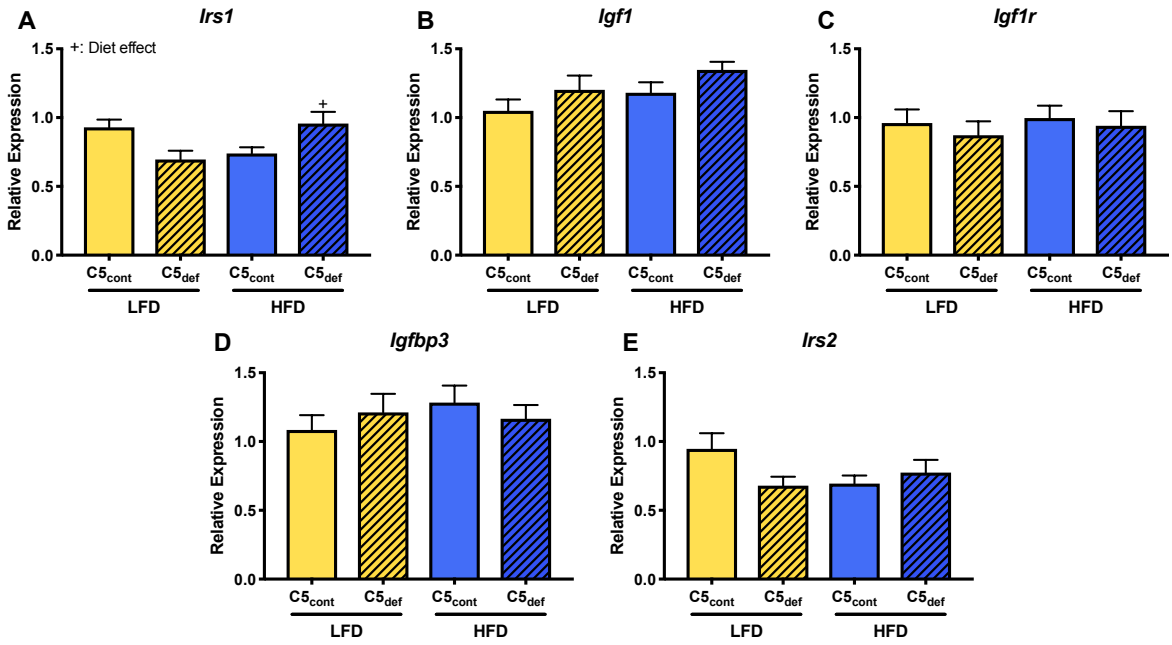

Figure 30. Insulin signaling gene expression in liver of $C5_{cont}$ and $C5_{def}$ mice

C5 control ($C5_{cont}$) and C5 deficient ($C5_{def}$) mice were maintained on LFD or HFD for 12 weeks. Liver was collected and RNA was isolated for gene expression analysis of A) insulin signaling adaptor molecular 1 (*Irs1*), B) insulin-like growth factor (*Igf1*), C) insulin-like growth factor 1 receptor (*Igf1r*), D) insulin-like growth factor-binding protein 3 (*Igfbp3*), and E) insulin signaling adaptor molecule 2 (*Irs2*). Data are expressed as mean ± SEM of 12-13 mice per group, and were analyzed by two-way ANOVA with multiple comparisons.
+ $p<0.05$ (diet effect)

Western blot analysis demonstrated a striking 50-70% decrease in the mature form of the β subunit of INSR (INSR-β) in liver and AT of $C5_{def}$ LFD-fed mice ($p<0.0001$, $p<0.01$, respectively, **Figure 31A-B**).

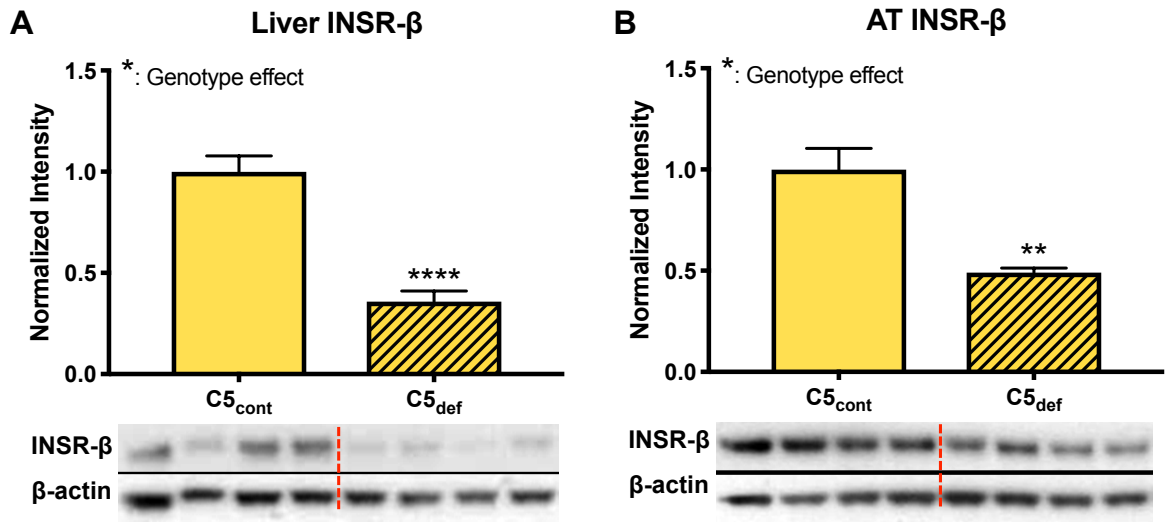

Figure 31. Insulin receptor protein levels in liver and adipose tissue of $C5_{cont}$ and $C5_{def}$ mice

C5 control ($C5_{cont}$) and C5 deficient ($C5_{def}$) mice were maintained on LFD for 6 weeks, and protein lysates were collected from liver and adipose tissue (AT). Protein expression was assessed by western blot analysis. β-actin was used as a protein loading control. INSR-β protein levels in liver (A) and AT (B), respectively. Data in bar graphs are shown as mean ± SEM from 8 mice per group, and were analyzed with student's t test. Representative images are below each graph.

** $p<0.01$ (genotype effect)

**** $p<0.0001$ (genotype effect)

A downstream indicator of INSR signaling, Akt phosphorylation (pAkt) at serine 473 was increased in liver of $C5_{cont}$ LFD-fed mice after insulin bolus ($p<0.0001$, **Figure 32A).** The insulin-stimulated increase in pAkt was blunted in liver of $C5_{def}$ LFD-fed mice ($p<0.001$, **Figure 32A**). In AT, pAkt trended towards an increase upon insulin stimulation in $C5_{cont}$ mice, and this effect appeared blunted in $C5_{def}$ mice (**Figure 32B**).

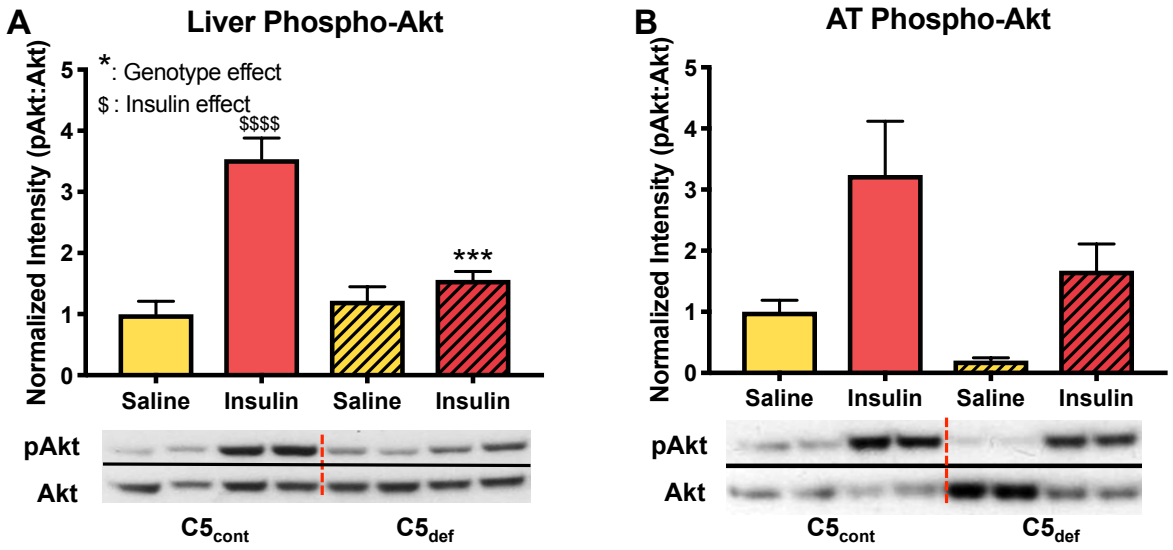

Figure 32. Insulin signaling in liver and adipose tissue of $C5_{cont}$ and $C5_{def}$ mice

C5 control ($C5_{cont}$) and C5 deficient ($C5_{def}$) mice were maintained on LFD for 6 weeks, and protein lysates were collected from liver and adipose tissue (AT). Mice were injected with saline or 1 U/kg insulin 15 min prior to being euthanized. Protein expression and phosphorylation levels was assessed by western blot analysis. β-actin was used as a protein loading control. Phospho-Akt levels relative to total total Akt in A) liver and B) AT, respectively. Data in bar graphs are shown as mean ± SEM from 4-6 mice per group, and were analyzed with two-way ANOVA with multiple comparisons. Representative images are below each graph.

*** $p<0.001$ (genotype effect)

$$$$ $p<0.0001$ (insulin effect)

Differential processing of the pro-INSR in $C5_{def}$ mice

Functional INSR is initially synthesized as a single polypeptide known as pro-insulin receptor (pro-INSR) [137], and subsequent processing results in a mature INSR with α and β subunits [138]. To determine if these mice had altered pro-INSR expression or processing, an antibody that recognizes both the mature INSR-β and the precursor form was used. In all tissues assessed (liver, AT, muscle, pancreas, and brain, **Figure 33**), a pro-INSR band of approximately 190 kDa was detected by Western blot analysis. Interestingly, in $C5_{def}$ mice, an additional pro-INSR band at 180 kDa was abundantly expressed in addition to the standard 190 kDa band.

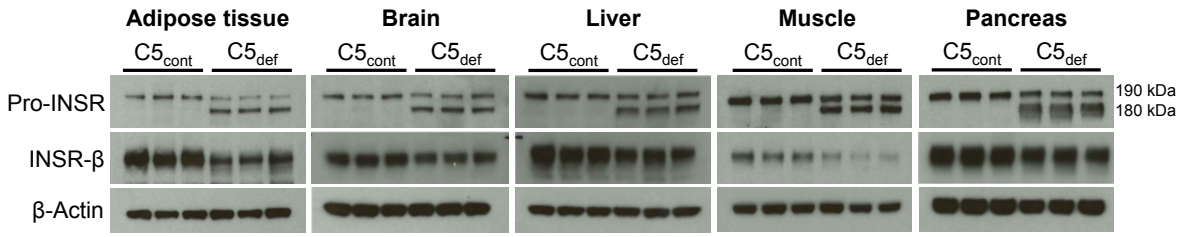

Figure 33. Improper processing of pro-INSR in $C5_{def}$ mice
Western blot analysis of the precursor of INSR (pro-INSR) in adipose tissue, brain, liver, muscle, and pancreas of C5 control ($C5_{cont}$) and C5 deficient ($C5_{def}$) mice. The normal pro-INSR band size is 190kDa. β-actin was used as a protein loading control.

To determine if the pro-INSR processing error was specific to INSR in $C5_{def}$ mice, western blotting of several other endocytic recycling receptors was performed. There were no differences in the molecular weight of the low density lipoprotein receptor (LDLR), epidermal growth factor receptor (EGFR), or transferrin receptor (Tfr1) in liver of the $C5_{cont}$ and $C5_{def}$ mice (**Figure 34**). Thus, the processing defect in $C5_{def}$ mice appears to be specific to the INSR.

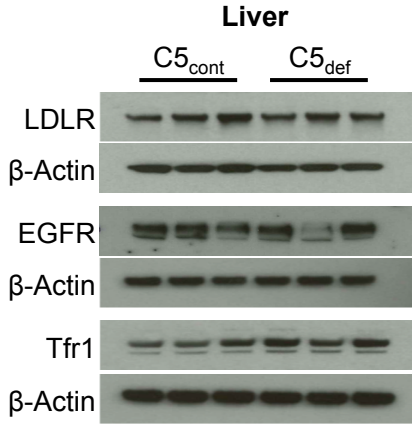

Figure 34. Western blot analysis of endocytic recycling receptors
Western blot analysis of low density lipoprotein receptor (LDLR), epidermal growth factor receptor (EGFR), or transferrin receptor (Tfr1) in liver of the C5 control ($C5_{cont}$) and C5 deficient ($C5_{def}$) mice. β-actin was used as a protein loading control.

Phenotype of $C5_{cont}$ and $C5_{def}$ mice is conserved in females

Female $C5_{def}$ mice were evaluated for their metabolic phenotype. When put on HFD for 6 weeks, $C5_{cont}$ mice gained more weight than $C5_{def}$ (**Figure 35A**). The $C5_{def}$ on HFD displayed a slight decrease in lean mass compared to $C5_{cont}$ (**Figure 35B**), but no statistically significant differences in AT mass (**Figure 35C**). Importantly, similar to the males (**Figure 23A**), $C5_{def}$ mice on LFD had impaired glucose tolerance ($p<0.01$, AUC) that was exacerbated on HFD ($p<0.001$, AUC, **Figure 35D**). The liver of female $C5_{def}$ animals also displayed reduced INSR-β expression and presence of the pro-INSR double band (**Figure 35E**).

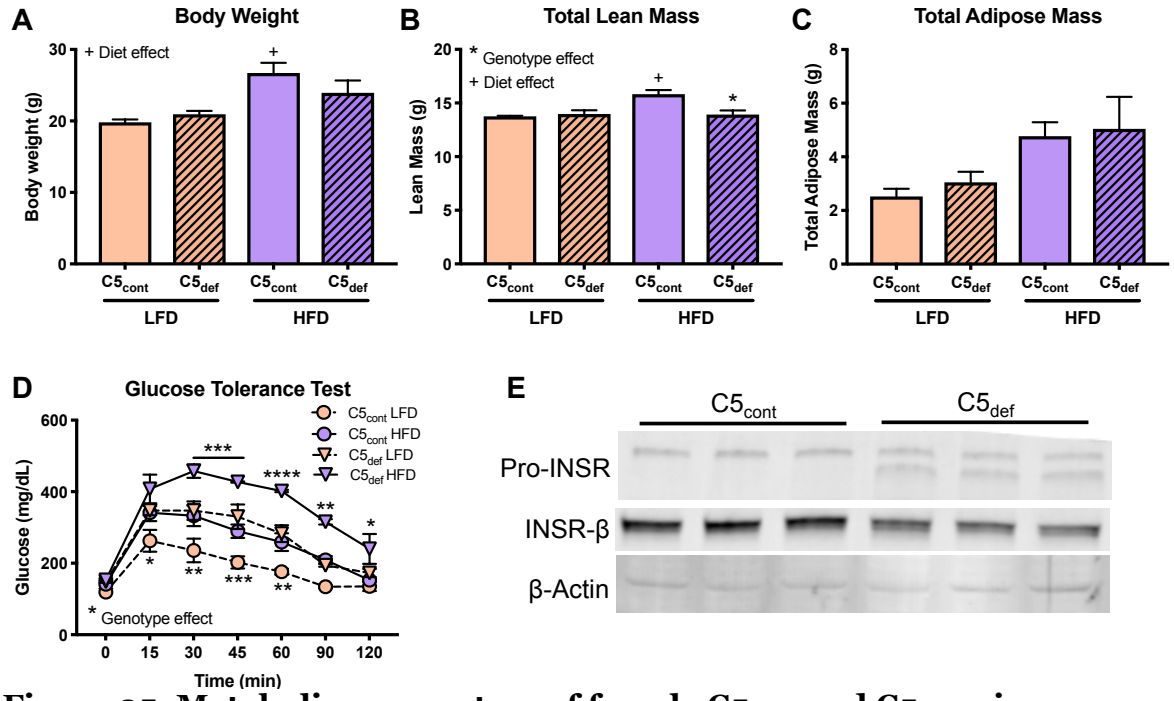

Figure 35. Metabolic parameters of female $C5_{cont}$ and $C5_{def}$ mice
Female C5 control ($C5_{cont}$) and C5 deficient ($C5_{def}$) mice were placed on LFD or HFD for 6 weeks. A) Body weight. B) Total lean mass and C) total adipose tissue mass as measured by NMR. D) Glucose tolerance test. E) Western blot analysis of liver pro-INSR and INSR-β. β-actin was used as a protein loading control. Data are presented as mean ± SEM of 3-4 mice per group, and were analyzed by two-way ANOVA with multiple comparisons, with repeating measures for GTT.
* $p<0.05$; ** $p<0.01$; *** $p<0.001$; **** $p<0.0001$ (genotype effect)
+ $p<0.05$ (diet effect)

Phenotype of C5 heterozygous mice

$C5_{cont}$ female and $C5_{def}$ male mice were bred to generate C5 heterozygous ($C5_{het}$) mice. Male mice of each genotype were fed HFD for 6 weeks, after which there were no observed differences in body weight, lean mass, or AT mass between groups (**Figure 36A-C**). Glucose tolerance tests revealed that $C5_{het}$ mice had the same degree of glucose intolerance as $C5_{def}$ mice ($p<0.05$, AUC, **Figure 36D**). The liver of $C5_{het}$ mice displayed reduced expression of INSR-β and the pro-INSR double band, similar to the $C5_{def}$ (**Figure 36E**).

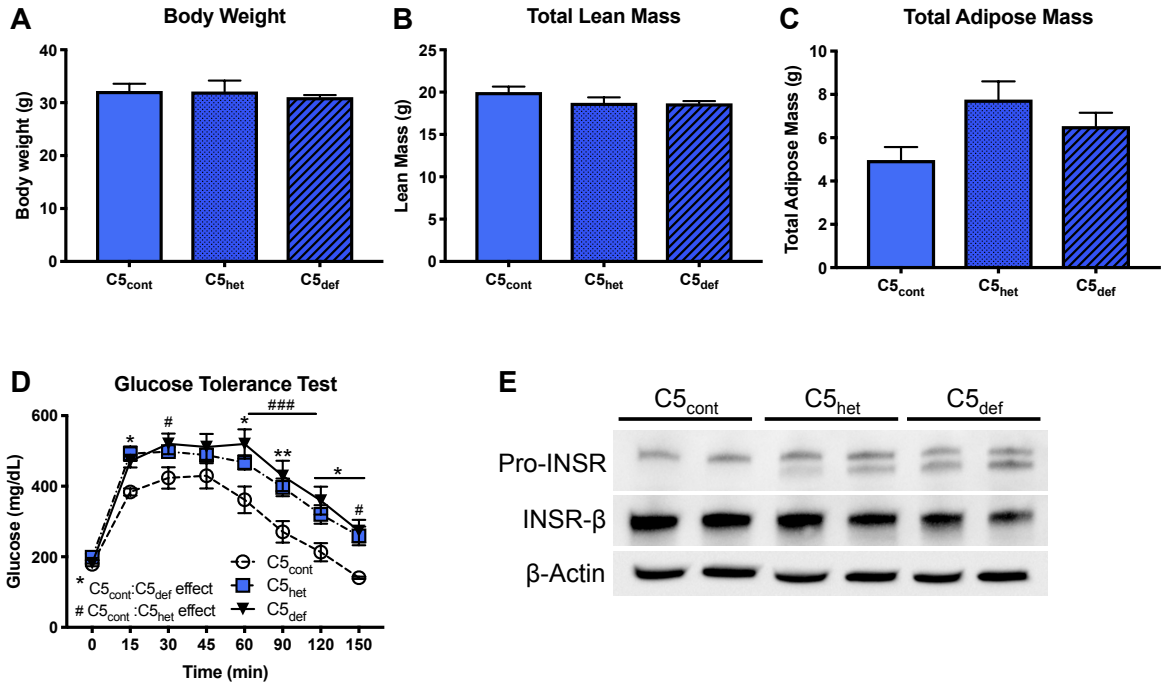

Figure 36. Metabolic parameters of $C5_{het}$ mice

C5 control ($C5_{cont}$), C5 heterozygous ($C5_{het}$), and C5 deficient ($C5_{def}$) mice were placed on HFD for 6 weeks. A) Body weight. B) Total lean mass as measured by NMR C) Total adipose tissue mass as measured by NMR. D) Glucose tolerance test. E) Western blot analysis of pro-INSR and INSR-β from liver of $C5_{cont}$, $C5_{het}$, and $C5_{def}$ mice. β-actin was used as a protein loading control. Data are presented as mean ± SEM of 4-5 mice per group, and were analyzed by two-way ANOVA with multiple comparisons, with repeating measures for GTT.

*,# $p<0.05$; **,## $p<0.01$; ***, ### $p<0.001$

Pro-INSR processing is not disrupted in other C5 deficient mouse models

The $C5_{def}$ Jackson Laboratory mouse characterized in these studies (B10.D2-*Hc^{o}H2^{d}H2-T18^{c}*/oSnJ) is one of several known mouse models deficient for C5. To rigorously assess the impact of C5 deficiency on INSR processing, seven other C5 deficient mouse models were obtained from Jackson Laboratory in order to determine whether mis-processed pro-INSR was present in all C5 deficient models. Western blot analysis was used to evaluate the INSR in livers from the mice. Surprisingly, none of the other C5 deficient models displayed the misprocessed pro-INSR or decreased INSR-β protein (**Figure 37**). Two of these mouse lines, AKR/J and DBA/2J (designated with * in the figure), have the same 2 base-pair deletion as the $C5_{def}$ mouse in these studies, but did not show any changes in INSR protein compared to C57BL/6J wildtype or $C5_{cont}$ mice.

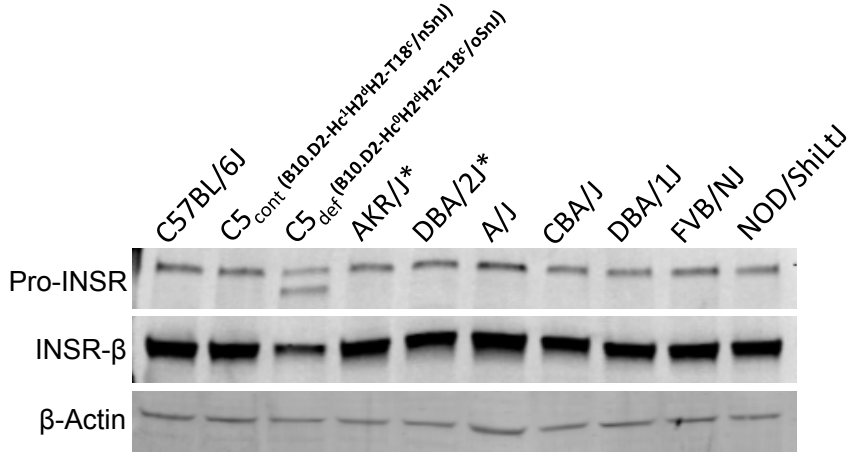

Figure 37. Pro-INSR processing in other C5 deficient mouse models
Western blot analysis of pro-INSR and INSR-β from liver of C57BL/6J, $C5_{cont}$, $C5_{def}$, AKR/J, DBA/2J, A/J, CBA/J, DBA/1J, FVB/NJ, and NOD/ShiLtJ mice. β-actin was used as a protein loading control. * denotes the same 2 base-pair deletion as $C5_{def}$.

Genetic analysis of the insulin receptor gene in $C5_{cont}$ and $C5_{def}$ mice

With the novel information that C5 deficiency alone cannot account for the metabolic phenotype of the $C5_{def}$ mice, whole genome sequencing was performed to determine whether there is a genetic basis for the INSR processing phenotype. Genomic DNA was isolated from liver of $C5_{cont}$ and $C5_{def}$ mice and sequenced. The 2-base pair mutation in Exon 6 of the *C5* gene in $C5_{def}$ was confirmed (**Figure 38**). Next, the *Insr* gene was analyzed for genetic variation. While there were no differences observed in the exons, we discovered a 31 base-pair deletion in the intronic region just upstream of Exon 2 (**Figure 39**).

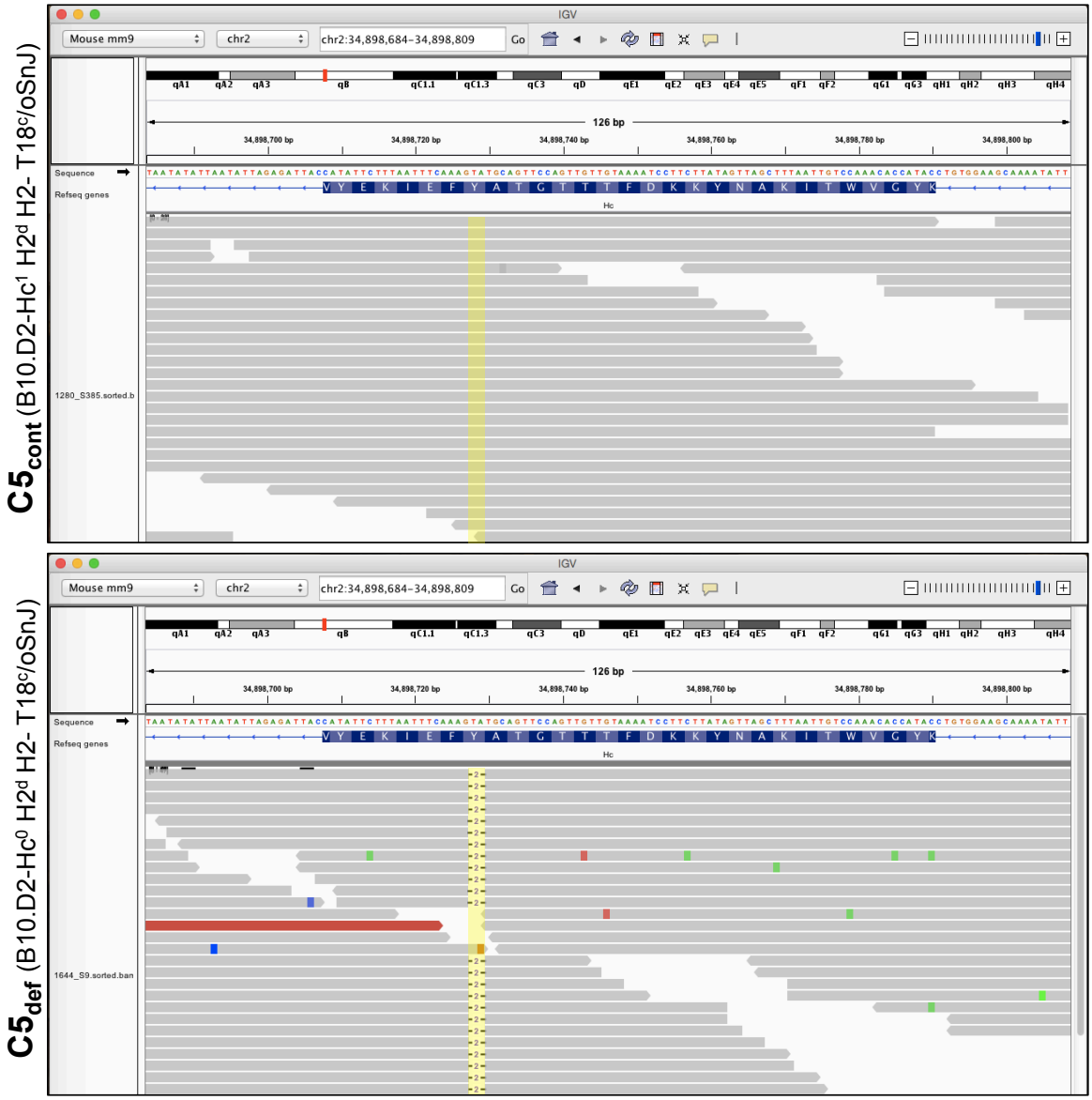

Figure 38. Genetic analysis of the *Hc* gene in $C5_{cont}$ and $C5_{def}$ mice
Integrative Genomics Viewer (IGV) screenshots from the *Hc* ($C5$) gene sequences across reads from FASTQ files generated by whole genome sequencing of $C5$ control ($C5_{cont}$) and $C5$ deficient ($C5_{def}$) murine liver. The top image shows a representative $C5_{cont}$ sample, and the bottom shows a representative $C5_{def}$ sample. The yellow rectangular shading denotes the location of the 2 base-pair deletion in Exon 6 of *Hc* in $C5_{def}$ mice. Other shading is a reflection of read attributes within the IGV software. Data are representative of 3 per group.

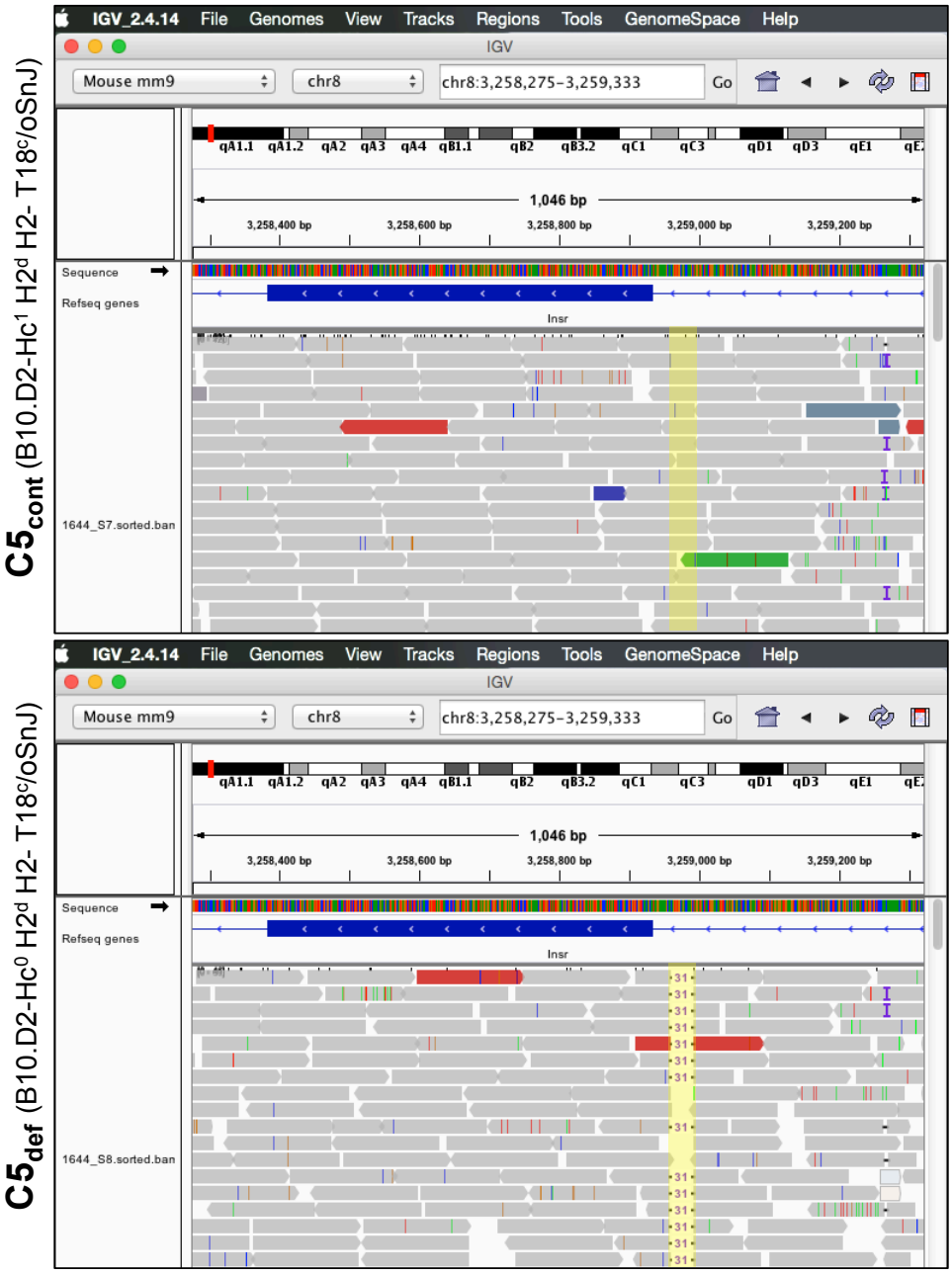

Figure 39. Genetic analysis of the insulin receptor gene in $C5_{cont}$ and $C5_{def}$ mice

Integrative Genomics Viewer (IGV) screenshots from the *Insr* gene sequences across reads from FASTQ files generated by whole genome sequencing of C5 control ($C5_{cont}$) and C5 deficient ($C5_{def}$) murine liver. The images on the left side show n=3 $C5_{cont}$ samples, and n=3 $C5_{def}$ samples on the right. The yellow rectangular shading denotes the location of the 31 base-pair deletion in an intronic region of the *Insr* gene in $C5_{def}$ mice. Other shading is a reflection of read attributes within the IGV software.

Forced C5 expression enhances glucose homeostasis and insulin sensitivity

To determine the contribution of INSR insufficiency versus C5 deficiency to the IR noted in $C5_{def}$ mice, we provided exogenous human C5 by systemic adenoviral (Ad) transfection. LFD-fed $C5_{cont}$ and $C5_{def}$ mice received an injection of either control (AdGFP) or human C5 (AdC5) adenovirus. During a hyperinsulinemic-euglycemic clamp, blood glucose concentrations were appropriately clamped so there were no differences between AdGFP and AdC5-treated mice regardless of genotype (**Figure 40A-B**). Adenoviral delivery of C5 increased the glucose infusion rate required to maintain euglycemia in both $C5_{cont}$ mice ($p<0.01$, **Figure 40C**) and $C5_{def}$ animals ($p<0.001$, **Figure 40D**).

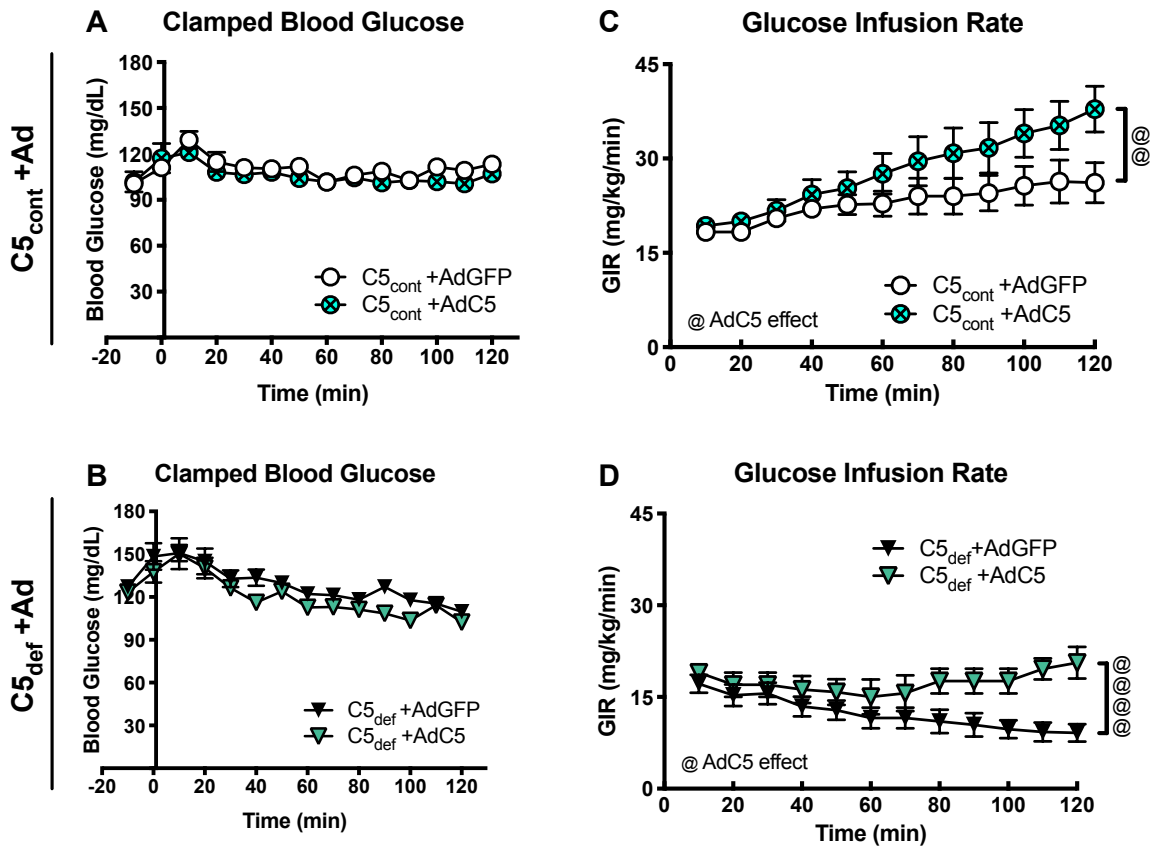

Figure 40. *In vivo* C5 delivery and insulin sensitivity via hyperinsulinemic-euglycemic clamp

C5 control ($C5_{cont}$) and C5 deficient ($C5_{def}$) mice were maintained on LFD for 14-16 weeks and received a single injection of adenoviral vector for control (AdGFP) or C5 (AdC5) four weeks prior to hyperinsulinemic-euglycemic clamps. A-B) Arterial blood glucose and C-D) glucose infusion rate during a hyperinsulinemic-euglycemic clamp. Data are presented as mean ± SEM of 5-7 mice per group. Curves were analyzed by two-way ANOVA with multiple comparisons and repeated measures.

@@ $p<0.01$; @@@@ $p<0.0001$ (AdC5 effect)

Basal insulin concentrations were higher in $C5_{def}$ compared to $C5_{cont}$ mice as expected (**Figure 41B** vs. **41A**), but were not affected by AdC5 treatment in either genotype. During the clamp, plasma insulin levels trended toward a decrease in AdC5 compared to AdGFP in both genotypes ($C5_{cont}$; p=0.08, **Figure 41A**) and ($C5_{def}$; p=0.07, **Figure 41B**). Relative to basal conditions, administration of AdC5 to $C5_{cont}$ mice attenuated insulin suppression of endoRa (**Figure 41C**). In contrast, AdC5 administration to $C5_{def}$ mice did not impair insulin suppression of endoRa ($p<0.01$, **Figure 41D**). The rate of glucose disappearance during the clamp was heightened in $C5_{def}$+AdC5 mice, while $C5_{cont}$+AdC5 animals showed a non-significant increase (**Figure 41E-F**).

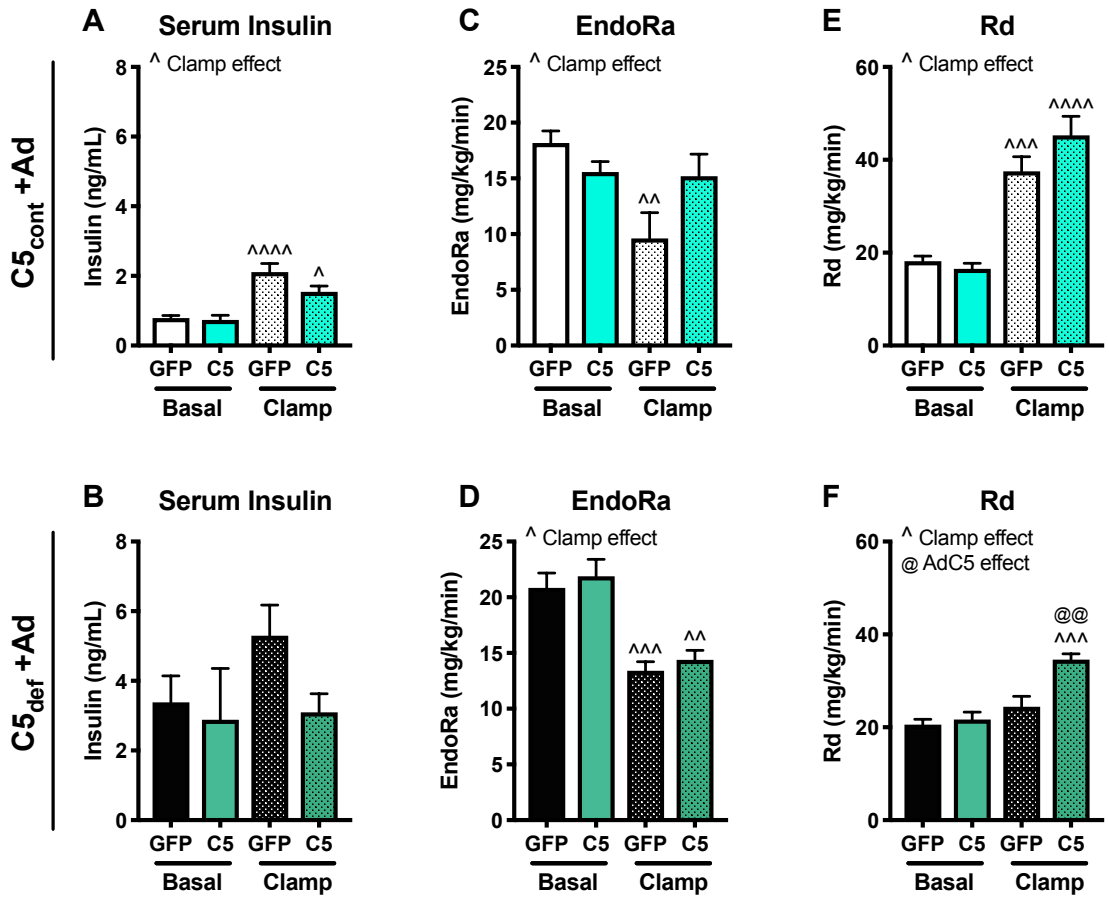

Figure 41. *In vivo* C5 delivery and insulin sensitivity via hyperinsulinemic-euglycemic clamp

C5 control ($C5_{cont}$) and C5 deficient ($C5_{def}$) mice were maintained on LFD for 14-16 weeks and received a single injection of adenoviral vector for control (AdGFP) or C5 (AdC5) four weeks prior to hyperinsulinemic-euglycemic clamps. Basal and clamp period A-B) plasma insulin, C-D) endoRa, and E-F) and whole body glucose disappearance Rd. Data are presented as mean ± SEM of 5-7 mice per group, and were analyzed by two-way ANOVA with multiple comparisons.

@@ $p<0.01$ (AdC5 effect)

^ $p<0.05$; ^^ $p<0.01$; ^^^ $p<0.001$; ^^^^ $p<0.0001$ (clamp effect)

Relative to respective AdGFP controls, $C5_{cont}$+AdC5 and $C5_{def}$+AdC5 animals showed increased glucose uptake specifically in BAT ($p<0.05$, **Figure 42A-B**); whereas, glucose disposal in the heart was also increased in $C5_{def}$+AdC5 mice ($p<0.05$, **Figure 42B**).

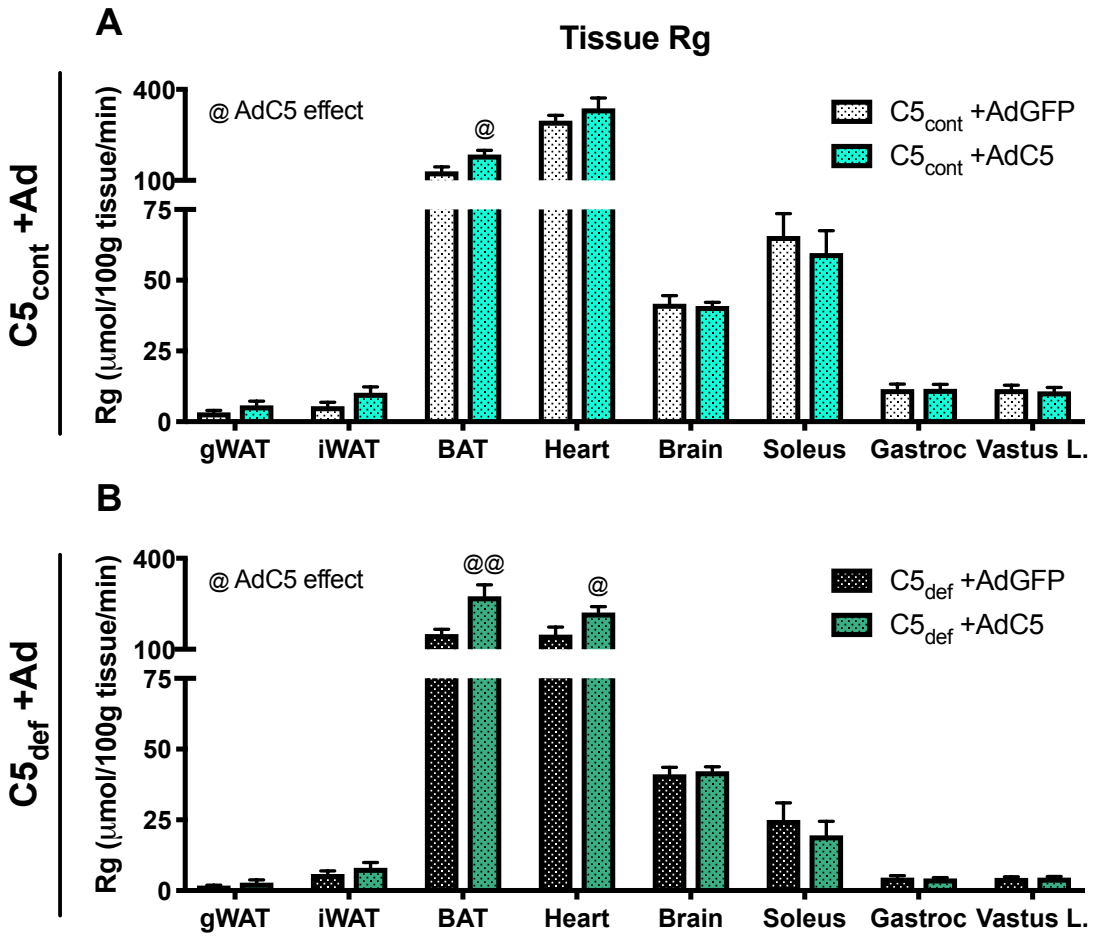

Figure 42. *In vivo* C5 delivery and insulin sensitivity via hyperinsulinemic-euglycemic clamp

C5 control ($C5_{cont}$) and C5 deficient ($C5_{def}$) mice were maintained on LFD for 14-16 weeks and received a single injection of adenoviral vector for control (AdGFP) or C5 (AdC5) four weeks prior to hyperinsulinemic-euglycemic clamps. A-B) Tissue specific glucose (Rg) uptake during clamp. Data are presented as mean ± SEM of 5-7 mice per group, and were analyzed by student's t test with multiple comparisons. @ $p<0.05$; @@ $p<0.01$ (AdC5 effect)

Together, these findings indicate that the IR in the $C5_{def}$ B10.D2-*Hc^{o} H2^{d} H2-T18^{c}*/oSnJ mice is indeed driven by the INSR mutation, and also show that forced expression of C5 improves insulin sensitivity irrespective of whether endogenous C5 is present and even on a background of extreme IR.

Discussion

Our studies aimed to elucidate the role of C5 in metabolic disease by utilizing the Jackson Laboratory $C5_{def}$ mouse, but have instead revealed a novel metabolic phenotype of the $C5_{def}$ B10.D2-*Hc^{0} H2^{d} H2-T18^{c}*/oSnJ strain that may be caused by a genetic alteration in the *Insr* gene. While unexpected, these results expose a novel mouse model for studying IR, and provide a previously unreported phenotype of the Jackson Laboratory $C5_{def}$ mouse with implications for other investigations that have utilized this model. Although the IR phenotype of the $C5_{def}$ model was driven by the *Insr* mutation, adenoviral delivery of human C5 improved insulin action in lean $C5_{cont}$ and $C5_{def}$ mice, suggesting that C5 does indeed have insulin sensitizing actions. Further work, beyond the scope of this study, will need to be performed to validate this observation.

$C5_{def}$ mice display an obesity- and inflammation-independent insulin resistant phenotype. Notwithstanding the lack of inflammation, $C5_{def}$ mice manifest severe IR characterized by glucose intolerance, hyperinsulinemia, and blunted insulin-mediated glucose disposal. These disturbances in glucose metabolism occur regardless of obesity, such that $C5_{def}$ mice fed a LFD display the same degree of glucose intolerance as HFD-fed $C5_{cont}$ animals. This remarkable degree of IR in $C5_{def}$ mice phenocopy several different tissue-specific INSR knockout mice, but unlike global INSR knockout mouse models, these mice are viable. For example, the dwarfing phenotype mimics disrupted INSR signaling during development, where the INSR is required for IGF-2 signaling to promote lean mass growth [139]. Additionally, the ~30% reduction in total fat mass and ~70% reduction in liver triglycerides are consistent with deficient INSR signaling

in AT and liver, as similar phenotypes were observed in mice with fat and liver-specific INSR deficiency [140, 141].

Several parameters were tested to determine a mechanism for the observed systemic IR of $C5_{def}$ mice. While ER and oxidative stress was unaffected in the liver, insulin-stimulated, AKT phosphorylation was impaired in liver and AT of $C5_{def}$ mice (**Figure 23**). Interestingly we did not detect impaired Akt signaling in skeletal muscle of the $C5_{def}$ mice. This result is similar to that obtained for the muscle-specific *Insr* knockout mouse where signaling downstream of IGF-1R was shown to play an important compensatory role in muscle [142]. Differential processing of pro-INSR was observed in metabolic tissues of the $C5_{def}$ mice (**Figure 33**). Further studies are needed to characterize the structure of the observed 180kDa pro-INSR translation product, and this is discussed in more detail in Chapter 4 of this Dissertation. Thus, we have shown that $C5_{def}$ mice have impaired INSR processing, decreased INSR mRNA and protein expression, and blunted INSR signaling, likely accounting for the observed glucose intolerance and severe systemic IR in this model.

The phenotype of the $C5_{het}$ mice (**Figure 36**) also presents potentially interesting genetics associated with the $C5_{def}$ mice. The glucose intolerance of the $C5_{het}$ mice mirrored that of the $C5_{def}$, suggesting a dominant negative expression pattern. Leprechaunism and Rabson-Mendenhall syndrome and other inherited forms of IR are difficult to diagnose, but human studies have characterized many associated mutations [143-147]. Often, these mutations occur in the tyrosine kinase domain of the protein and act dominantly, possibly by forming hybrid dimers [145, 147] or by sequestering IRS-1 substrate [148]. The only mutation we detected in the

INSR of the $C5_{def}$ B10.D2-*Hc^{o} H2^{d} H2-T18^{c}*/oSnJ mice was in an intronic region, leading to a truncated protein. The mechanism by which this truncation causes IR in a dominant negative fashion is an area of future investigation as it may prove to be relevant to human disease as well, and is discussed further in Chapter 4 of this Dissertation.

With the elucidation of the extreme IR in the Jackson Laboratory B10.D2-Hc0H2dH2-T18c/oSnJ $C5_{def}$ mice, it is important to recognize that these mice have been used extensively in many fields of study – fields in which IR could influence disease outcomes. As expected, $C5_{def}$ mice have been used in studies of bacteriology and pathogenesis, but it is now appreciated that IR in humans is associated with a higher incidence of infection and associated complications, especially in diabetic patients [149, 150]. In addition to the inflammation-specific applications of this mouse model, it has also been used to investigate the role of C5 in areas less traditionally associated with innate immunity. For example, Ehrnthaller *et al.* studied the role of complement in fracture healing by evaluating C3-/- and $C5_{def}$ mice. They reported that C5 is required for proper healing [151], but it is well known that diabetic subjects are at higher risk for bone fracture, and that their healing processes are impaired [152]. Additionally, Pasinetti *et al.* reported that C5 influences glutamatergic neurotransmission and neurodegenerative disease [153], but it has also been shown that diabetes influences the genetic basis of glutamatergic signaling [154]. Thus, the insulin resistant phenotype of the $C5_{def}$ mice may introduce variables that were not previously appreciated in investigations that have used this mouse line.

Although mutation of the INSR in the $C5_{def}$ mice likely accounts for the insulin resistant phenotype, our studies reveal that adenoviral delivery of C5 enhances insulin sensitivity and improves glucose homeostasis. This notable finding indicates that C5 is an important regulator of metabolic function that is not fundamentally linked to insulin signaling. Interestingly, as early as 1979 it was discovered that C5a can induce the uptake of deoxyglucose in neutrophils by as much as 700% [103]. The authors suggested that upon activation of complement, immune cells require a burst of energy and thus, the cells must have a way to regulate their glucose uptake. Because neutrophils don't upregulate glucose uptake in response to insulin, the authors put forth the titillating hypothesis that "C5a might have developed phylogenetically as an 'insulin' for phagocytes [103]." A similar induction of glucose uptake in eosinophils has also been reported [104], and it was published that C5a and C3a have insulin-like effects on 3T3-L1 adipocytes [155]. Thus, our *in vivo* adenoviral studies extend what has previously been shown *in vitro* and reinvigorates the novel idea that C5 has beneficial effects on metabolic homeostasis.

Conclusions

It is now well-established that the inflammatory state of the AT and other metabolic organs is an important determinant of disease phenotypes associated with the onset and progression of obesity. The complement system is intricately involved in inflammation and associated metabolic disease, but C5 specifically has also been shown to have metabolically beneficial effects by promoting glucose uptake. These connections, as well as our data showing increased *Hc* expression in

diet-induced obese mice, led to the experiments shown here asking how C5 deficiency influences metabolism. Our data show that the B10.D2-*Hc*^{o}*H2*^{d}*H2-T18*^{c}/oSnJ C5$_{def}$ mouse is severely insulin resistant, which is also associated with misprocessing of the INSR precursor, pro-INSR, due to a genetic deletion in an intronic region of the *Insr* gene. Furthermore, we show for the first time that forced expression of C5 improves insulin sensitivity, presenting an opportunity to further investigate the therapeutic potential of C5 on insulin action and glucose homeostasis.

CHAPTER 4

DISCUSSION AND FUTURE DIRECTIONS

The immunophenotype of brown adipose tissue

It is well-appreciated that immune cells and the cytokines they secrete and signal through contribute to WAT homeostasis, and that this microenvironment changes with the onset and progression of obesity. In contrast to the lipid storage role of WAT, BAT can burn lipid through thermogenesis. These AT depots have very different functions, and as such, our data presented in Chapter 2 are not particularly surprising in highlighting not only the very low numbers of immune cells in BAT, but also the obesity-driven changes that do not align with WAT literature. There have not been many studies that characterize BAT immune cells since the publication of my manuscript detailed in Chapter 2. A review article from 2018 [156] summarized the field's knowledge of immune cells in BAT by describing changes in cytokine gene expression rather than actual cell numbers, as we performed in [89]. There is evidence that brown adipocytes are also capable of secreting cytokines such as TNF-α and IL-6 [157], so gene expression alone is not an appropriate method by which cell population discoveries are made. Since my study, flow cytometry has not been used to characterize the BAT SVF; however, there have been advances for its use in adipocyte studies [158, 159]. These methods will be helpful for future studies in this field because it will allow for more detailed analysis of AT cells, regardless of depot. Historically, adipocytes have been separated from the SVF by buoyancy, and the entire floating fraction is evaluated as one entity. Histological studies have shown that AT does not necessarily change

in a uniform way with disease onset and progression though, so it will be interesting to have a molecular tool to further evaluate adipocytes in ways similar to the SVF. Furthermore, histology of beiged AT also shows a spectrum of changes over time of treatment (i.e. cold exposure), and these studies will benefit from more advanced adipocyte characterization.

Concomitantly with the field's shift of focus to the adipocytes in BAT and beige AT is a shift in the literature discussing the role of immune cells in thermogenesis. One paper that sparked the studies presented in Chapter 2 showed alternatively activated macrophages as producers of catecholamines that can activate thermogenesis [96]. This discovery was had vast implications because macrophages are so intricately involved with AT homeostasis. One may propose that these macrophages could be targeted to produce norepinephrine locally in order to initiate thermogenesis. Unfortunately, these findings have since been disputed and the alternative findings were published not long before our article in *Obesity* (Chapter 2) [93]. Hence, the focus in the field has since returned to understanding the different types of adipocytes and how to therapeutically alter their phenotype, potentially in UCP1-independent ways [160].

The role of complement in metabolism

The studies presented in Chapter 3 showed that the Jackson Laboratory B10.D2-*Hc^{o} H2^{d} H2-T18^{c}*/oSnJ $C5_{def}$ mice are severely insulin resistant, but this is attributed to an INSR defect, rather than C5 deficiency alone. This was an unexpected finding that has made the necessity of a novel mouse model of C5 deficiency obvious, but there are still further investigations necessary in the $C5_{def}$

mice. Namely, the Pro-INSR misprocessing and INSR genetics of the $C5_{def}$ mice may be applicable to IR research in general. It is also of upmost importance to ask our original question about the role of C5 deficiency in metabolism using a model that does not have these confounding factors. This will allow for further mechanistic analyses about the role of C5 and other complement proteins in the realm of metabolism. Each of these areas will be discussed in detail below.

Pro-INSR is misprocessed in $C5_{def}$ mice

Metabolic tissues from $C5_{def}$ mice exhibit a second band of lower molecular weight for the INSR translation product, Pro-INSR, when analyzed by western blot (**Figure 33**). Such data typically indicates two versions of the protein that have been processed differently during protein maturation. Posttranslational processing occurs in the endoplasmic reticulum and/or Golgi. Typically, if a protein is not properly glycosylated, the consequence is decreased mature receptor at the membrane because of improper protein folding, as seen in **Figure 31**.

In preliminary work, a PNGase F assay was used to determine whether there were differences in N-linked glycosylation between the normal single band in $C5_{cont}$ animals and the lower band from $C5_{def}$ (**Figure 43**). PNGase F removes N-linked glycosylation from the protein, so if different degrees of glycosylation are the difference between the two bands, both bands should shift lower to become one single non-glycosylated Pro-INSR. In contrast, the data show that both $C5_{def}$ bands migrate, confirming that N-linked glycans were removed, but two distinct bands remained, indicating additional modifications exist between the bands. Additionally, the active subunit of INSR, INSR-β, also showed a double band in

$C5_{def}$ samples after PNGase F treatment. Further studies to uncover the differences between the bands could utilize mass spectrometry, but protein purity may be problematic without different antibodies specific to each band.

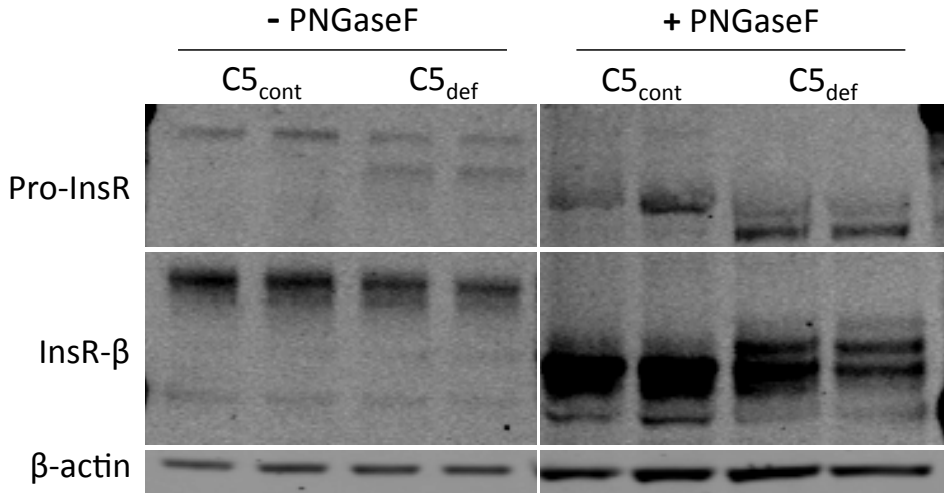

Figure 43. Glycosylation analysis by PNGase F assay
Western blot analysis of liver from C5 control ($C5_{cont}$) and C5 deficient ($C5_{def}$) treated with (+) and without (-) F-glycosidase (PNGase F) treatment to remove N-linked glycosylation. Pro-INSR and INSR-β are indicated, and β-actin was used as a loading control.

Nonetheless, these data show that $C5_{cont}$ and $C5_{def}$ Pro-INSR have differential N-linked glycosylation, as well as other modifications. Such modifications may include addition of fatty acids by amide or ester linkages [161]. Because the $C5_{def}$ mice present with such a remarkable alteration in posttranslational processing of InsR, we expect that this would also lead to altered expression at the cell surface, which could be measured by biotinylation or radioligand binding assays. This is interesting as it has been shown that mice with a tissue specific deletion of InsR in liver [141], pancreas [162], and brain [163] exhibit phenotypes that mirror our $C5_{def}$ mice including elevated plasma insulin levels and IR. Given the improper InsR processing that occurred in the tissues of $C5_{def}$ mice, it is not surprising that they

have a metabolic phenotype similar to various tissue specific InsR knockout models.

Genetic defect in the insulin receptor gene of $C5_{def}$ mice

Whole genome sequencing analysis of liver from $C5_{cont}$ and $C5_{def}$ mice revealed an intronic 31 base pair deletion in the *Insr* gene of the $C5_{def}$ animals (**Figure 39**). While this particular defect has not been previously reported, there are many known *Insr* mutations in humans with T2D or severe inherited IR [143, 164-170]. Most of the known mutations occur in the portion of the gene that codes for the tyrosine kinase domain, exons 17-21 (**Figure 44**), but some have also been shown in intronic regions throughout the gene [171-173]. The relative location of our discovered deletion in the intronic region near exon 2 is indicated in Figure 44 with a red arrow.

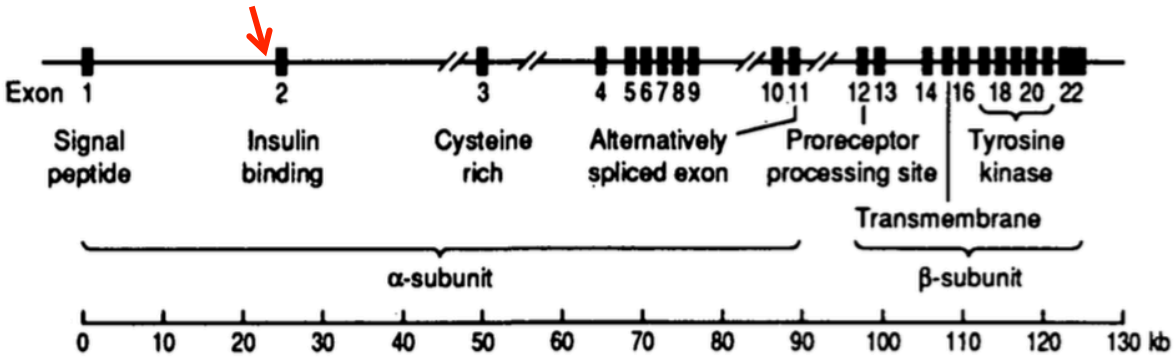

Figure 44. *Insr* gene map
Adapted from Olefsky, Diabetes (1990) [174]
The 22 exons and their functional protein domains in the insulin receptor (*Insr*) gene are shown as labeled. The red arrow indicates the relative location of the intronic 31 base pair deletion we discovered in C5 deficient ($C5_{def}$) mice.

Alternative splicing is known to occur in the *Insr* gene, most notably via excision of exon 11 to form two INSR isoforms with variable insulin action and

function [175-177]. Because the $C5_{def}$ *Insr* deletion was in the intronic region between exons 1 and 2, we aimed to determine whether this led to a splicing event that affected the flanking exons. Primers were designed to amplify these exons by polymerase chain reaction (PCR) so that we could determine whether transcription was affected. The data show an expected decrease in mRNA expression in the $C5_{def}$ exons (similar to **Figure 29**), but do not show band size differences between $C5_{cont}$ and $C5_{def}$ (**Figure 45**). This indicates that the *Insr* mutation did not alter exons 1 or 2 at the transcriptional level. It is possible that other areas of the gene may be affected, but further analysis by PCR and/or Northern Blot would be required.

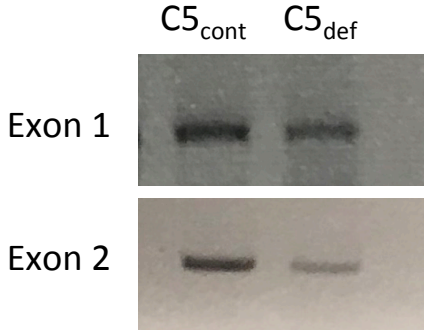

Figure 45. Gel electrophoresis of *Insr* exons 1 and 2
mRNA from liver of C5 control ($C5_{cont}$) and C5 deficient ($C5_{def}$) mice was isolated and reverse transcribed to cDNA. Polymerase chain reaction was used to amplify exons 1 and 2 from the *Insr* gene via gel electrophoresis on a 1% agarose gel visualized by ethidium bromide.

Interestingly, several N-linked glycosylation sites are located in the INSR α-subunit that is coded for in exon 2 [178]. While the mutation in $C5_{def}$ mice may not affect splicing or transcription, it is possible that the deletion affects nearby glycosylation, which could also explain the Pro-INSR double band observed in **Figure 33**. Further *in vitro* and biochemical analyses are necessary fully understand the consequence of the *Insr* mutation observed in $C5_{def}$ mice.

Utilization of CRISPR technology for a novel mouse model of C5 deficiency

With the knowledge that the Jackson Laboratory $C5_{def}$ mouse also has a 31 base pair deletion in an intronic region of the INSR gene, it is necessary to ask how C5 deficiency influences systemic metabolism in a cleaner mouse model. Accordingly, we worked with the Vanderbilt Genome Editing Resource to utilize CRISPR-Cas9 editing technology to generate an *Hc* (*C5*) knockout mouse via deletion of Exon 3 from C57BL/6J mice. Upon injection of 92 embryos, 76 implanted, and 11 live births occurred. Four mice (1 female, 3 males) had the deletion of Exon 3 and are currently being bred with C57BL/6J wildtype animals to expand the colony for evaluation. In caution of off-target effects from the CRISPR-Cas9 system, each knockout animal's colony will be kept separate until initial characterization. Although unlikely, if there are differences in phenotypes between the knockout lines, this will provide evidence of off-target effects and genetic variation outside of the *Hc* gene.

Mechanisms by which C5 improves insulin action

While the INSR defect in the $C5_{def}$ mice certainly confounded the questions addressed in Chapter 3, adenoviral delivery of C5 improved insulin sensitivity in both the insulin resistant $C5_{def}$ and healthy $C5_{cont}$ mice (**Figures 40-42**). These data show metabolically beneficial effects of C5, and lead us to hypothesize that the Hc (C5) CRISPR-Cas9 knockout mice will have worsened systemic metabolism than controls. There are other hints in the literature that support this premise as well. For example, and as mentioned in the Discussion of Chapter 3, C5 has been shown to induce glucose uptake. Delving deeper into a potential mechanism

behind these effects requires a closer look at the C5 signaling pathway (**Figure 46**).

C5 receptors and metabolism

There are two known receptors for C5a, C5aR1 and C5aR2 (also called C5L2). Both are expressed on many immune [179] and non-immune cells, including adipocytes and hepatocytes [180]. C5aR1 was discovered in 1991 as a $G_{\alpha i}$ or $G_{\alpha 16}$-coupling GPCR with high binding affinity to C5a [181-186]. In contrast, C5aR2 has been shown to bind C3a, $C3a_{desArg}$, C5a, and $C5a_{desArg}$, with highest affinity to the latter two [187, 188]. Like C5aR1, C5aR2 is a seven-transmembrane receptor, but studies suggest that binding does not lead to G-protein coupling, and it has been thought to be a decoy receptor for C5aR1 [187-189].

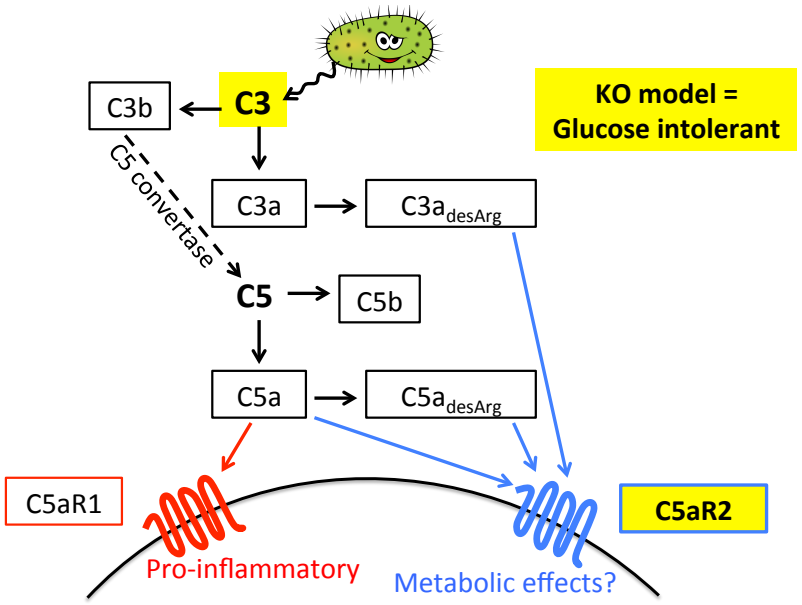

Figure 46. C5 signaling pathway

C3, C3aR, C5aR1, and C5aR2 knockout mice have been generated and evaluated for their metabolic phenotype. As expected, C3aR and C5aR1 knockout mice show decreased inflammation and protection against IR [107, 190],

presumably due to dampened inflammatory responses. In contrast, both $C3^{-/-}$ and $C5aR2^{-/-}$ have a phenotype of elevated plasma insulin and decreased glucose tolerance [191-193]. Given that $C3^{-/-}$ mice also lack C3a, $C3a_{desArg}$, C5a, C5b, and $C5a_{desArg}$, the results obtained in these two models could be a consequence of absence of signaling through C5aR2. Interestingly, studies also show that polymorphisms in C5aR2 are associated with T2D in humans [194], suggesting an important role for C5aR2 in metabolism.

In addition to what is known about C5's ability to influence glucose uptake, HEK cells made to over-express C5aR2 have enhanced glucose uptake in response to $C3a_{desArg}$ [195] and antibody neutralization of C5aR2 has been shown to increase blood glucose levels after a fat load (indicating reduced glucose uptake) [102]. In fact, most of the work on complement and adipose-related metabolism has been on $C3a_{desArg}$ (also called acylation stimulating protein, ASP), showing its role in glucose uptake [196, 197], TG synthesis [198, 199], adipocyte differentiation [200], postprandial TG clearance [201], and insulin secretion [202]. Recent evidence also suggests that in response to $C3a_{desArg}$, C5aR2 can be phosphorylated, and subsequently signal through Akt and ERK1/2, leading to glucose uptake and TG synthesis [195, 203].

Thus, the current literature shows that C5a or $C3a_{desArg}$ treatment stimulates glucose uptake in a way similar to insulin action on metabolic cells, and that the receptor for these mediators, C5aR2, is necessary for proper metabolic action *in vivo*. The studies presented in Chapter 3 show that adenoviral delivery of C5 improves insulin action (**Figures 40-42**). *Based on these observations, we propose the novel hypothesis that C5a mediates inflammatory effects via C5aR1*

while C5a$_{desArg}$ mediates metabolic benefits via C5aR2 (**Figure 45**). Future studies will test this hypothesis by administration of C5a$_{desArg}$ in the Hc (C5) knockout CRISPR-Cas9 mice to determine if this assumed inactive protein can improve insulin sensitivity *in vivo*. Furthermore, *in vitro* studies can be utilized to isolate parts of the C5 signaling pathway and determine whether C3a$_{desArg}$ and/or C5a$_{desArg}$ signaling specifically via C5aR2 leads to the metabolic effects.

Conclusion

This Dissertation details my contributions to the field of Immunometabolism, specifically in the areas of BAT immune cells and the role of C5 in insulin action. I discovered B cells in BAT and showed that the numbers of these cells, as well as macrophages and eosinophils, change in change in response to HFD-induced obesity, but not during aging (Chapter 2). I also revealed that the Jackson Laboratory mouse model of C5 deficiency has a phenotype of severe IR that may be attributed to a genetic variant in the *Insr* gene. Additionally, adenoviral C5 delivery showed that C5 has beneficial effects on systemic insulin action (Chapter 3). Many questions remain in these areas, and it will be interesting to see where the trajectory of these studies goes next.

APPENDIX

MACROPHAGE-TARGETED THERAPEUTICS FOR METABOLIC DISEASE

This Appendix were adapted from
a review article published in *Trends in Pharmacological Sciences* titled,
Macrophage-Targeted Therapeutics for Metabolic Disease
written by Peterson, Cottam, Kennedy, and Hasty [204],

Abstract

Macrophages are cells of the innate immune system that are resident in all tissues, including metabolic organs such as the liver and adipose tissue. Because of their phenotypic flexibility, they play beneficial roles in tissue homeostasis, but they also contribute to the progression of metabolic disease. Thus, they are ideal therapeutic targets for diseases such as insulin resistance, non-alcoholic fatty liver disease, and atherosclerosis. Recently, discoveries in the area of drug delivery have facilitated phenotype-specific targeting of macrophages. In this review, we discuss advances in potential therapeutics for metabolic diseases via macrophage-specific delivery. We highlight micro- and nano-particles, liposomes, and oligopeptide complexes, and how they can be used to alter macrophage phenotype for a more metabolically favorable tissue environment.

Glossary

ATM (Adipose tissue macrophage): Macrophages in the adipose tissue.

CD163: A high affinity scavenger receptor for the hemoglobin-haptoglobin complex used to identify an M2-polarized macrophage marker.

CCL2, CCL3, and CCL5 (Chemokine (C-C motif) ligands 2, 3, and 5, respectively): Cytokine ligands involved in the recruitment of leukocytes.

CRISPR-Cas9: Bacterial-based immune defense that leads to destruction of specific genetic sequences. This can be delivered and utilized in other systems to silence target genes of interest.

GeRPs (β1,3-d-glucan-encapsulated siRNA particles): Yeast-derived glucan shells that encapsulate macrophage-targeted siRNA.

iNOS2 (Inducible nitric oxide synthase 2): An enzyme that produces reactive free radicals of nitric oxide when induced by a combination of cytokines and lipopolysaccharide.

IR (Insulin resistance): A condition in which cellular response to the hormone insulin is reduced, leading to dysfunctional glucose homeostasis.

IL-1β (Interleukin 1 beta): Pro-inflammatory cytokine produced by activated macrophages.

IL-4 (Interleukin 4): Anti-inflammatory cytokine produced by T cells that promotes alternative activation and inhibits classical activation of macrophages.

IL-6 (Interleukin 6): Pro-inflammatory cytokine produced by T cells and macrophages that stimulates an immune response.

IL-13 (Interleukin 13): Anti-inflammatory cytokine produced by T cells, basophils, and eosinophils that promotes alternative activation of macrophages.

IL-33 (Interleukin 33): Anti-inflammatory cytokine produced by macrophages and dendritic cells that drives production of other anti-inflammatory cytokines, including IL-4 and IL-13 by T cells.

Kupffer cells: Macrophages that are resident in the liver.

M1-like macrophage: Classically activated macrophage with a pro-inflammatory phenotype most often associated with host defense.

M2-like macrophage: Alternatively activated macrophage with an anti-inflammatory and pro-fibrogenic phenotype most often associated with tissue repair.

MMe (Metabolically active macrophages): Macrophages that are activated by metabolic growth factors and are resident to adipose tissue. They produce pro-inflammatory cytokines, but express markers that are more similar to M2-like macrophages, including ABCA1, CD36, and PLIN2.

MFe^{hi}: ATMs with high iron content that can recycle iron and display a M2-like phenotype.

M(Hb): Macrophages with unique phenotype resulting from uptake of haptoglobin-hemoglobin complexes.

Mhem: Macrophages with unique phenotype resulting from uptake of heme.

NAFLD (Non-alcoholic fatty liver disease): A class of liver disease characterized by fat deposition in the liver that is not associated with alcohol consumption.

ROS (Reactive oxygen species): Oxygen containing chemical species that are produced by cells at high levels in response to pathogens or inflammatory stimuli.

siRNA (Small interfering RNA): Gene silencing technology that interferes with transcription of genes.

SPIONs (Superparamagnetic iron oxide nanoparticles): Engineered tool that targets macrophages and was originally used for imaging techniques, but can also be targeted for delivery of compounds to M2-polarized macrophages.

TNF-α (Tumor necrosis factor alpha): Pro-inflammatory cytokine produced by macrophages and adipocytes that activates NF-κB and induces insulin resistance.

TACE (Tumor necrosis factor-α converting enzyme): Metalloproteinase that generates soluble TNF-α.

Y-BGs (Yeast-derived β-glucans): β-D-glucose polysaccharides extracted from the cell walls of *Saccharomyces cerevisiae* that have shown promise in altering obesity via IL-10 mediated effects.

Rationale for macrophages as therapeutic targets in metabolic disease

Cells of the immune system have important functions in health and disease. Their roles in autoimmune and inflammatory diseases are obvious; however, more recently, their contributions to cancer [205], cardiovascular disease [206, 207], and diabetes [65, 208, 209], have also been elucidated. Although all cells of the immune system can theoretically impact tissue homeostasis and contribute to disease, macrophages are particularly important to consider as therapeutic targets because they are resident in all tissues and show tremendous plasticity. Furthermore, they are phagocytic [210] and thus capable of endocytosing particles that are nanometers to micrometers in size. This review will focus on recent literature that shows the therapeutic potential of targeting macrophages in metabolic diseases as well as novel delivery systems being developed to capitalize on their phenotypic variability.

Contribution of macrophages to metabolic disease

Macrophages are historically understood for their role as recruited and differentiated monocytes that respond to acute infection as phagocytes and secretors of inflammatory cytokines [210]. Resident macrophages are present in every tissue and are involved in development, as well as maintenance of tissue homeostasis, and have been given special names based upon their tissue-of-residence, *e.g.* adipose tissue macrophages (ATMs) and Kupffer cells of the liver (Reviewed in [4, 65]; **Figure 47**). Macrophages can act as accessory cells and positively contribute to tissue homeostasis [211]. Briefly, macrophages secrete chemokines, cytokines, growth factors, and extracellular vesicle-encapsulated

Figure 47. Tissue Associated Macrophages
Resident macrophages are known to play critical roles in tissue homeostasis and in disease. These macrophages are given special names based upon their tissue-intrinsic function. Most tissue resident macrophages are yolk sac-derived and self-renew; however, circulating monocytes can also infiltrate tissues. Macrophages from each tissue also have distinct cell surface markers that could ultimately be used for tissue specific macrophage targeting in the future [4, 5].

Arterial Macrophages: Lipid laden foamy macrophages in atherosclerotic plaques are thought to contribute to lesion formation due to their accumulation of cholesterol and secretion of inflammatory cytokines. In addition, they may contribute to plaque instability, intraplaque hemorrhage, and rupture. In this setting, targeting them to reduce their inflammatory nature and increase their pro-fibrotic tendencies are strategies to improve CVD [7].

Kupffer Cells: Kupffer cells play roles in liver iron handling, bilirubin processing, scavenging of gut-derived pathogens, cholesterol metabolism, and immune surveillance [8]. When over-activated, they can also be pathogenic by accumulating lipid, secreting inflammatory cytokines, and activating stellate cells to produce α-smooth muscle actin, leading to fibrosis and ultimately non-alcoholic fatty liver disease (NAFLD). Elimination of macrophages is known to reduce progression of NAFLD. It should be noted that monocytes can be recruited from the circulation to the liver and subsequently differentiate into macrophages; however, these have distinct cell surface markers compared to Kupffer cells.

Red pulp macrophages (RPMs): RPMs are responsible for recycling iron retrieved from senescent red blood cells following erythrophagocytosis [10]. In fact, 10 times more iron is recycled in RPMs than is absorbed by enterocytes. Because elevated tissue iron stores are correlated with systemic IR, RPMs could be a potential target for metabolic disease in certain settings.

Tumor Associate Macrophages (TAMs): Myeloid cells are recruited to the tumor microenvironment where they can be differentiated into TAMs. They retain an M2-like phenotype and are thereby immunosuppressive – preventing immune detection and destruction of malignant cells [11]. Thus, their presence is associated with increased tumor burden and worsened prognosis. Use of mannosylated, siRNA delivery nanoparticles has been recently utilized to activate NF-κB in macrophages and is a promising anti-cancer therapy [13].

Microglia: Macrophages in the brain are called microglia and are essential to central nervous system homeostasis [15]. Developmental programming, synapse remodeling, phagocytosis of dead cells are among their many functions. Microglial activation is a feature of neurodegeneration and also diabetic retinopathy, and thus, reducing their inflammatory potential is a potential target for these diseases.

material that can influence the function of neighboring parenchymal cells. Ongoing studies are focused on macrophage-parenchymal cells in tissue homeostasis; however, to date, this has most often been studied in the context of disease, *e.g*. inflammatory cytokines can cause IR, rather than how these interactions promote tissue health. Thus, many times, the pathogenicity of macrophages derives from their ability to modulate the function of neighboring cells – a characteristic that can be exploited when considering their potential as therapeutic targets.

Macrophages are polarized across a broad spectrum, from an M1-like state that is considered to be pro-inflammatory, to an M2-like state in which they are anti-inflammatory and pro-fibrogenic. This diversity of phenotype is relevant to acute infections where macrophages initially fight off pathogens and phagocytose dead cells, but then convert their phenotype and subsequently assist in the wound healing process. The various properties of macrophages have been reviewed [212], but it is important to note that traditional M1 and M2 classification has been challenged, and more recent studies have suggested a spectrum of inflammatory phenotypes for macrophages [213]. Nonetheless, these same M1-like and M2-like properties can be detrimental when exaggerated or unregulated in chronic inflammation. For example, excess inflammatory cytokine secretion can lead to IR in neighboring cells – a finding particularly relevant in AT. Conversely, excess fibrogenic stimulation can lead to fibrosis in diseases such as NAFLD. Thus, when considering macrophages as therapeutic targets, one needs to be discerning about the phenotype of the macrophages targeted and pathogenesis of the disease treated. Although it is now appreciated that macrophages can contribute to the development of metabolic diseases, their contributions are tissue-specific and

context-dependent. Understanding the complexity and diversity of macrophages is also critical.

Macrophages in obesity-related adipose tissue inflammation and IR

Due to the contribution of M1-like inflammatory macrophages to obesity-related IR, the selection of macrophage-specific therapeutics should focus on their involvement. Potential areas of modification are to reduce M1-like polarization and inflammatory cytokine production via targeting of specific cytokines such as tumor necrosis factor alpha (TNF-α), Interleukin 6 (IL-6), and Interleukin 1 beta (IL-1β), or chemokines such as Chemokine (C-C motif) ligands 2, 3, and 5 (CCL2, CCL3, and CCL5, respectively). Other inflammatory signal transduction intermediates such as nuclear factor kappa-light-chain-enhancer of activated B cells (NF-κB) and signaling molecules in the inflammasome pathway may prove reasonable targets as well. Conversely, increasing the M2-like anti-inflammatory ATM phenotype via adiponectin, peroxisome proliferator-activated receptor gamma (PPARγ), or type 2 cytokines such as Interleukins 4, 13, and 33 (IL-4, IL-13, and IL-33, respectively) is an alternative [reviewed in [214]]. There are at least 3 caveats with this strategy that should be noted: 1) M1 macrophage content is increased in obese human AT, but not to the same degree as mouse adipose [215-218]. 2) Systemic reduction of inflammation has not been effective at improving metabolic parameters [214], but it is possible that specifically modifying ATMs may be a more viable approach due to the paracrine rather than endocrine nature of M1 macrophage interactions with nearby parenchymal cells. 3) In early stages of AT expansion, mild inflammation is beneficial [219], so the timing of this approach needs to be carefully considered.

Despite these caveats, reducing ATM inflammatory potential remains a promising avenue for treatment of obesity-accelerated IR and diabetes.

Other macrophage subsets in adipose tissue

Recently, a new population of metabolically active macrophages (MMe) in the AT has been described [220, 221]. Although MMe macrophages secrete pro-inflammatory cytokines, they have distinct cell surface markers that distinguish them from both M1 and M2 macrophages. Specifically, MMes do not express CD38, CD319, or CD273, which are traditional M1 markers, but instead express ABCA1, CD36, and PLIN2, which are associated with M2 macrophages.

In addition to MMes, macrophages with iron-related phenotypes have also been identified in AT. Iron-handling macrophages were first identified in atherosclerotic plaques [222-225] and have been shown to be M2-like and to express high levels of mannose receptor and the haptoglobin/hemoglobin receptor, CD163. They have been given names such as M(Hb) and Mhem and are reviewed in [226]. In plaques, these iron-handling macrophages are considered to play a role in clearing intra-plaque hemorrhage. Our laboratory has found a similar population of iron handling macrophages in AT that we call MFe^{hi} [67]. These MFe^{hi} macrophages have a 2-fold increase in iron content and in iron handling genes compared with non iron-handling AT macrophages. Interesting, they have a strong M2-like phenotype with high expression of mannose receptor and CD163 – just like the M(Hb) and Mhem macrophages, even in the presence of excess iron. Their relevance to AT homeostasis and protection from IR is under investigation, but

they highlight the point that both M1-like and M2-like macrophages could be targets of therapy for obesity-related metabolic disorders.

Hepatic macrophages in nonalcoholic fatty liver disease

Similar to the AT transition, hepatic macrophages undergo changes in polarization, recruitment, and proliferation during the pathogenesis of NAFLD [227]. Hepatic macrophages are dynamic players in maintaining liver homeostasis, via protection against bacteria and microbes from the intestine and restoring tissue integrity following liver injury [reviewed in [8]]. The liver contains a number of distinct macrophage subsets important for liver disease, with embryonic-derived Kupffer cells and monocyte-derived macrophages being the primary subsets driving the progression of NAFLD. Kupffer cells are the resident macrophages of the liver and make up ~20-25% of the non-parenchymal cell content [228]. NAFLD develops due to long-term high carbohydrate or fat consumption, resulting in hepatocyte lipid accumulation and cell death. The inflamed hepatocytes secrete chemokines, such as CCL2 and TNF-α, leading to the activation and proliferation of Kupffer cells and conversion to what could be considered an M1-like phenotype, with expression and secretion of cytokines such as IL-6, IL-1β, TNF-α, and inducible nitric oxide synthase 2 (iNOS2) [229]. In addition inflamed hepatocytes and Kupffer cells signal for the infiltration of CCR2+Ly6C+ monocytes that differentiate into monocyte-derived macrophages, also expressing an M1 phenotype [230, 231].

Recently, macrophage inflammation has been targeted for treatment of NAFLD. Impairment of recruitment and/or depletion of hepatic macrophage

subsets have been shown to successfully suppress hepatic steatosis and inflammation in mouse models of NAFLD [232, 233]. It has been shown that pediatric NAFLD prognosis could be improved through treatment with docosahexaenoic acid due to its effects on macrophage polarization, pushing them toward an M2-like phenotype [234]. Dietary carotenoids have also been proposed for NAFLD treatment due to their effects on macrophage polarization [reviewed in [235]]. More recently, altering the polarization state of hepatic macrophages to an M2 phenotype by increasing PPARγ activity was found to reduce NAFLD in mice [229].

Macrophages in atherosclerosis

Like AT and the liver, the healthy artery wall contains resident macrophages [236], and in hyperlipidemic conditions, the recruitment of additional macrophages leads to atherosclerotic lesion formation [7]. High fat feeding and hyperlipidemia can both induce myelopoiesis in the bone marrow and recruitment of monocytes into the intimal space [237, 238]. Once there, they differentiate into macrophages and express scavenger receptors allowing them to endocytose oxidized lipids. This lipid accumulation results in foamy macrophages that are highly inflammatory and that also send chemotactic signals to recruit additional monocytes, exacerbating the lipid-enriched inflammatory milieu [239]. Recently, a subset of arterial macrophages [Mhem, M(Hb)] have been shown to express receptors involved in heme scavenging and can clear debris during intraplaque hemorrhage as discussed earlier [240]. In addition, a novel macrophage population that uniquely responds to oxidatively modified lipids in the

atherosclerotic plaque, called “Mox”, has been identified [241]. Understanding the biology of these unique subsets of arterial macrophages and developing strategies similar to those suggested for AT, *i.e.* reduction of their inflammatory potential, may provide therapeutic opportunities for atherosclerosis. Additionally, decreasing their ability to take up lipid or increasing their ability to efflux lipid are other possibilities. In fact, mannose functionalized nanoparticles have recently been utilized to deliver therapeutic molecules to plaque macrophages in a mouse model of atherosclerosis [242]. Although, this is a very new area of research, the high level of mannose receptor expression on M(Hb) and Mhem cells, could provide a method to target them with mannosylated particles in order to dampen inflammation and improve their iron handling phenotype.

Macrophages as a therapeutic target in metabolic disease

Targeting strategies: Intracellular access

Currently, most macrophage-targeted therapeutic strategies provide specificity by capitalizing on receptor-mediated phagocytosis. Compounds designed to encapsulate therapeutics can have surface modifications that are recognized by receptors on macrophages. There are defining receptors such as F4/80, CD11b, and CD68 that are expressed on all macrophages [243-245], but subpopulations can additionally express others – such as those for mannose, lectin, adenosine [246], and folate [247]. Although not exclusively macrophage-specific, they allow targeting of cells of particular phenotypes and activation states. This receptor-focused approach offers a direct route of import into macrophages while minimizing off-target effects.

There are at least three methods of internalization that can be exploited for delivery purposes [reviewed in [248]]. 1) *Activation of therapeutic agents in the acidic lysosomal compartment*: Once recognized and engulfed, entrapped particles are packaged into a phagosome prior to fusion with destructive lysosomes. Utilizing the microenvironment of the phagosome or lysosome to initiate therapeutic activity is promising, but has been primarily limited to nanoparticle encapsulation approaches. In these strategies, the acidic lysosomal interior initiates breakdown of the nanoparticle capsule and release of its contents [249] Alternatively, lysosomal enzymes degrade the nanoparticle shell to release core contents [250]. 2) *Cytoplasmic delivery via endocytosis and lysosomal escape:* Another strategy to avoid phagocytic destruction is to design particles that escape phagosomes after endocytosis but prior to fusion with the lysosome [251]. 3) *Utilization of endocytic receptors:* A third strategy takes advantage of active transport into the macrophage mediated by coat proteins, such as clathrin and caveolin [252]. Once a particle has entered the intracellular space, it can deliver its phenotype/function altering cargo. Methods to accomplish this in macrophages are discussed below.

Therapeutic strategies: Changing the role of the macrophage

Once inside the macrophage, therapeutic strategies are diverse - depletion, proliferation, inflammation, and gene silencing are commonly used. Approaches that modulate macrophage number often aim to deplete macrophages by inducing apoptosis following accumulation of toxic particles that are released into the macrophage [253]. Targeting proliferation may also reduce macrophage number

[254], and could be relevant for atherosclerosis; however, macrophages are often recruited in the context of obesity, so this strategy may not be as useful for IR. Modification of inflammatory signal transduction pathways inside the macrophage is another approach. By introducing anti-inflammatory agents to the macrophage cytoplasm, inflammatory cytokine production and release can be modulated [255]. Perhaps the most attractive approach to modifying macrophage polarization is to reduce inflammatory gene expression through RNA interference, as multiple genes can be downregulated simultaneously. Potential targets include inflammatory mediators such as cytokines, *e.g* TNF-α, IL-6, IL-1β; chemokines, *e.g*. CCL2, CCL3, CCL5; and transduction targets involved in promoting inflammation such as members of the NF-κB signaling cascade [256, 257]. These therapeutic strategies, coupled with techniques to target specific macrophage subsets, offer a variety of ways to modulate macrophage number and activity at the site of metabolic disease.

Methods of delivery

Nanoparticles

Nanoparticle design and delivery is a logical strategy for macrophage therapeutics. By definition, nanoparticles are small agents ranging from 1-1000 nm. Their surface coating dictates whether they target a particular cell type – due to receptor-mediated specificity – or an entire tissue due to chemical properties that encourage attraction to that depot [258]. This approach provides target specificity that aims to minimize toxicity and off-target effects. One area of particular interest is development of nanoparticles that target antigen presenting

cells, such as macrophages and dendritic cells, via receptors of the C-type lectin family, [reviewed in [259]].

In one recent example, polysaccharide-based delivery systems were utilized to target inflammatory ATMs in obese mice [260]. The 4-30 nm particles were made with dextran and were readily taken up by macrophages following recognition by dextran-binding C-type lectins and scavenger receptors. In lean mice, the nanoparticles preferentially accumulated in liver after intraperitoneal (IP) injection, but in obese mice they accumulated in the adipose depots. The authors showed that ~90% of the cells taking up the particles in gonadal, perirenal, and subcutaneous AT were of myeloid origin. The nanocarriers were used to deliver the anti-inflammatory drug, dexamethasone, specifically to the obesity-associated inflammatory macrophages. Upon delivery, there was a marked decrease in pro-inflammatory genes, *Tnf*□, *Il6*, and *Ccl2*. Although, these preliminary studies show promise in the nontoxic treatment of chronic inflammation in obese AT, the IP delivery method is not realistic for clinical use. The investigators suggest that extended release will be necessary in order to minimize the invasiveness of delivery, but other modes of delivery will need to be explored, and AT specificity will need to be confirmed regardless of the administration route.

There are nanoparticle technologies that have targeted macrophage receptors in other diseases, but not yet in metabolic disease. For example, superparamagnetic iron oxide nanoparticles (SPIONs) have traditionally been used as imaging tools, but now have also been shown to impact M2 macrophages by altering their activation state and iron handling capabilities [261]. The M2-like

phenotype of iron-handling macrophages means that their use as a therapeutic target must be considered differently than M1-like macrophages. With regard to MFe^{hi}, Mhem, and M(Hb) macrophages, a potential use for SPIONs could be to induce an iron recycling phenotype and/or increase their anti-inflammatory phenotype. Along these lines, "click" chemistry has been used to create mannosylated nanoparticles that deliver siRNA specifically to M2-polarized TAMs that express mannose receptor on their surface [262]. While these The ability of these nanoparticles to specifically target the M2 macrophages that are present in lean AT makes them a potentially promising technology for further exploration. More research is needed regarding the roles of MFe^{hi}, Mhem, and M(Hb) macrophages in AT and the artery wall so that siRNA therapy can be targeted to pathways that are relevant to these iron-handling macrophages.

Liposomes

Liposomes are a third drug delivery platform that has been investigated. Liposomes are phospholipid vesicles, about 15-1000 nm in size, that can carry either hydrophilic or lipophilic drugs in their bilayer membrane or core, respectively. The encapsulation design allows for drug protection and stabilization; one method of which is PEGylation, which increases circulation time [263]. As with nanoparticles, liposome shells can be engineered with ligands or antibodies to target specific macrophage phenotypes based on receptor specificity. For example, F4/80-targeted liposomes would go to all macrophages, while IL-6 receptor or CD163-targeted liposomes would be taken up by M1 or M2 polarized macrophages, respectively. Additionally, the contents of the liposomes can be altered. These

design features allow for more effective and efficient targeting because the outer shell of the compound can be changed depending on where it needs to go, while the inner contents can be altered according to therapeutic needs. While advances have been made in the design of liposomes [reviewed in [264-266]], clinical usage has proven difficult. Due to the complexity of liposome compounds, the associated trials are typically longer and more complex, which leads to cost burden. Off-target effects of treatment are also common because of leakiness of the liposome and degradation of the particles through circulation. Nonetheless, liposomes remain attractive therapeutics as there are many ways that they can be engineered to target macrophages in metabolic disease.

Liposomes can enter macrophages purely because of the cells' phagocytic properties. Clodronate-loaded liposomes are used to deplete macrophages by inducing apoptosis when internalized. This technology has been historically used in many tissues, but in 2011 depletion of visceral ATMs with consequent effects on tissue health was shown. IP injection of clodronate liposomes, resulted in an improved glucose and insulin tolerance that was associated with increased circulating adiponectin, an insulin sensitizing adipokine [70]. In 2013, another study showed similar data: under the same conditions – animals fed a high fat diet gained less weight, showed improved glucose tolerance and decreased fasting glucose, insulin, and free fatty acid levels, compared to control groups [267]. Notably, these studies potentially represent an additional disease preventative approach. Current efforts focus on lifestyle changes in diet and exercise, but adjuvant therapy to reduce the inflammatory environment of AT by targeting ATMs should be considered. Nonetheless, this research tool provides mechanistic

insight into obesity-related disease progression and is a method that can be further optimized to more specifically target macrophage subsets involved in metabolic disease.

As with the nanoparticle technologies, discoveries in liposome delivery outside of the metabolism field may prove interesting for the treatment of metabolic disease. For example, CD163 antibody coated liposomes were shown to be taken up by CD163+ monocytes *in vitro* and to kill cells when loaded with doxorubicin [268]. CD163+ macrophages are resident in lean healthy AT, but their numbers are overshadowed during obesity related inflammation. If the healthy cells can be targeted and encouraged to proliferate, the obese tissue microenvironment can conceivably be therapeutically altered to resemble its lean, and healthier, counterpart.

Glucan shell microparticles

β-glucans are sugars most commonly found in the cell walls of bacteria. Dectin-1, a macrophage receptor for β-glucans has been proposed as a potential therapeutic with antitumor and antimicrobial activity [269, 270]. Yeast-derived β-glucans (Y-BGs) have been reviewed recently and are known to have beneficial effects in models of obesity, allergy, and cancer [271]. For example, orally administrated Y-BGs induced expression of the anti-inflammatory cytokine, IL-10, in the AT of obese humans and increased serum IL-10 levels [272]. Once taken up by macrophages, Y-BGs appear to cause increased reactive oxygen species (ROS) formation and phagosomal maturation, ultimately resulting in the induction of autophagy [273]. A recent study suggests IL-10 is an important mediator of

macrophage autophagy necessary for removing dysfunctional mitochondria [274]. Taken together, these findings suggest Y-BGs promote anti-inflammatory activity in macrophages through an IL-10 mediated mechanism.

Interestingly, Y-BGs have been used as unique encapsulation tools that can target macrophages in an activation-independent manner. These 2-4 μm hollow particles are able to encapsulate potential therapeutics, including siRNA and small molecules [275-277]. For example, glucan shells have been utilized to encapsulate gene-silencing molecules for macrophage targeted therapies. Orally delivered β1,3-d-glucan-encapsulated siRNA particles (GeRPs) containing siRNA directed toward mitogen activated protein kinase kinase kinase kinase 4 (*Map4k4*) reduced systemic inflammation by reducing *Tnf*□ mRNA in macrophages [275]. In this design, the siRNA is anchored to Endo-Porter peptide, which simplifies compound preparation and also facilitates release of internalized GeRPs into the macrophage cytoplasm. This peptide-facilitated phagosomal escape is critical for siRNA to reach the cytoplasm where it can function to silence inflammatory genes. Macrophages exposed to orally delivered GeRPs migrated to other tissues and resulted in a 40-80% knockdown of *Map4k4* expression depending on tissue site. These data also suggest that delivery of GeRPs to specific tissue sites can be carried out by the macrophages themselves upon migration to peripheral tissues. IP injection of GeRPs resulted in specific delivery to epididymal ATMs in obese mice, resulting in silencing of *Tnf*-α and *Opn* [278]. While these studies show promise, IP delivery of GeRPs would not be favorable for clinical use. Upon further analysis of their efficacy, the investigators should determine whether other modes of delivery are possible.

Oligopeptide Complexes

Oligopeptides have been known for decades to display tissue specificity [279-281]. Many tissues are difficult to target for non-viral mediated gene delivery, and oligopeptides complexed with gene modulating molecules are an attractive solution. These oligopeptide complexes exhibit specificity by utilizing peptide-bound oligonucleotide sequences designed to target specific cell populations and are complexed with modulatory molecules, such as siRNA or shRNA, that function by silencing genes. One such oligopeptide gene carrier has been designed and is effectively taken up by mature adipocytes through binding a cell surface protein called prohibitin [280]. However, ATMs have also been shown to express prohibitin, and these oligopeptide gene carriers were found in the the stromal vascular fraction of AT that contains immune cells. This unexpected finding may prove to be beneficial in attempts to specifically deliver non-viral gene altering technology to adipose depots and ATMs.

Another potential way to therapeutically target ATMs is through tumor necrosis factor-α converting enzyme (TACE) oligopeptides. TACE is an anti-inflammatory metalloproteinase, which is critical for generating soluble TNF-α, and therefore presents a remarkable opportunity for disrupting TNF-α mediated inflammation [282]. Complexes of TACE shRNA (shTACE) and adipocyte-targeting sequence (ATS-9R) oligopeptides have been produced and are specifically taken up by visceral ATMs following IP injection. These complexes display specificity for AT, and function by silencing TACE, resulting in the cell's inability to generate soluble TNF-α. Accumulation of injected oligopeptides in visceral ATMs without accumulation in the spleen or liver after 4 hours has been observed [281].

Although shTACE oligopeptide complexes are enzymatically degraded, 8 repeated injections over a month long period resulted in improved insulin sensitivity and glucose tolerance, which was attributed to reductions in adipose TACE activity.

Concluding remarks and future perspectives

Macrophages have become a unique target for treating metabolic disease since the discovery of their importance in metabolic tissues and their change in phenotype upon disease progression. This review presents discoveries that couple the ability to alter macrophage function with the technologies that ensure their specific targeting. There is ongoing research to define specific macrophage subsets, identify surface markers unique to these subsets, and capitalize on their unique properties to target specific functions. Many of the delivery systems described in this review can be engineered to transport gene-silencing agents such as siRNA; however; challenges remain in successfully eliminating the targeted gene expression. While CRISPR-Cas9 technology can not yet be used *in vivo* [283], it would be interesting to determine whether this technology could be delivered specifically to tissue macrophage subsets in order to alter their polarization and functional phenotype. Additionally, it has recently been elucidated that epigenetic regulation is involved in macrophage polarization, [284]. Targeting epigenetic modifications via genetic or pharmacological perturbation is another promising area of research.

While strides have been made in elucidating mechanisms involved in maintaining healthy macrophages in metabolic tissues, questions still remain regarding the therapeutic potential and feasibility of specifically treating macrophages in metabolic disease (see Outstanding Questions). Ultimately, the future of macrophage-specific treatment relies on continued efforts to identify and produce therapeutics that can be specifically targeted to cells of the appropriate phenotype and tissue location.

Figure 48. Outstanding Questions

- Can we identify and utilize unique macrophage markers to provide tissue-specific therapy?
- Will antisense oligonucleotide therapies targeting macrophages be useful for treatment of metabolic disease?
- Are there less expensive and more streamlined methods to design liposomes that target specific phenotypes of macrophages in metabolic tissues?
- What are the long-term effects of all of these novel strategies?
- Modulation of epigenetic programming and permanent genetic alteration via CRISPR are both innovative and cutting edge techniques. What is the future of these discoveries as it relates to metabolic disease? How responsive will the public be to therapeutics that alter the genome or epigenome in particular cells?

REFERENCES

1. Weiss, R. et al. (2004) Obesity and the metabolic syndrome in children and adolescents. N Engl J Med 350 (23), 2362-74.
2. Olshansky, S.J. et al. (2005) A potential decline in life expectancy in the United States in the 21st century. N Engl J Med 352 (11), 1138-45.
3. Benjamin, E.J. et al. (2018) Heart Disease and Stroke Statistics-2018 Update: A Report From the American Heart Association. Circulation 137 (12), e67-e492.
4. Gordon, S. and Pluddemann, A. (2017) Tissue macrophages: heterogeneity and functions. BMC Biol 15 (1), 53.
5. Cho, K.W. et al. (2014) Flow cytometry analyses of adipose tissue macrophages. Methods Enzymol 537, 297-314.
6. Hales, C.M. et al. (2017) Prevalence of Obesity Among Adults and Youth: United States, 2015-2016. NCHS Data Brief (288), 1-8.
7. Park, I. et al. (2017) Functional diversity of macrophages in vascular biology and disease. Vascul Pharmacol 99, 13-22.
8. Krenkel, O. and Tacke, F. (2017) Liver macrophages in tissue homeostasis and disease. Nat Rev Immunol 17 (5), 306-321.
9. Kershaw, E.E. and Flier, J.S. (2004) Adipose tissue as an endocrine organ. J Clin Endocrinol Metab 89 (6), 2548-56.
10. Ganz, T. (2016) Macrophages and Iron Metabolism. Microbiol Spectr 4 (5).
11. Schupp, J. et al. (2017) Targeting myeloid cells in the tumor sustaining microenvironment. Cell Immunol.
12. Chusyd, D.E. et al. (2016) Relationships between Rodent White Adipose Fat Pads and Human White Adipose Fat Depots. Front Nutr 3, 10.
13. Ortega, R.A. et al. (2016) Manipulating the NF-kappaB pathway in macrophages using mannosylated, siRNA-delivering nanoparticles can induce immunostimulatory and tumor cytotoxic functions. Int J Nanomedicine 11, 2163-77.
14. Lagathu, C. et al. (2003) Chronic interleukin-6 (IL-6) treatment increased IL-6 secretion and induced insulin resistance in adipocyte: prevention by rosiglitazone. Biochem Biophys Res Commun 311 (2), 372-9.
15. Li, Q. and Barres, B.A. (2017) Microglia and macrophages in brain homeostasis and disease. Nat Rev Immunol.
16. Rutkowski, J.M. et al. (2015) The cell biology of fat expansion. J Cell Biol 208 (5), 501-12.
17. Bjorndal, B. et al. (2011) Different adipose depots: their role in the development of metabolic syndrome and mitochondrial response to hypolipidemic agents. J Obes 2011, 490650.
18. Harms, M. and Seale, P. (2013) Brown and beige fat: development, function and therapeutic potential. Nat Med 19 (10), 1252-63.
19. Rothwell, N.J. and Stock, M.J. (1983) Luxuskonsumption, diet-induced thermogenesis and brown fat: the case in favour. Clin Sci (Lond) 64 (1), 19-23.
20. Cannon, B. and Nedergaard, J. (2004) Brown adipose tissue: function and physiological significance. Physiol Rev 84 (1), 277-359.
21. Young, P. et al. (1984) Brown adipose tissue in the parametrial fat pad of the mouse. FEBS Lett 167 (1), 10-4.

22. Gnad, T. et al. (2014) Adenosine activates brown adipose tissue and recruits beige adipocytes via A2A receptors. Nature 516, 395-399.
23. Whittle, A.J. et al. (2012) BMP8B increases brown adipose tissue thermogenesis through both central and peripheral actions. Cell 149 (4), 871-85.
24. Ramage, L.E. et al. (2016) Glucocorticoids Acutely Increase Brown Adipose Tissue Activity in Humans, Revealing Species-Specific Differences in UCP-1 Regulation. Cell Metab 24 (1), 130-41.
25. Wang, W. and Seale, P. (2016) Control of brown and beige fat development. Nat Rev Mol Cell Biol 17 (11), 691-702.
26. Wu, J. et al. (2013) Adaptive thermogenesis in adipocytes: is beige the new brown? Genes Dev 27 (3), 234-50.
27. Qian, S.W. et al. (2013) BMP4-mediated brown fat-like changes in white adipose tissue alter glucose and energy homeostasis. Proc Natl Acad Sci U S A 110 (9), E798-807.
28. Madsen, L. et al. (2010) UCP1 induction during recruitment of brown adipocytes in white adipose tissue is dependent on cyclooxygenase activity. PLoS One 5 (6), e11391.
29. Fisher, F.M. et al. (2012) FGF21 regulates PGC-1alpha and browning of white adipose tissues in adaptive thermogenesis. Genes Dev 26 (3), 271-81.
30. Klaus, S. et al. (2001) Effect of the beta(3)-adrenergic agonist Cl316,243 on functional differentiation of white and brown adipocytes in primary cell culture. Biochim Biophys Acta 1539 (1-2), 85-92.
31. Vernochet, C. et al. (2009) C/EBPalpha and the corepressors CtBP1 and CtBP2 regulate repression of select visceral white adipose genes during induction of the brown phenotype in white adipocytes by peroxisome proliferator-activated receptor gamma agonists. Mol Cell Biol 29 (17), 4714-28.
32. Ohno, H. et al. (2012) PPARgamma agonists induce a white-to-brown fat conversion through stabilization of PRDM16 protein. Cell Metab 15 (3), 395-404.
33. Seale, P. et al. (2011) Prdm16 determines the thermogenic program of subcutaneous white adipose tissue in mice. J Clin Invest 121 (1), 96-105.
34. Zuriaga, M.A. et al. (2017) Humans and Mice Display Opposing Patterns of "Browning" Gene Expression in Visceral and Subcutaneous White Adipose Tissue Depots. Front Cardiovasc Med 4, 27.
35. Kajimura, S. et al. (2015) Brown and Beige Fat: Physiological Roles beyond Heat Generation. Cell Metab 22 (4), 546-59.
36. Carpaij, O.A. and van den Berge, M. (2018) The asthma-obesity relationship: underlying mechanisms and treatment implications. Curr Opin Pulm Med 24 (1), 42-49.
37. Liu, Y. et al. (2017) Impact of Obesity on Remission and Disease Activity in Rheumatoid Arthritis: A Systematic Review and Meta-Analysis. Arthritis Care Res (Hoboken) 69 (2), 157-165.
38. George, M.D. and Baker, J.F. (2016) The Obesity Epidemic and Consequences for Rheumatoid Arthritis Care. Curr Rheumatol Rep 18 (1), 6.
39. McCrindle, B.W. (2015) Cardiovascular consequences of childhood obesity. Can J Cardiol 31 (2), 124-30.

40. Hanson, C. et al. (2014) Influence of diet and obesity on COPD development and outcomes. Int J Chron Obstruct Pulmon Dis 9, 723-33.
41. Harper, J.W. and Zisman, T.L. (2016) Interaction of obesity and inflammatory bowel disease. World J Gastroenterol 22 (35), 7868-81.
42. Whaley-Connell, A. and Sowers, J.R. (2017) Obesity and kidney disease: from population to basic science and the search for new therapeutic targets. Kidney Int 92 (2), 313-323.
43. Ronan, L. et al. (2016) Obesity associated with increased brain age from midlife. Neurobiol Aging 47, 63-70.
44. Cheke, L.G. et al. (2017) Obesity and insulin resistance are associated with reduced activity in core memory regions of the brain. Neuropsychologia 96, 137-149.
45. Rhea, E.M. et al. (2017) Blood-Brain Barriers in Obesity. AAPS J 19 (4), 921-930.
46. Milic, S. et al. (2014) Non-alcoholic fatty liver disease and obesity: biochemical, metabolic and clinical presentations. World J Gastroenterol 20 (28), 9330-7.
47. Leitner, D.R. et al. (2017) Obesity and Type 2 Diabetes: Two Diseases with a Need for Combined Treatment Strategies - EASO Can Lead the Way. Obes Facts 10 (5), 483-492.
48. Pulgaron, E.R. and Delamater, A.M. (2014) Obesity and type 2 diabetes in children: epidemiology and treatment. Curr Diab Rep 14 (8), 508.
49. Muppala, S. et al. (2017) Adiponectin: Its role in obesity-associated colon and prostate cancers. Crit Rev Oncol Hematol 116, 125-133.
50. Zheng, J. et al. (2017) Obesity-associated digestive cancers: A review of mechanisms and interventions. Tumour Biol 39 (3), 1010428317695020.
51. Loo, T.M. et al. (2017) Gut Microbiota Promotes Obesity-Associated Liver Cancer through PGE2-Mediated Suppression of Antitumor Immunity. Cancer Discov 7 (5), 522-538.
52. Engin, A. (2017) Obesity-associated Breast Cancer: Analysis of risk factors. Adv Exp Med Biol 960, 571-606.
53. Olefsky, J.M. and Glass, C.K. (2010) Macrophages, inflammation, and insulin resistance. Annu Rev Physiol 72, 219-46.
54. Gregor, M.F. and Hotamisligil, G.S. (2011) Inflammatory mechanisms in obesity. Annu Rev Immunol 29, 415-45.
55. Mathis, D. and Shoelson, S.E. (2011) Immunometabolism: an emerging frontier. Nat Rev Immunol 11 (2), 81.
56. Spranger, J. et al. (2003) Inflammatory cytokines and the risk to develop type 2 diabetes: results of the prospective population-based European Prospective Investigation into Cancer and Nutrition (EPIC)-Potsdam Study. Diabetes 52 (3), 812-7.
57. Rask-Madsen, C. and Kahn, C.R. (2012) Tissue-specific insulin signaling, metabolic syndrome, and cardiovascular disease. Arterioscler Thromb Vasc Biol 32 (9), 2052-9.
58. Boucher, J. et al. (2014) Insulin receptor signaling in normal and insulin-resistant states. Cold Spring Harb Perspect Biol 6 (1).
59. Weisberg, S.P. et al. (2003) Obesity is associated with macrophage accumulation in adipose tissue. J Clin Invest 112 (12), 1796-808.
60. Xu, H. et al. (2003) Chronic inflammation in fat plays a crucial role in the development of obesity-related insulin resistance. J Clin Invest 112 (12), 1821-30.

61. McGillicuddy, F.C. et al. (2009) Interferon gamma attenuates insulin signaling, lipid storage, and differentiation in human adipocytes via activation of the JAK/STAT pathway. J Biol Chem 284 (46), 31936-44.
62. Rotter, V. et al. (2003) Interleukin-6 (IL-6) induces insulin resistance in 3T3-L1 adipocytes and is, like IL-8 and tumor necrosis factor-alpha, overexpressed in human fat cells from insulin-resistant subjects. J Biol Chem 278 (46), 45777-84.
63. Hotamisligil, G.S. et al. (1994) Tumor necrosis factor alpha inhibits signaling from the insulin receptor. Proc Natl Acad Sci U S A 91 (11), 4854-8.
64. Ferrante, A.W., Jr. (2013) The immune cells in adipose tissue. Diabetes Obes Metab 15 Suppl 3, 34-8.
65. Hill, A.A. et al. (2014) A decade of progress in adipose tissue macrophage biology. Immunol Rev 262 (1), 134-52.
66. Wu, D. et al. (2011) Eosinophils sustain adipose alternatively activated macrophages associated with glucose homeostasis. Science 332 (6026), 243-7.
67. Orr, J.S. et al. (2014) Obesity alters adipose tissue macrophage iron content and tissue iron distribution. Diabetes 63 (2), 421-32.
68. Nishimura, S. et al. (2013) Adipose Natural Regulatory B Cells Negatively Control Adipose Tissue Inflammation. Cell Metab.
69. Wu, L. et al. (2014) Spleen supports a pool of innate-like B cells in white adipose tissue that protects against obesity-associated insulin resistance. Proc Natl Acad Sci U S A 111 (43), E4638-47.
70. Lynch, L. et al. (2015) Regulatory iNKT cells lack expression of the transcription factor PLZF and control the homeostasis of T(reg) cells and macrophages in adipose tissue. Nat Immunol 16 (1), 85-95.
71. Feuerer, M. et al. (2009) Lean, but not obese, fat is enriched for a unique population of regulatory T cells that affect metabolic parameters. Nat Med 15 (8), 930-9.
72. Deiuliis, J. et al. (2011) Visceral adipose inflammation in obesity is associated with critical alterations in tregulatory cell numbers. PLoS One 6 (1), e16376.
73. Winer, D.A. et al. (2011) B cells promote insulin resistance through modulation of T cells and production of pathogenic IgG antibodies. Nat Med 17 (5), 610-7.
74. DeFuria, J. et al. (2013) B cells promote inflammation in obesity and type 2 diabetes through regulation of T-cell function and an inflammatory cytokine profile. Proc Natl Acad Sci U S A 110 (13), 5133-8.
75. Bertola, A. et al. (2012) Identification of adipose tissue dendritic cells correlated with obesity-associated insulin-resistance and inducing Th17 responses in mice and patients. Diabetes 61 (9), 2238-47.
76. Lumeng, C.N. et al. (2007) Obesity induces a phenotypic switch in adipose tissue macrophage polarization. J Clin Invest 117 (1), 175-84.
77. Liu, J. et al. (2009) Genetic deficiency and pharmacological stabilization of mast cells reduce diet-induced obesity and diabetes in mice. Nat Med 15 (8), 940-5.
78. Elgazar-Carmon, V. et al. (2008) Neutrophils transiently infiltrate intra-abdominal fat early in the course of high-fat feeding. J Lipid Res 49 (9), 1894-903.
79. Nishimura, S. et al. (2009) CD8+ effector T cells contribute to macrophage recruitment and adipose tissue inflammation in obesity. Nat Med 15 (8), 914-20.

80. Rocha, V.Z. et al. (2008) Interferon-gamma, a Th1 cytokine, regulates fat inflammation: a role for adaptive immunity in obesity. Circ Res 103 (5), 467-76.
81. Kanda, H. et al. (2006) MCP-1 contributes to macrophage infiltration into adipose tissue, insulin resistance, and hepatic steatosis in obesity. J Clin Invest 116 (6), 1494-505.
82. Medrikova, D. et al. (2015) Brown adipose tissue harbors a distinct sub-population of regulatory T cells. PLoS One 10 (2), e0118534.
83. Ricklin, D. et al. (2010) Complement: a key system for immune surveillance and homeostasis. Nat Immunol 11 (9), 785-97.
84. Banda, N.K. et al. (2009) Complement activation pathways in murine immune complex-induced arthritis and in C3a and C5a generation in vitro. Clin Exp Immunol 159 (1), 100-8.
85. Snyderman, R. et al. (1975) Quantification of mouse macrophage chemotaxis in vitro: role of C5 for the production of chemotactic activity. Infect Immun 11 (3), 488-92.
86. Jauneau, A.C. et al. (2003) Complement component anaphylatoxins upregulate chemokine expression by human astrocytes. FEBS Lett 537 (1-3), 17-22.
87. Weinrauch, Y. et al. (1996) The potent anti-Staphylococcus aureus activity of a sterile rabbit inflammatory fluid is due to a 14-kD phospholipase A2. J Clin Invest 97 (1), 250-7.
88. Trouw, L.A. et al. (2017) The complement system as a potential therapeutic target in rheumatic disease. Nat Rev Rheumatol 13 (9), 538-547.
89. Peterson, K.R. et al. (2017) Obesity Alters B Cell and Macrophage Populations in Brown Adipose Tissue. Obesity (Silver Spring) 25 (11), 1881-1884.
90. Orr, J.S. et al. (2013) Isolation of adipose tissue immune cells. J Vis Exp (75), e50707.
91. Wolf, Y. et al. (2017) Brown-adipose-tissue macrophages control tissue innervation and homeostatic energy expenditure. Nature Immunology (18), 665-674.
92. Palmer, A.K. and Kirkland, J.L. (2016) Aging and adipose tissue: potential interventions for diabetes and regenerative medicine. Exp Gerontol 86, 97-105.
93. Fischer, K. et al. (2017) Alternatively activated macrophages do not synthesize catecholamines or contribute to adipose tissue adaptive thermogenesis. Nat Med 23 (5), 623-630.
94. Fitzgibbons, T.P. et al. (2011) Similarity of mouse perivascular and brown adipose tissues and their resistance to diet-induced inflammation. Am J Physiol Heart Circ Physiol 301 (4), H1425-37.
95. Dowal, L. et al. (2017) Intrinsic Properties of Brown and White Adipocytes Have Differential Effects on Macrophage Inflammatory Responses. Mediators Inflamm 2017, 9067049.
96. Nguyen, K.D. et al. (2011) Alternatively activated macrophages produce catecholamines to sustain adaptive thermogenesis. Nature 480 (7375), 104-8.
97. Kin, N.W. and Sanders, V.M. (2006) It takes nerve to tell T and B cells what to do. J Leukoc Biol 79 (6), 1093-104.
98. Saze, Z. et al. (2013) Adenosine production by human B cells and B cell-mediated suppression of activated T cells. Blood 122 (1), 9-18.

99. Sanders, V.M. (2012) The beta2-adrenergic receptor on T and B lymphocytes: do we understand it yet? Brain Behav Immun 26 (2), 195-200.
100. Vlaicu, S.I. et al. (2016) The role of complement system in adipose tissue-related inflammation. Immunol Res 64 (3), 653-64.
101. Maslowska, M. et al. (2005) Novel roles for acylation stimulating protein/C3adesArg: a review of recent in vitro and in vivo evidence. Vitam Horm 70, 309-32.
102. Cui, W. et al. (2007) Acylation-stimulating protein/C5L2-neutralizing antibodies alter triglyceride metabolism in vitro and in vivo. Am J Physiol Endocrinol Metab 293 (6), E1482-91.
103. McCall, C.E. et al. (1979) Enhancement of hexose uptake in human polymorphonuclear leukocytes by activated complement component C5a. Proc Natl Acad Sci U S A 76 (11), 5896-900.
104. Bass, D.A. et al. (1981) Stimulation of hexose uptake by human eosinophils with chemotactic factors. J Infect Dis 143 (5), 719-25.
105. Moreno-Navarrete, J.M. et al. (2010) Complement factor H is expressed in adipose tissue in association with insulin resistance. Diabetes 59 (1), 200-9.
106. Lim, J. et al. (2013) C5aR and C3aR antagonists each inhibit diet-induced obesity, metabolic dysfunction, and adipocyte and macrophage signaling. FASEB J 27 (2), 822-31.
107. Roy, C. et al. (2013) C5a receptor deficiency alters energy utilization and fat storage. PLoS One 8 (5), e62531.
108. Poursharifi, P. et al. (2013) C5L2 and C5aR interaction in adipocytes and macrophages: insights into adipoimmunology. Cell Signal 25 (4), 910-8.
109. Le, A.D. et al. (1994) Alcohol consumption by C57BL/6, BALB/c, and DBA/2 mice in a limited access paradigm. Pharmacol Biochem Behav 47 (2), 375-8.
110. Braem, K. et al. (2012) Spontaneous arthritis and ankylosis in male DBA/1 mice: further evidence for a role of behavioral factors in "stress-induced arthritis". Biol Proced Online 14 (1), 10.
111. Paigen, B. et al. (1990) Atherosclerosis susceptibility differences among progenitors of recombinant inbred strains of mice. Arteriosclerosis 10 (2), 316-23.
112. Paigen, B. et al. (1985) Variation in susceptibility to atherosclerosis among inbred strains of mice. Atherosclerosis 57 (1), 65-73.
113. Nishina, P.M. et al. (1993) Atherosclerosis and plasma and liver lipids in nine inbred strains of mice. Lipids 28 (7), 599-605.
114. Bekesi, J.G. et al. (1976) Treatment of spontaneous leukemia in AKR mice with chemotherapy, immunotherapy, or interferon. Cancer Res 36 (2 pt 2), 631-9.
115. Belinsky, S.A. et al. (1993) The A/J mouse lung as a model for developing new chemointervention strategies. Cancer Res 53 (2), 410-6.
116. Rossmeisl, M. et al. (2003) Variation in type 2 diabetes--related traits in mouse strains susceptible to diet-induced obesity. Diabetes 52 (8), 1958-66.
117. Chaparro, R.J. and Dilorenzo, T.P. (2010) An update on the use of NOD mice to study autoimmune (Type 1) diabetes. Expert Rev Clin Immunol 6 (6), 939-55.
118. Yoshimura, T. et al. (1994) Differences in circadian photosensitivity between retinally degenerate CBA/J mice (rd/rd) and normal CBA/N mice (+/+). J Biol Rhythms 9 (1), 51-60.

119. Chang, B. et al. (1999) Interacting loci cause severe iris atrophy and glaucoma in DBA/2J mice. Nat Genet 21 (4), 405-9.
120. Gimenez, E. and Montoliu, L. (2001) A simple polymerase chain reaction assay for genotyping the retinal degeneration mutation (Pdeb(rd1)) in FVB/N-derived transgenic mice. Lab Anim 35 (2), 153-6.
121. Noben-Trauth, K. and Johnson, K.R. (2009) Inheritance patterns of progressive hearing loss in laboratory strains of mice. Brain Res 1277, 42-51.
122. Myint, A. et al. (2016) Large-scale phenotyping of noise-induced hearing loss in 100 strains of mice. Hear Res 332, 113-120.
123. Ohlemiller, K.K. et al. (2011) Divergence of noise vulnerability in cochleae of young CBA/J and CBA/CaJ mice. Hear Res 272 (1-2), 13-20.
124. Goldsworthy, M. et al. (2016) Haploinsufficiency of the Insulin Receptor in the Presence of a Splice-Site Mutation in Ppp2r2a Results in a Novel Digenic Mouse Model of Type 2 Diabetes. Diabetes 65 (5), 1434-46.
125. Wheat, W.H. et al. (1987) The fifth component of complement (C5) in the mouse. Analysis of the molecular basis for deficiency. J Exp Med 165 (5), 1442-7.
126. Ooi, Y.M. and Colten, H.R. (1979) Genetic defect in secretion of complement C5 in mice. Nature 282 (5735), 207-8.
127. Wetsel, R.A. et al. (1990) Deficiency of the murine fifth complement component (C5). A 2-base pair gene deletion in a 5'-exon. J Biol Chem 265 (5), 2435-40.
128. Ayala, J.E. et al. (2011) Hyperinsulinemic-euglycemic clamps in conscious, unrestrained mice. J Vis Exp (57).
129. Ayala, J.E. et al. (2006) Considerations in the design of hyperinsulinemic-euglycemic clamps in the conscious mouse. Diabetes 55 (2), 390-7.
130. Kraegen, E.W. et al. (1985) Dose-response curves for in vivo insulin sensitivity in individual tissues in rats. Am J Physiol 248 (3 Pt 1), E353-62.
131. Mulligan, K.X. et al. (2012) Disassociation of muscle insulin signaling and insulin-stimulated glucose uptake during endotoxemia. PLoS One 7 (1), e30160.
132. Gutierrez, D.A. et al. (2011) Aberrant accumulation of undifferentiated myeloid cells in the adipose tissue of CCR2-deficient mice delays improvements in insulin sensitivity. Diabetes 60 (11), 2820-9.
133. Pfaffl, M.W. (2001) A new mathematical model for relative quantification in real-time RT-PCR. Nucleic Acids Res 29 (9), e45.
134. Li, H. and Durbin, R. (2009) Fast and accurate short read alignment with Burrows-Wheeler transform. Bioinformatics 25 (14), 1754-60.
135. Li, H. et al. (2009) The Sequence Alignment/Map format and SAMtools. Bioinformatics 25 (16), 2078-9.
136. Thorvaldsdottir, H. et al. (2013) Integrative Genomics Viewer (IGV): high-performance genomics data visualization and exploration. Brief Bioinform 14 (2), 178-92.
137. Jacobs, S. et al. (1983) Monensin blocks the maturation of receptors for insulin and somatomedin C: identification of receptor precursors. Proc Natl Acad Sci U S A 80 (5), 1228-31.
138. Hedo, J.A. et al. (1983) Biosynthesis and glycosylation of the insulin receptor. Evidence for a single polypeptide precursor of the two major subunits. J Biol Chem 258 (16), 10020-6.

139. Louvi, A. et al. (1997) Growth-promoting interaction of IGF-II with the insulin receptor during mouse embryonic development. Dev Biol 189 (1), 33-48.
140. Bluher, M. et al. (2002) Adipose tissue selective insulin receptor knockout protects against obesity and obesity-related glucose intolerance. Dev Cell 3 (1), 25-38.
141. Michael, M.D. et al. (2000) Loss of insulin signaling in hepatocytes leads to severe insulin resistance and progressive hepatic dysfunction. Mol Cell 6 (1), 87-97.
142. Bruning, J.C. et al. (1998) A muscle-specific insulin receptor knockout exhibits features of the metabolic syndrome of NIDDM without altering glucose tolerance. Mol Cell 2 (5), 559-69.
143. Ardon, O. et al. (2014) Sequencing analysis of insulin receptor defects and detection of two novel mutations in INSR gene. Mol Genet Metab Rep 1, 71-84.
144. Hojlund, K. et al. (2004) A novel syndrome of autosomal-dominant hyperinsulinemic hypoglycemia linked to a mutation in the human insulin receptor gene. Diabetes 53 (6), 1592-8.
145. Moller, D.E. et al. (1990) A naturally occurring mutation of insulin receptor alanine 1134 impairs tyrosine kinase function and is associated with dominantly inherited insulin resistance. J Biol Chem 265 (25), 14979-85.
146. Magre, J. et al. (1997) Dominant transmission of insulin resistance in a type A family resulting from a heterozygous nonsense mutation in the insulin receptor gene and associated with decreased mRNA level and insulin binding sites. Diabetes 46 (11), 1901-3.
147. Odawara, M. et al. (1989) Human diabetes associated with a mutation in the tyrosine kinase domain of the insulin receptor. Science 245 (4913), 66-8.
148. Levy-Toledano, R. et al. (1994) Investigation of the mechanism of the dominant negative effect of mutations in the tyrosine kinase domain of the insulin receptor. EMBO J 13 (4), 835-42.
149. Abu-Ashour, W. et al. (2018) Diabetes and the occurrence of infection in primary care: a matched cohort study. BMC Infect Dis 18 (1), 67.
150. Carey, I.M. et al. (2018) Risk of Infection in Type 1 and Type 2 Diabetes Compared With the General Population: A Matched Cohort Study. Diabetes Care 41 (3), 513-521.
151. Ehrnthaller, C. et al. (2013) Complement C3 and C5 deficiency affects fracture healing. PLoS One 8 (11), e81341.
152. Jiao, H. et al. (2015) Diabetes and Its Effect on Bone and Fracture Healing. Curr Osteoporos Rep 13 (5), 327-35.
153. Pasinetti, G.M. et al. (1996) Hereditary deficiencies in complement C5 are associated with intensified neurodegenerative responses that implicate new roles for the C-system in neuronal and astrocytic functions. Neurobiol Dis 3 (3), 197-204.
154. Lau, J.C. et al. (2013) Diabetes changes expression of genes related to glutamate neurotransmission and transport in the Long-Evans rat retina. Mol Vis 19, 1538-53.
155. Lim, J. et al. (2012) C5aR and C3aR antagonists each inhibit diet-induced obesity, metabolic dysfunction, and adipocyte and macrophage signaling. FASEB J.
156. Villarroya, F. et al. (2018) Inflammation of brown/beige adipose tissues in obesity and metabolic disease. J Intern Med 284 (5), 492-504.

157. Bae, J. et al. (2014) Activation of pattern recognition receptors in brown adipocytes induces inflammation and suppresses uncoupling protein 1 expression and mitochondrial respiration. Am J Physiol Cell Physiol 306 (10), C918-30.
158. Boumelhem, B.B. et al. (2017) Flow cytometric single cell analysis reveals heterogeneity between adipose depots. Adipocyte 6 (2), 112-123.
159. Hagberg, C.E. et al. (2018) Flow Cytometry of Mouse and Human Adipocytes for the Analysis of Browning and Cellular Heterogeneity. Cell Rep 24 (10), 2746-2756 e5.
160. Ikeda, K. et al. (2018) The Common and Distinct Features of Brown and Beige Adipocytes. Trends Endocrinol Metab 29 (3), 191-200.
161. Knutson, V.P. (1991) Cellular trafficking and processing of the insulin receptor. FASEB J 5 (8), 2130-8.
162. Kulkarni, R.N. et al. (1999) Tissue-specific knockout of the insulin receptor in pancreatic beta cells creates an insulin secretory defect similar to that in type 2 diabetes. Cell 96 (3), 329-39.
163. Bruning, J.C. et al. (2000) Role of brain insulin receptor in control of body weight and reproduction. Science 289 (5487), 2122-5.
164. Jiang, S. et al. (2011) Functional characterization of insulin receptor gene mutations contributing to Rabson-Mendenhall syndrome - phenotypic heterogeneity of insulin receptor gene mutations. Endocr J 58 (11), 931-40.
165. Kazemi, B. et al. (2009) Insulin receptor gene mutations in iranian patients with type II diabetes mellitus. Iran Biomed J 13 (3), 161-8.
166. Longo, N. et al. (1999) Progressive decline in insulin levels in Rabson-Mendenhall syndrome. J Clin Endocrinol Metab 84 (8), 2623-9.
167. Seino, S. et al. (1990) Human insulin-receptor gene. Diabetes 39 (2), 129-33.
168. Saito-Hakoda, A. et al. (2018) A follow-up during puberty in a Japanese girl with type A insulin resistance due to a novel mutation in INSR. Clin Pediatr Endocrinol 27 (1), 53-57.
169. Kirel, B. et al. (2017) A case of Donohue syndrome "Leprechaunism" with a novel mutation in the insulin receptor gene. Turk Pediatri Ars 52 (4), 226-230.
170. Huang, Z. et al. (2018) Glimepiride treatment in a patient with type A insulin resistance syndrome due to a novel heterozygous missense mutation in the insulin receptor gene. J Diabetes Investig 9 (5), 1075-1083.
171. Shimada, F. et al. (1992) Abnormal messenger ribonucleic acid (mRNA) transcribed from a mutant insulin receptor gene in a patient with type A insulin resistance. Diabetologia 35 (7), 639-44.
172. Moller, D.E. et al. (1994) Prevalence of mutations in the insulin receptor gene in subjects with features of the type A syndrome of insulin resistance. Diabetes 43 (2), 247-55.
173. Kadowaki, T. et al. (1990) Five mutant alleles of the insulin receptor gene in patients with genetic forms of insulin resistance. J Clin Invest 86 (1), 254-64.
174. Olefsky, J.M. (1990) The insulin receptor. A multifunctional protein. Diabetes 39 (9), 1009-16.
175. Seino, S. and Bell, G.I. (1989) Alternative splicing of human insulin receptor messenger RNA. Biochem Biophys Res Commun 159 (1), 312-6.
176. Belfiore, A. et al. (2017) Insulin Receptor Isoforms in Physiology and Disease: An Updated View. Endocr Rev 38 (5), 379-431.

177. McClain, D.A. (1991) Different ligand affinities of the two human insulin receptor splice variants are reflected in parallel changes in sensitivity for insulin action. Mol Endocrinol 5 (5), 734-9.
178. De Meyts, P. and Whittaker, J. (2002) Structural biology of insulin and IGF1 receptors: implications for drug design. Nat Rev Drug Discov 1 (10), 769-83.
179. Ohno, M. et al. (2000) A putative chemoattractant receptor, C5L2, is expressed in granulocyte and immature dendritic cells, but not in mature dendritic cells. Mol Immunol 37 (8), 407-12.
180. Lee, H. et al. (2008) Receptors for complement C5a. The importance of C5aR and the enigmatic role of C5L2. Immunol Cell Biol 86 (2), 153-60.
181. Gerard, N.P. and Gerard, C. (1991) The chemotactic receptor for human C5a anaphylatoxin. Nature 349 (6310), 614-7.
182. Boulay, F. et al. (1991) Expression cloning of a receptor for C5a anaphylatoxin on differentiated HL-60 cells. Biochemistry 30 (12), 2993-9.
183. Amatruda, T.T., 3rd et al. (1993) Specific interactions of chemoattractant factor receptors with G-proteins. J Biol Chem 268 (14), 10139-44.
184. Buhl, A.M. et al. (1994) Mapping of the C5a receptor signal transduction network in human neutrophils. Proc Natl Acad Sci U S A 91 (19), 9190-4.
185. Vanek, M. et al. (1994) Coupling of the C5a receptor to Gi in U-937 cells and in cells transfected with C5a receptor cDNA. Mol Pharmacol 46 (5), 832-9.
186. Yang, M. et al. (2001) G alpha 16 couples chemoattractant receptors to NF-kappa B activation. J Immunol 166 (11), 6885-92.
187. Cain, S.A. and Monk, P.N. (2002) The orphan receptor C5L2 has high affinity binding sites for complement fragments C5a and C5a des-Arg(74). J Biol Chem 277 (9), 7165-9.
188. Kalant, D. et al. (2003) The chemoattractant receptor-like protein C5L2 binds the C3a des-Arg77/acylation-stimulating protein. J Biol Chem 278 (13), 11123-9.
189. Scola, A.M. et al. (2009) The human complement fragment receptor, C5L2, is a recycling decoy receptor. Mol Immunol 46 (6), 1149-62.
190. Mamane, Y. et al. (2009) The C3a anaphylatoxin receptor is a key mediator of insulin resistance and functions by modulating adipose tissue macrophage infiltration and activation. Diabetes 58 (9), 2006-17.
191. Paglialunga, S. et al. (2008) Acylation-stimulating protein deficiency and altered adipose tissue in alternative complement pathway knockout mice. Am J Physiol Endocrinol Metab 294 (3), E521-9.
192. Gauvreau, D. et al. (2013) Deficiency of C5L2 increases macrophage infiltration and alters adipose tissue function in mice. PLoS One 8 (4), e60795.
193. Fisette, A. et al. (2013) C5L2 receptor disruption enhances the development of diet-induced insulin resistance in mice. Immunobiology 218 (1), 127-33.
194. Zheng, Y.Y. et al. (2012) Relationship between type 2 diabetes mellitus and a novel polymorphism C698T in C5L2 in the Chinese Han population. Endocrine 41 (2), 296-301.
195. Kalant, D. et al. (2005) C5L2 is a functional receptor for acylation-stimulating protein. J Biol Chem 280 (25), 23936-44.
196. Maslowska, M. et al. (1997) ASP stimulates glucose transport in cultured human adipocytes. Int J Obes Relat Metab Disord 21 (4), 261-6.

197. Yasruel, Z. et al. (1991) Effect of acylation stimulating protein on the triacylglycerol synthetic pathway of human adipose tissue. Lipids 26 (7), 495-9.
198. Cianflone, K. (1997) The acylation stimulating protein pathway: clinical implications. Clin Biochem 30 (4), 301-12.
199. Cianflone, K. et al. (1999) Acylation stimulating protein (ASP), an adipocyte autocrine: new directions. Semin Cell Dev Biol 10 (1), 31-41.
200. Cianflone, K. and Maslowska, M. (1995) Differentiation-induced production of ASP in human adipocytes. Eur J Clin Invest 25 (11), 817-25.
201. Saleh, J. et al. (1998) Coordinated release of acylation stimulating protein (ASP) and triacylglycerol clearance by human adipose tissue in vivo in the postprandial period. J Lipid Res 39 (4), 884-91.
202. Ahren, B. et al. (2003) Acylation stimulating protein stimulates insulin secretion. Int J Obes Relat Metab Disord 27 (9), 1037-43.
203. Chen, N.J. et al. (2007) C5L2 is critical for the biological activities of the anaphylatoxins C5a and C3a. Nature 446 (7132), 203-7.
204. Peterson, K.R. et al. (2018) Macrophage-Targeted Therapeutics for Metabolic Disease. Trends Pharmacol Sci 39 (6), 536-546.
205. Chen, D.S. and Mellman, I. (2017) Elements of cancer immunity and the cancer-immune set point. Nature 541 (7637), 321-330.
206. Zlatanova, I. et al. (2016) Immune Modulation of Cardiac Repair and Regeneration: The Art of Mending Broken Hearts. Front Cardiovasc Med 3, 40.
207. Sanmarco, L.M. et al. (2017) New Insights into the Immunobiology of Mononuclear Phagocytic Cells and Their Relevance to the Pathogenesis of Cardiovascular Diseases. Front Immunol 8, 1921.
208. Clark, M. et al. (2017) Type 1 Diabetes: A Chronic Anti-Self-Inflammatory Response. Front Immunol 8, 1898.
209. Winer, S. and Winer, D.A. (2012) The adaptive immune system as a fundamental regulator of adipose tissue inflammation and insulin resistance. Immunol Cell Biol 90 (8), 755-62.
210. Gordon, S. (2016) Phagocytosis: An Immunobiologic Process. Immunity 44 (3), 463-475.
211. Man, K. et al. (2017) Tissue Immunometabolism: Development, Physiology, and Pathobiology. Cell Metab 25 (1), 11-26.
212. Murray, P.J. et al. (2014) Macrophage activation and polarization: nomenclature and experimental guidelines. Immunity 41 (1), 14-20.
213. Mosser, D.M. and Edwards, J.P. (2008) Exploring the full spectrum of macrophage activation. Nat Rev Immunol 8 (12), 958-69.
214. Reilly, S.M. and Saltiel, A.R. (2017) Adapting to obesity with adipose tissue inflammation. Nat Rev Endocrinol 13 (11), 633-643.
215. Curat, C.A. et al. (2004) From blood monocytes to adipose tissue-resident macrophages: induction of diapedesis by human mature adipocytes. Diabetes 53 (5), 1285-92.
216. Cancello, R. et al. (2005) Reduction of macrophage infiltration and chemoattractant gene expression changes in white adipose tissue of morbidly obese subjects after surgery-induced weight loss. Diabetes 54 (8), 2277-86.

217. Cancello, R. et al. (2006) Increased infiltration of macrophages in omental adipose tissue is associated with marked hepatic lesions in morbid human obesity. Diabetes 55 (6), 1554-61.
218. Shapiro, H. et al. (2013) Adipose tissue foam cells are present in human obesity. J Clin Endocrinol Metab 98 (3), 1173-81.
219. Sun, K. et al. (2011) Adipose tissue remodeling and obesity. J Clin Invest 121 (6), 2094-101.
220. Kratz, M. et al. (2014) Metabolic dysfunction drives a mechanistically distinct proinflammatory phenotype in adipose tissue macrophages. Cell Metab 20 (4), 614-25.
221. Coats, B.R. et al. (2017) Metabolically Activated Adipose Tissue Macrophages Perform Detrimental and Beneficial Functions during Diet-Induced Obesity. Cell Rep 20 (13), 3149-3161.
222. Boyle, J.J. et al. (2009) Coronary intraplaque hemorrhage evokes a novel atheroprotective macrophage phenotype. Am J Pathol 174 (3), 1097-108.
223. Boyle, J.J. et al. (2012) Activating transcription factor 1 directs Mhem atheroprotective macrophages through coordinated iron handling and foam cell protection. Circ Res 110 (1), 20-33.
224. Finn, A.V. et al. (2012) Macrophage subsets in human atherosclerosis. Circ Res 110 (9), e64; author reply e65-6.
225. Bories, G. et al. (2013) Liver X receptor activation stimulates iron export in human alternative macrophages. Circ Res 113 (11), 1196-205.
226. Hasty, A.H. and Yvan-Charvet, L. (2013) Liver X receptor alpha-dependent iron handling in M2 macrophages: The missing link between cholesterol and intraplaque hemorrhage? Circ Res 113 (11), 1182-5.
227. Meli, R. et al. (2014) Role of innate immune response in non-alcoholic Fatty liver disease: metabolic complications and therapeutic tools. Front Immunol 5, 177.
228. Guilliams, M. et al. (2016) Unsupervised High-Dimensional Analysis Aligns Dendritic Cells across Tissues and Species. Immunity 45 (3), 669-684.
229. Luo, W. et al. (2017) Effect of modulation of PPAR-gamma activity on Kupffer cells M1/M2 polarization in the development of non-alcoholic fatty liver disease. Sci Rep 7, 44612.
230. Obstfeld, A.E. et al. (2010) C-C chemokine receptor 2 (CCR2) regulates the hepatic recruitment of myeloid cells that promote obesity-induced hepatic steatosis. Diabetes 59 (4), 916-25.
231. Krenkel, O. et al. (2017) Therapeutic Inhibition of Inflammatory Monocyte Recruitment Reduces Steatohepatitis and Liver Fibrosis. Hepatology.
232. Ju, C. and Tacke, F. (2016) Hepatic macrophages in homeostasis and liver diseases: from pathogenesis to novel therapeutic strategies. Cell Mol Immunol 13 (3), 316-27.
233. Ray, I. et al. (2016) Obesity: An Immunometabolic Perspective. Front Endocrinol (Lausanne) 7, 157.
234. Carpino, G. et al. (2016) Macrophage Activation in Pediatric Nonalcoholic Fatty Liver Disease (NAFLD) Correlates with Hepatic Progenitor Cell Response via Wnt3a Pathway. PLoS One 11 (6), e0157246.

235. Ni, Y. et al. (2016) Novel Action of Carotenoids on Non-Alcoholic Fatty Liver Disease: Macrophage Polarization and Liver Homeostasis. Nutrients 8 (7).
236. Ensan, S. et al. (2016) Self-renewing resident arterial macrophages arise from embryonic CX3CR1(+) precursors and circulating monocytes immediately after birth. Nat Immunol 17 (2), 159-68.
237. Huang, J.Y. et al. (2017) Neutrophil Elastase Regulates Emergency Myelopoiesis Preceding Systemic Inflammation in Diet-induced Obesity. J Biol Chem 292 (12), 4770-4776.
238. Singer, K. et al. (2015) Differences in Hematopoietic Stem Cells Contribute to Sexually Dimorphic Inflammatory Responses to High Fat Diet-induced Obesity. J Biol Chem 290 (21), 13250-62.
239. Tabas, I. and Bornfeldt, K.E. (2016) Macrophage Phenotype and Function in Different Stages of Atherosclerosis. Circ Res 118 (4), 653-67.
240. Boyle, J.J. (2012) Heme and haemoglobin direct macrophage Mhem phenotype and counter foam cell formation in areas of intraplaque haemorrhage. Curr Opin Lipidol 23 (5), 453-61.
241. Kadl, A. et al. (2010) Identification of a novel macrophage phenotype that develops in response to atherogenic phospholipids via Nrf2. Circ Res 107 (6), 737-46.
242. He, H. et al. (2017) Development of mannose functionalized dendrimeric nanoparticles for targeted delivery to macrophages: use of this platform to modulate atherosclerosis. Transl Res.
243. Morris, D.L. et al. (2011) Adipose tissue macrophages: phenotypic plasticity and diversity in lean and obese states. Curr Opin Clin Nutr Metab Care 14 (4), 341-6.
244. Gordon, S. et al. (2014) Macrophage heterogeneity in tissues: phenotypic diversity and functions. Immunol Rev 262 (1), 36-55.
245. Murray, P.J. and Wynn, T.A. (2011) Protective and pathogenic functions of macrophage subsets. Nat Rev Immunol 11 (11), 723-37.
246. Merino, M. et al. (2017) Role of adenosine receptors in the adipocyte-macrophage interaction during obesity. Endocrinol Diabetes Nutr 64 (6), 317-327.
247. Zhao, X. et al. (2008) Targeted drug delivery via folate receptors. Expert Opin Drug Deliv 5 (3), 309-19.
248. Hillaireau, H. and Couvreur, P. (2009) Nanocarriers' entry into the cell: relevance to drug delivery. Cell Mol Life Sci 66 (17), 2873-96.
249. Yu, S.S. et al. (2012) Size- and charge-dependent non-specific uptake of PEGylated nanoparticles by macrophages. Int J Nanomedicine 7, 799-813.
250. Vlasova, II et al. (2016) Enzymatic oxidative biodegradation of nanoparticles: Mechanisms, significance and applications. Toxicol Appl Pharmacol 299, 58-69.
251. Ahsan, F. et al. (2002) Targeting to macrophages: role of physicochemical properties of particulate carriers--liposomes and microspheres--on the phagocytosis by macrophages. J Control Release 79 (1-3), 29-40.
252. Kuhn, D.A. et al. (2014) Different endocytotic uptake mechanisms for nanoparticles in epithelial cells and macrophages. Beilstein J Nanotechnol 5, 1625-36.
253. van Rooijen, N. and van Kesteren-Hendrikx, E. (2003) "In vivo" depletion of macrophages by liposome-mediated "suicide". Methods Enzymol 373, 3-16.
254. Tang, J. et al. (2015) Inhibiting macrophage proliferation suppresses atherosclerotic plaque inflammation. Sci Adv 1 (3).

255. Dinarello, C.A. (2010) Anti-inflammatory Agents: Present and Future. Cell 140 (6), 935-50.
256. Tornatore, L. et al. (2012) The nuclear factor kappa B signaling pathway: integrating metabolism with inflammation. Trends Cell Biol 22 (11), 557-66.
257. Turner, M.D. et al. (2014) Cytokines and chemokines: At the crossroads of cell signalling and inflammatory disease. Biochim Biophys Acta 1843 (11), 2563-2582.
258. Singh, R. and Lillard, J.W., Jr. (2009) Nanoparticle-based targeted drug delivery. Exp Mol Pathol 86 (3), 215-23.
259. Frenz, T. et al. (2015) Antigen presenting cell-selective drug delivery by glycan-decorated nanocarriers. Eur J Pharm Biopharm 95 (Pt A), 13-7.
260. Ma, L. et al. (2016) Efficient Targeting of Adipose Tissue Macrophages in Obesity with Polysaccharide Nanocarriers. ACS Nano 10 (7), 6952-62.
261. Rojas, J.M. et al. (2016) Superparamagnetic iron oxide nanoparticle uptake alters M2 macrophage phenotype, iron metabolism, migration and invasion. Nanomedicine 12 (4), 1127-1138.
262. Yu, S.S. et al. (2013) Macrophage-specific RNA interference targeting via "click", mannosylated polymeric micelles. Mol Pharm 10 (3), 975-87.
263. Suk, J.S. et al. (2016) PEGylation as a strategy for improving nanoparticle-based drug and gene delivery. Adv Drug Deliv Rev 99 (Pt A), 28-51.
264. Kelly, C. et al. (2011) Targeted liposomal drug delivery to monocytes and macrophages. J Drug Deliv 2011, 727241.
265. Sercombe, L. et al. (2015) Advances and Challenges of Liposome Assisted Drug Delivery. Front Pharmacol 6, 286.
266. Zylberberg, C. and Matosevic, S. (2016) Pharmaceutical liposomal drug delivery: a review of new delivery systems and a look at the regulatory landscape. Drug Deliv 23 (9), 3319-3329.
267. Bu, L. et al. (2013) Intraperitoneal injection of clodronate liposomes eliminates visceral adipose macrophages and blocks high-fat diet-induced weight gain and development of insulin resistance. AAPS J 15 (4), 1001-11.
268. Etzerodt, A. et al. (2012) Efficient intracellular drug-targeting of macrophages using stealth liposomes directed to the hemoglobin scavenger receptor CD163. J Control Release 160 (1), 72-80.
269. Brown, G.D. and Gordon, S. (2001) Immune recognition. A new receptor for beta-glucans. Nature 413 (6851), 36-7.
270. Brown, G.D. et al. (2002) Dectin-1 is a major beta-glucan receptor on macrophages. J Exp Med 196 (3), 407-12.
271. Samuelsen, A.B. et al. (2014) Effects of orally administered yeast-derived beta-glucans: a review. Mol Nutr Food Res 58 (1), 183-93.
272. Kohl, A. et al. (2009) Increased interleukin-10 but unchanged insulin sensitivity after 4 weeks of (1, 3)(1, 6)-beta-glycan consumption in overweight humans. Nutr Res 29 (4), 248-54.
273. Fatima, N. et al. (2017) Particulate beta-glucan induces early and late phagosomal maturation in murine macrophages. Front Biosci (Elite Ed) 9, 129-140.
274. Ip, W.K.E. et al. (2017) Anti-inflammatory effect of IL-10 mediated by metabolic reprogramming of macrophages. Science 356 (6337), 513-519.

275. Aouadi, M. et al. (2009) Orally delivered siRNA targeting macrophage Map4k4 suppresses systemic inflammation. Nature 458 (7242), 1180-4.
276. Soto, E.R. et al. (2016) Targeted Delivery of Glucan Particle Encapsulated Gallium Nanoparticles Inhibits HIV Growth in Human Macrophages. J Drug Deliv 2016, 8520629.
277. Upadhyay, T.K. et al. (2017) Preparation and characterization of beta-glucan particles containing a payload of nanoembedded rifabutin for enhanced targeted delivery to macrophages. EXCLI J 16, 210-228.
278. Aouadi, M. et al. (2013) Gene silencing in adipose tissue macrophages regulates whole-body metabolism in obese mice. Proc Natl Acad Sci U S A 110 (20), 8278-83.
279. Liu, M. et al. (2012) An oligopeptide ligand-mediated therapeutic gene nanocomplex for liver cancer-targeted therapy. Biomaterials 33 (7), 2240-50.
280. Won, Y.W. et al. (2014) Oligopeptide complex for targeted non-viral gene delivery to adipocytes. Nat Mater 13 (12), 1157-64.
281. Yong, S.B. et al. (2017) Visceral adipose tissue macrophage-targeted TACE silencing to treat obesity-induced type 2 diabetes. Biomaterials 148, 81-89.
282. Black, R.A. (2002) Tumor necrosis factor-alpha converting enzyme. Int J Biochem Cell Biol 34 (1), 1-5.
283. Dai, W.J. et al. (2016) CRISPR-Cas9 for in vivo Gene Therapy: Promise and Hurdles. Mol Ther Nucleic Acids 5, e349.
284. Wang, X. et al. (2016) Epigenetic regulation of macrophage polarization and inflammation by DNA methylation in obesity. JCI Insight 1 (19), e87748.